



The $\eta/\eta' \rightarrow \pi^+\pi^-\gamma$ decays within BHLS₂ and the muon HVP

M. Benayoun¹, L. DelBuono^{1,a} , F. Jegerlehner²

¹ LPNHE des Universités Paris VI et Paris VII, IN2P3/CNRS, 75252 Paris, France

² Institut für Physik, Humboldt-Universität zu Berlin, Newtonstrasse 15, 12489 Berlin, Germany

Received: 28 September 2023 / Accepted: 25 February 2024 / Published online: 21 March 2024
© The Author(s) 2024, corrected publication 2024

Abstract The departure of the latest FNAL experimental average for the muon anomalous magnetic moment $a_\mu = (g_\mu - 2)/2$ measurements, having increased from 4.2σ (Abi et al. in Measurement of the positive muon anomalous magnetic moment to 0.46 ppm, [arXiv:2104.03281](https://arxiv.org/abs/2104.03281), 2021) to 5.0σ (Muon g-2, D.P. Aguillard et al. in Measurement of the positive muon anomalous magnetic moment to 0.20 ppm, [arXiv:2308.06230](https://arxiv.org/abs/2308.06230), 2023) with respect to the white paper (WP) consensus (Aoyama et al. in Phys Rep 887:1, [arXiv:2006.04822](https://arxiv.org/abs/2006.04822), 2020), may indicate a hint for new physics. As the most delicate piece of a_μ is its leading-order hadronic vacuum polarization (HVP) part a_μ^{HVP-LO} , methods to ascertain its theoretical value are crucial to appropriately interpreting this departure from the measurement. We, therefore, propose to closely examine the dipion spectra from the $\eta/\eta' \rightarrow \pi^+\pi^-\gamma$ decays in the hidden local symmetry (HLS) context using its BHLS₂ broken variant. We thus have at our disposal a framework where the close relationship of the dipion spectra from the η/η' and τ decays and of the $e^+e^- \rightarrow \pi^+\pi^-$ annihilation can be simultaneously considered. A special focus is given to the high-statistics dipion spectra from the η decay collected by the KLOE/KLOE2 Collaboration and η' decay collected by the BESIII Collaboration, and it is shown that the BHLS₂ framework provides a fair account of their dipion spectra. More precisely, it is first proven that a single Omnès representation real polynomial is required, common to both the η and η' dipion spectra. Moreover, it is shown that fits involving the $\eta/\eta'/\tau$ dipion spectra, and excluding the $e^+e^- \rightarrow \pi^+\pi^-$ annihilation data, allow for a prediction of the pion vector form factor data $F_\pi(s)$ which agrees fairly well with the usual dipion spectra collected in the $e^+e^- \rightarrow \pi^+\pi^-$ annihilation channel. Even if more precise $\eta/\eta'/\tau$ dipion spectra would help to be fully conclusive, this confirms the dispersive approach results for

a_μ^{HVP-LO} and points toward a common non-experimentally dependent origin to this tension with the now well-accepted LQCD result.

Contents

1 Preamble: various aspects of the dispersive approach to the muon HVP	2
2 Introduction	3
3 The Kroll conditions and VPP Lagrangian pieces	5
4 The $\eta/\eta' \rightarrow \pi^+\pi^-\gamma$ decays in the BHLS ₂ framework	6
5 The $\eta \rightarrow \pi^+\pi^-\gamma$ amplitude within BHLS ₂	6
6 The $\eta' \rightarrow \pi^+\pi^-\gamma$ amplitude within BHLS ₂	7
7 BHLS ₂ and the WZW box anomalies	7
8 η/η' radiative decays: the BHLS ₂ dipion mass spectra	8
9 Pion form factor in the η/η' radiative decays	9
10 Fits of the η/η' radiative decay spectra within BHLS ₂	12
10.1 Available dipion spectra from the $\eta/\eta' \rightarrow \pi^+\pi^-\gamma$ decays	12
10.2 η/η' experimental spectra: fits in isolation	13
10.3 The η/η' experimental spectra: analysis within the BHLS ₂ context	13
10.4 $P_X(s)$: BHLS ₂ fit results versus others	16
10.5 Brief analysis of the BHLS ₂ parameter values	18
10.6 The $T^{R2}(\eta/\eta')$ terms in BHLS ₂ : the role of ρ^\pm exchanges	20
10.7 Dealing with the absolute scale of the η/η' dipion spectra	22
11 η/η' decays: the muon anomalous magnetic moment	22
11.1 Accuracy of the $P_X(s)$ parameterization	22
11.2 The η/η' spectra and HVP estimates	25
11.3 The case for the τ data	25
11.3.1 Fitting the τ data	25
11.3.2 τ data and a_μ	27
11.4 η/η' -based evaluations of the HVP	27

Maurice Benayoun passed on September 15, 2023.

^a e-mail: luigi.delbuono@lpnhe.in2p3.fr (corresponding author)

12 Concluding remarks	28
Appendices	29
A Brief outline of the HLS/BHLS ₂ approach	29
A.1 The unbroken non-anomalous HLS Lagrangian	29
A.2 Breaking the HLS Lagrangian I: the BKY mechanism	29
A.3 Breaking the HLS Lagrangian II: the covariant derivative (CD) breaking	30
A.4 Breaking the HLS Lagrangian III: dynamical vector meson mixing	30
A.5 The kinetic breaking and the $[\pi^0, \eta, \eta']$ system	31
B Erratum: the VPP/APP interaction pieces in BHLS ₂	32
C A_{\pm} solutions: the AAP and VVP Lagrangians	32
C.1 The AAP Lagrangian	32
C.2 The VVP Lagrangian	33
C.2.1 The $VV\pi$ Lagrangians	33
C.2.2 The $VV\eta$ Lagrangian	33
C.2.3 The $VV\eta'$ Lagrangian	33
D A_{\pm} solutions: the APPP and VPPP Lagrangians	34
D.1 The APPP Lagrangian	34
D.2 The VPPP Lagrangian	34
References	35

1 Preamble: various aspects of the dispersive approach to the muon HVP

The hadronic vacuum polarization (HVP) $a_{\mu} \equiv (g_{\mu} - 2)/2$ plays a central role in precision physics, in particular in the Standard Model prediction of the muon anomalous magnetic moment, but equally importantly for a precise calculation of the running electromagnetic fine structure constant $\alpha_{em}(s)$ and the electroweak mixing parameter $\sin^2 \theta_W(s)$. Therefore, accurate predictions suffer from the non-perturbative contributions from low-lying hadron physics that are difficult to address precisely from first principles.

Recently [2], the Fermi National Accelerator Laboratory (FNAL) Muon $g - 2$ experiment re-estimated the previous average value of their run 1 data sample [2] and the latest Brookhaven National Laboratory (BNL) measurement [4] by also considering their run 2 and 3 data samples; this turns out to increase the statistics by a factor of $\simeq 4$. Moreover, the Muon $g - 2$ FNAL Collaboration achieved an improvement in their systematic uncertainty by about a factor of 2. The derived updated average

$$a_{\mu}^{exp.} = 116592059(22) \times 10^{-11} (0.19 \text{ ppm})$$

increases the deviation from the white paper (WP) Standard Model consensus [3] from 4.2σ [1] to 5.0σ [2]. The difference $\delta_a = a_{\mu}^{exp.} - a_{\mu}^{th.}$ is now $\delta_a = 24.4 \pm 4.5$ in units of 10^{-10} , dominated by the uncertainty agreed upon by the WP theory consensus [3]. Of course, this departure from theoretical expectations deserves to be explored, as the overall

pattern reflected by the various model/theoretical approaches is indeed unclear, even contradictory.

The WP Standard Model consensus for $a_{\mu}^{th.}$ resorts to a data-driven dispersion relation (DR) approach, where the experimental low-energy hadron production cross sections provide the non-perturbative input to calculate the HVP effects. Fortunately, the problem can be restricted to precise knowledge of the process $e^+e^- \rightarrow \gamma^* \rightarrow \text{hadrons}$, and for what concerns the muon $g - 2$, the $e^+e^- \rightarrow \pi^+\pi^-$ channel provides the dominant contribution to the model uncertainty.

Regarding its non-perturbative hadronic content, the standard dispersion-based (DR) evaluation of the HVP consists of deriving the contribution of *each* $e^+e^- \rightarrow \gamma^* \rightarrow \text{hadrons}$ annihilation channel by combining the different spectra collected by the different experiments in the hadronic channel considered, employing algorithms of different levels of sophistication. The full HVP value is then defined, for what concerns its non-perturbative content, by the sum of these different contributions. The WP Standard Model consensus [3] is based on a combination of two such evaluations [5, 6].

Although the main challenge is then, seemingly, the simple $\pi\pi$ production process, the experimental challenge is highly complex, depending on a precise understanding of the detectors and, on the theory side, the radiative corrections required to disentangle hadronic effects from electromagnetic contamination. Unfortunately, the data samples provided by the different experiments do not exhibit satisfactory consistency—and some can even be in strong contradiction [7] with the others. The use of the $\tau \rightarrow \pi^-\pi^0\nu_{\tau}$ decay information, first proposed by [8], has been considered to discriminate among the $\pi^+\pi^-$ spectra, but it did not lead to convincing enough conclusions.

It is widely considered that all low-energy hadronic processes derive from quantum chromodynamics (QCD), even though in the non-perturbative low-energy regime, tools to make valid predictions of real-time hadronic cross sections are missing. Nevertheless, as hadron physics is accepted to derive from QCD, it follows that *the various specific hadronic decay processes are highly correlated with each other*. This motivates the need to address these correlations, especially in order to constrain the non-perturbative sector of the $e^+e^- \rightarrow \gamma^* \rightarrow \text{hadrons}$ annihilations.

Although we lack methods to predict a process like $e^+e^- \rightarrow \pi^+\pi^-$, we know that QCD implies well-defined symmetry patterns such as approximate chiral symmetry, and gives rise to chiral perturbation theory (ChPT), a systematic expansion about the chiral symmetry point. It allows one to work out reliable predictions from first principles for the low-energy tail of the QCD hadron spectrum (up to about the η meson mass).

With this in mind, an attempt to consider the $e^+e^- \rightarrow \pi^+\pi^-$ annihilation not only in relation to the $\tau^{\pm} \rightarrow \pi^{\pm}\pi^0\nu_{\tau}$ decay *but also in relation to other related spectra* is impor-

tant; it motivates a unified modeling¹ by a version of the resonance Lagrangian approach (RLA) [9, 10]—we adopted the hidden local symmetry (HLS) version² [12, 13]—needed to extend the chiral perturbation theory toward higher energy to cover the ρ , ω , and ϕ energy range.³ To practically succeed in such a program, the original HLS model (see, for instance, [16] for a review) has been supplied with appropriate symmetry-breaking mechanisms with various levels of sophistication to derive the earlier versions of the BHLS model in [17–19], or the more refined BHLS₂ version [20], updated in [21].

One thus achieved a simultaneous consistent fit of the $e^+e^- \rightarrow \pi^+\pi^-$ data from CMD-2 [22], SND [23], KLOE [24–26], BaBar [27, 28], BESIII [29, 30], and CLEO-c [31], and the $\tau \rightarrow \pi^-\pi^0\nu_\tau$ decay spectral functions collected by ALEPH [32], CLEO [33], and Belle [34] (see [17, 18, 20, 21]). This updated BHLS₂ fairly recovers the known properties of the $[\pi^0, \eta, \eta']$ system thanks to its kinetic breaking mechanism [21].

Besides keeping the neutral vector current conserved, this breaking mechanism also generates a violation of the charged vector current conservation and a departure of $F_\pi^T(s=0) = 1$ by a few per mil. Such an option finds support in [34] in Belle own in their own fit results reported in their Table VII; additional τ spectra are needed to conclude—see the discussion in Section 3 of [21]—as such a breaking mechanism might affect τ -based predictions for the muon HVP.

Alongside the $\pi^+\pi^-$ annihilation channel and the $\tau \rightarrow \pi^-\pi^0\nu_\tau$ decay spectra, BHLS₂ [20, 21] also successfully addressed the $\pi^+\pi^-\pi^0$, $(\pi^0/\eta)\gamma$ and $K\bar{K}$ final states in a fully correlated way represented by a single Lagrangian. A few additional radiative partial width decays are also considered, notably those for $\pi^0/\eta/\eta' \rightarrow \gamma\gamma$, and some more $VP\gamma$ radiative decays.

In view of the significant inconsistencies in the data samples collected by some experiments, the global fit approach has two advantages: first, the additional data are expected to reduce the uncertainties of the HVP evaluations, and second, it provides consistency checks of each $e^+e^- \rightarrow \gamma^* \rightarrow$ hadrons data set versus the other samples collected in the same annihilation channel *or in another one*.

In the present work, we go a step further by also involving the $\eta/\eta' \rightarrow \pi^+\pi^-\gamma$ decay modes in order to obtain additional $\pi\pi$ dipion spectra from experiments with systematics quite different from those encountered in e^+e^- anni-

hilations. As will be seen below, these decays allow for a new test of the self-consistency of the DR-based estimates of a_μ . Indeed, the η/η' decay spectra can provide a DR evaluation for $a_\mu(\pi^+\pi^-, \sqrt{s} < 1 \text{ GeV})$, which can be fruitfully compared with those directly derived by directly integrating the $e^+e^- \rightarrow \pi^+\pi^-$ annihilation data. One may expect that the η/η' dipion spectra benefit from systematics largely independent of those in the e^+e^- annihilation.

Besides the DR approach which gave rise to several evaluations of the muon HVP a_μ listed in the white paper [3], the challenging lattice QCD (LQCD) approach has been used by several groups and produced results with relatively poor precision at the time of the white paper. They were not used to define the so-called WP Standard Model consensus reported in [3] which, based on some DR estimates, provided the leading-order (HVP-LO) consensus $a_\mu^{\text{LO}}[\text{th.}] = 693.1(4.0) \times 10^{-10}$. Using the LQCD approach, the BMW Collaboration, which first got [3, 35] $a_\mu^{\text{LO}} = (711.1 \pm 7.5 \pm 17.4) \times 10^{-10}$, later improved their calculation and got $a_\mu^{\text{LO}} = (707.5 \pm 5.5) \times 10^{-10}$ [36], at clear variance with the WP consensus just mentioned. This evaluation finds support from the new evaluations by other LQCD groups: $a_\mu^{\text{LO}} = (720.0 \pm 12.4_{\text{stat}} \pm 9.9_{\text{syst}}) \times 10^{-10}$ (Mainz/CLS 19) [37, 38] and $a_\mu^{\text{LO}} = (715.4 \pm 16.3_{\text{stat}} \pm 9.2_{\text{syst}}) \times 10^{-10}$ (RBC/UKQCD18) [39].

The lattice calculation of a_μ^{LO} thus brings the SM prediction of a_μ into acceptable agreement with the experiment but generates significant disagreement between the LQCD results and the different data-driven dispersive results; this now looks well established. It adds to the former puzzle from data versus predictions a puzzle between LQCD and the DR approaches, which deserves clarification.

2 Introduction

In this article, we focus on the traditional way of estimating the contribution of the non-perturbative energy region to the photon HVP which relies on dispersive methods using as basic ingredients the e^+e^- annihilation cross sections to all the possible exclusive hadronic final states collected up to $\sqrt{s} \simeq 2 \text{ GeV}$.

The different successive broken variants of the HLS model, especially BHLS₂ [20, 21], provide a well-adapted framework to address the most relevant e^+e^- annihilations to hadronic channels in the crucial part of the low-energy region ($\sqrt{s} \leq 1.05 \text{ GeV}$), namely the e^+e^- annihilations to the $\pi^+\pi^-$, $K\bar{K}/\pi^+\pi^-\pi^0/\pi^0\gamma/\eta\gamma$ final states; these already provide more than 80% of the muon HVP, when integrated up to the ϕ meson mass.

A BHLS₂-based computer code was used for this analysis which considered the large number of available data samples (several dozen), more than 1400 data points and, thus,

¹ Considering individual channels in isolation, as is usually done, does not help much to uncover inconsistencies between different experimental data sets sometimes involving different final states.

² See also [11] for an equivalent version.

³ A precise evaluation of the photon HVP implies a precise account of the energy range $\sqrt{s} \equiv [2m_\pi, 1.05 \text{ GeV}]$, the largest contribution of the non-perturbative region which extends up to $\simeq 2 \text{ GeV}$, as experimentally observed [14, 15].

practically the whole set of the available data samples has been exhausted. They have been listed, analyzed, and discussed in full detail previously, especially in the recent articles [20,21], where a large number of previous references can be found.⁴ This computer code faithfully takes into account all the uncertainty information provided together with these data samples, and therefore, yielding satisfactory global fit probabilities turns out to simultaneously have a satisfactory model, satisfactory handling of data of the samples collected in several physics channels, and also satisfactory dealing with their reported uncertainty information.

In this perspective, the given data samples exhibiting contradictory aspects compared to most of the others either may lead to discarding them or, when meaningful, may motivate several solutions that avoid mixing up contradictory spectra; this has led us in our previous studies [20,21] to provide different HVP evaluations based on some of the reported dipion KLOE samples—namely [24–26]—on the one hand, and separately on their BaBar analog [27,28] on the other hand.

Regarding the various dipion spectra, the studies found strong contradictions between the so-called KLOE8 data sample [40] or the recently published SND spectrum [41], and the bulk of the other considered data samples have been discarded.

Comparing our own evaluations with those based on dispersion relations collected in [3], one does not observe any loss in precision with any of the various reported values of the muon $g - 2$; however, differences between central values can be observed, clearly related to the contradictory properties of some data samples, especially KLOE [24,25] versus BaBar [27,28], reported long ago [18,19,42].

As noted above, the contribution of the listed HLS channels to the HVP is large; however, it is also worth mentioning that their contribution to the HVP uncertainty is almost negligible compared to that of the rest of the non-perturbative region. Moreover, as the HLS approach implies tight connections between the various annihilation channels, it allows one to perform stringent consistency checks on the different data samples involving the same physics channels or the other channels addressed by the HLS Lagrangian. It is worthwhile pointing out this important property specific to global models like the BHLS₂ model and also stressing that, by far, most of the available data samples fulfill this stringent constraint.

⁴ The CMD-3 Collaboration has recently published a high-statistics measurement of the $e^+e^- \rightarrow \pi^+\pi^-$ cross section [7] which deserves a specific analysis beyond the scope of the present work, which is focused on a quite different topic. Nevertheless, the information provided by the CMD-3 Collaboration in their article regarding the consistency of their spectrum with the previously collected data samples may indicate that, as it is, their measurement is not consistent with any subset of the relevant existing data samples and thus should hardly accommodate a global framework like HLS, so it should not impact the conclusions of the present work.

On the other hand, as indicated in the previous section, the updated version BHLS₂ variant [21] of the broken HLS model [20] allows us to fairly address the physics of the $[\pi^0, \eta, \eta']$ system within the HLS corpus. Indeed, besides the $e^+e^- \rightarrow (\pi^0/\eta)\gamma$ annihilations, the PS decays to $\gamma\gamma$, and the $VP\gamma$ couplings, the pseudoscalar meson (PS) mixing properties in the octet-singlet [43–45] and quark flavor [46–48] basis parameterizations have been analyzed, leading to a satisfactory comparison with expectations.

Among the other processes involving the properties of the $[\pi^0, \eta, \eta']$ system, the $\eta' \rightarrow \pi^+\pi^-\gamma$ decay spectrum deserves special attention. The measurements of this decay process started long ago—as early as 1975 [49]—and several experiments have collected samples of limited statistics [50–57], motivated by a reported 20 MeV mass shift of the ρ peak compared to its observed value in the $e^+e^- \rightarrow \pi^+\pi^-$ annihilation.

This effect was soon attributed to an interference between the $\eta' \rightarrow \rho\gamma$ ($\rho \rightarrow \pi^+\pi^-$) resonant amplitude and the Wess–Zumino–Witten (WZW) anomalous $\eta'\pi^+\pi^-\gamma$ contact term [58,59]; this so-called box anomaly was expected to occur alongside the triangle anomaly responsible for the two-photon decays of the π^0, η and η' mesons. A basic HLS approach including this anomalous interaction term alongside the dominant $\eta'\rho^0\gamma$ coupling [60] confirmed this guess.

However, the dipion η' spectrum from the BESIII Collaboration [61] published much later, thanks to its large statistics (970,000 events), modified the picture: It led to the conclusion that supplementing the (ρ^0, ω) resonance contributions by only a contact term is insufficient to reach a satisfactory description of the dipion spectrum.

On the other hand, the reported dipion spectrum observed in the parent $\eta \rightarrow \pi^+\pi^-\gamma$ decay has undergone many fewer measurements. Besides former spectra⁵ from Layter et al. [62] and Gormley et al. [63], WASA-at-COSY reported for a 14,000-event spectrum [64], whereas the KLOE/KLOE2 Collaboration collected a 205,000-event spectrum [65].

As the dipion spectra reported from the recent measurements of the $\eta/\eta' \rightarrow \pi^+\pi^-\gamma$ decays carry high statistics, it thus becomes relevant to re-examine whether (and how) they fit within the recently defined BHLS₂ framework of the HLS model, especially thanks to its kinetic breaking (see Appendix A.5), which has already allowed for a satisfactory description of the $[\pi^0, \eta, \eta']$ system properties [21]. Moreover, even if the physics of the η/η' mesons is interesting per se, a better understanding of their properties is important, given their important role in the light-by-light (LbL) contribution to the muon anomalous magnetic moment.

The paper is organized as follows. Section 3 recalls the Kroll conditions [66] which reduce the number of free param-

⁵ The numerical content of these spectra can only be derived from the paper figures.

eters of the kinetic breaking mechanism from 3 to 1; it also recalls and corrects Lagrangian pieces relevant for the present study. Section 4 identifies the Lagrangian pieces contributing to the considered η and η' radiative decays and displays the involved diagrams; the BHLS₂ amplitudes for these are constructed in Sect. 5 for the $\eta \rightarrow \pi^+\pi^-\gamma$ decay and in Sect. 6 for the $\eta' \rightarrow \pi^+\pi^-\gamma$ one. The relation between the anomalous HLS amplitudes and their WZW [58,59] analogs is given in Sect. 7. The derivation of the dipion mass spectrum in the η/η' radiative decays is done in Sect. 8, and the role of the additional polynomial factor in the η/η' radiative decays is thoroughly examined in Sect. 9. The polynomial factors accompanying the pion form factor parameterize an approximation to higher inelastic effects (beyond the two-pion channel) and are associated with the production vertex.⁶

Section 10 constitutes the central part of the present study. Section 10.1 provides an exhaustive presentation of the available $\eta/\eta' \rightarrow \pi^+\pi^-\gamma$ data samples; for this purpose it is important to note that all the available spectra carry an arbitrary absolute normalization, and that accounting for the $\eta/\eta' \rightarrow \pi^+\pi^-\gamma$ partial widths also implies using an external piece of (PDG [70]) information. A detailed study of the additional polynomial degrees is the subject of Sect. 10.2, which reports on the fits performed separately with the η and η' spectra to find the appropriate degrees of the requested polynomials. This allows us to perform the fits of the dipion spectra reported in Sect. 10.3, where it is proved that a unique polynomial can satisfactorily account for both the η and η' dipion spectra simultaneously.

Section 10.4 is devoted to comparing our polynomial results with those reported in the literature. The role of intermediate ρ^\pm exchanges is emphasized in Sect. 10.6. The global BHLS₂ fits performed to simultaneously describe the dipion spectral line shapes examined in the previous subsections and the PDG information for the partial widths $\Gamma(\eta/\eta' \rightarrow \pi^+\pi^-\gamma)$ are worked out in Sect. 10.7. A brief numerical analysis of some parameter values returned by the fits of the η/η' dipion spectra is the subject of Sect. 10.5. Finally, in Sect. 11, we examine the issues relative to the connection between the $\eta/\eta' \rightarrow \pi^+\pi^-\gamma$ decays (and also the τ decay data) and the hadronic contribution to the muon

anomalous magnetic moment a_μ . Section 12 summarizes the conclusions reached in the present study.

For ease of reading, the main pieces of information regarding the HLS model are briefly revisited in Appendix A.1, whereas its symmetry-breaking mechanisms are briefly summarized in Appendices A.2 to A.5. An erratum to the previous broken version of the BHLS₂ version is the subject of Appendix B. Also for ease of reading in the present work, it is appropriate to give the most relevant parts of the non-anomalous and anomalous BHLS₂ pieces under the Kroll conditions—mentioned just below—in Appendices C and D.

3 The Kroll conditions and VPP Lagrangian pieces

In the Feldmann–Kroll–Stech (FKS) approach [46–48] to the $[\pi^0, \eta, \eta']$ system, it has been found appropriate to impose the Kroll conditions [66] to axial current matrix elements. Applied to the BHLS₂ axial currents, these conditions,

$$\begin{aligned} \langle 0 | J_\mu^a | \eta_b(p) \rangle &= i p_\mu f_a \delta_{ab}, \quad | \eta_b(p) \rangle = | b \bar{b}(p) \rangle, \\ J_\mu^a &= \bar{a} \gamma_\mu \gamma_5 a, \quad \{a, b = u, d, s\}, \end{aligned} \tag{1}$$

lead to two nontrivial relations [21]—referred to below as A_\pm solutions—among the λ_i parameters of the generalized 't Hooft term [45,71] (see Appendix B); one gets

$$\left\{ \text{Solutions } A_\pm \iff \lambda_0 = \sqrt{2} \lambda_8 = \pm \sqrt{\frac{3}{2}} \lambda_3 \right\}, \tag{2}$$

which reduces the actual parameter freedom of the kinetic breaking from three to only one.

One thus should note that the Kroll conditions tightly couple the breaking in the BHLS₂ Lagrangian of the original U(3) symmetry to SU(3)×U(1) and a particular isospin-breaking piece (via $\lambda_3 \neq 0$); it also leads to $F_\pi^\tau(s=0) = 1 - \lambda_3^2/2$.

The ± 1 factor in Eq. (2) is propagated below as d_\pm ; thus, A_+ corresponds to d_+ and A_- to d_- . The non-anomalous pieces $\mathcal{L}_{\eta'\pi^\pm}$ and $\mathcal{L}_{\eta\pi^\pm}$ of the BHLS₂ Lagrangian acquire simplified expressions compared to [21]:

$$\begin{cases} \mathcal{L}_{\pi^0\pi^\pm} = \frac{iag}{2} (1 + \Sigma_V) \left(1 - \frac{\lambda_0^2}{3} \right) \left[\rho^- \cdot \pi^+ \overleftrightarrow{\partial} \pi^0 - \rho^+ \cdot \pi^- \overleftrightarrow{\partial} \pi^0 \right] \\ \mathcal{L}_{\eta\pi^\pm} = -\frac{iag}{2} [1 + \Sigma_V] \left[\epsilon - \frac{A_\pm}{2} \sin \delta_P \right] \left[\rho^- \cdot \pi^+ \overleftrightarrow{\partial} \eta - \rho^+ \cdot \pi^- \overleftrightarrow{\partial} \eta \right] \\ \mathcal{L}_{\eta'\pi^\pm} = -\frac{iag}{2} [1 + \Sigma_V] \left[\epsilon' + \frac{A_\pm}{2} \cos \delta_P \right] \left[\rho^- \cdot \pi^+ \overleftrightarrow{\partial} \eta' - \rho^+ \cdot \pi^- \overleftrightarrow{\partial} \eta' \right] \end{cases} \tag{3}$$

⁶ The polynomials addressed here are process-dependent and also appear in the Omnès representation of the pion form-factor-related $\pi\pi$ production in e^+e^- annihilation [67–69].

where

$$A_\pm = \Delta_A + d_\pm \lambda_0^2, \tag{4}$$

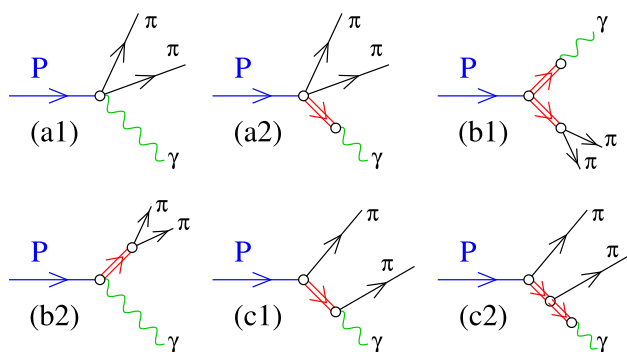


Fig. 1 The classes of tree diagrams. P stands for either of η and η' . In diagrams a and b , the double lines stand for the neutral vector mesons (subject to mixing). In the c diagrams, the intermediate vector meson is ρ^\pm , whereas the external one is neutral. The pions are charged. The vanishing of the AVP couplings (see text) implies that diagrams (b2) and (c1) do not contribute to the decay amplitudes

exhibiting the Bando–Kugo–Yamawaki (BKY) Δ_A , and δ_P is defined by

$$\begin{aligned} \cos \delta_P &= \frac{1}{\sqrt{3}} \left[\sin \theta_P + \sqrt{2} \cos \theta_P \right], \\ \sin \delta_P &= -\frac{1}{\sqrt{3}} \left[\cos \theta_P - \sqrt{2} \sin \theta_P \right] \end{aligned} \tag{5}$$

in terms of θ_P , the third mixing angle [72] which is one of the BHLS₂ fit parameters. It was shown in [21] that the BKY parameter Σ_V can be dropped out without any loss in generality.

One should note that if $\mathcal{L}_{\pi^0\pi^\pm}$ is the leading order, both $\mathcal{L}_{\eta\pi^\pm}$ and $\mathcal{L}_{\eta'\pi^\pm}$ are manifestly $\mathcal{O}(\delta)$, i.e., first order in breakings. Finally, it is worthwhile to recall that terms of order $\mathcal{O}(\delta^2)$ or higher in amplitudes are discarded.

4 The $\eta/\eta' \rightarrow \pi^- \pi^+ \gamma$ decays in the BHLS₂ framework

The amplitudes for the $\eta/\eta' \rightarrow \pi^- \pi^+ \gamma$ decays a priori involve the $APPP$, $VPPP$, and AVP sectors of the full BHLS₂ Lagrangian [20,21]. The interaction terms involved are displayed in Appendices C and D in terms of the *physical* pseudoscalar fields and *ideal* vector fields which should be replaced by their physical partners following the method developed in [20]. The $V - \gamma$ transition couplings can be found in [20], Appendix A, and the relevant non-anomalous VPP couplings have been displayed for convenience in Sect. 3 just above.

The classes of diagrams involved a priori in the η/η' decays to $\pi^- \pi^+ \gamma$ are displayed in Fig. 1. Namely, diagram (a1) illustrates the $APPP$ interaction, whereas diagram (a2) sketches the $VPPP$ contributions with $V - \gamma$ transitions ($V = \rho^0, \omega, \phi$) provided by the non-anomalous BHLS₂

Lagrangian ([20], Appendix A). These two kinds of diagrams are generally named box anomaly terms.

Diagram (b1) sketches the diagram class involving VVP couplings; these diagrams provide the major contribution to the η/η' dipion spectra. As one assumes that $c_3 = c_4$ thanks to former works [18], all contributions involving AVP couplings, such as those depicted in Figs. (b2) and (c1), identically vanish. Finally, the (c2) diagram class illustrates the diagrams reflecting the two possible choices for the $\pi^\pm \pi^\mp$ pair, each involving an intermediate ρ^\pm exchange.

In the following, for the η and η' decays, the non-resonant (a1) and (a2) contributions are gathered into the T^{NR} partial amplitude, whereas the (b1) and (c2) resonant contributions are given by the T^{R1} and T^{R2} terms, respectively.

5 The $\eta \rightarrow \pi^+ \pi^- \gamma$ amplitude within BHLS₂

As three kinds of diagrams contribute, the full $T(\eta)$ amplitude for the $\eta \rightarrow \pi^+ \pi^- \gamma$ decay is written as

$$T(\eta) = T^{NR}(\eta) + T^{R1}(\eta) + T^{R2}(\eta), \tag{6}$$

and they include the common tensor object

$$F = \epsilon^{\mu\nu\alpha\beta} \epsilon_\mu(\gamma, q) q_\nu P_\alpha^- P_\beta^+ \tag{7}$$

typical of the anomalous Lagrangian piece expressions; F exhibits the obvious momentum notations. This factor is understood in the $T(\eta/\eta')$ amplitude expressions here and below to lighten the writing; it is restored in the final expressions involving the differential decay widths.

As already stated, the first term in the expansion (6) gathers the non-resonant ($APPP/VPPP$) contributions, whereas the second and third terms collect the resonant contributions of different structures generated via the VVP Lagrangian as noted in the section just above.

The T_{NR}^η term can be written ($A_\pm = \Delta_A + d_\pm \lambda_0^2$):

$$\begin{aligned} T^{NR}(\eta) &= -\frac{ie}{4\pi^2 f_\pi^3} \left[1 - \frac{3c_3}{2} \right] g_{\eta\pi^+\pi^-\gamma} \text{ with} \\ g_{\eta\pi^+\pi^-\gamma} &= \epsilon + \left\{ 1 - \frac{A_\pm}{2} - \frac{3\lambda_0^2}{4} \right\} \sin \delta_P. \end{aligned} \tag{8}$$

It is worth noting that (i) the dependence upon $c_1 - c_2$ drops out when summing up the $APPP$ and $VPPP$ contributions, and (ii) if one cancels out the symmetry-breaking contributions, $T^{NR}(\eta)$ remains nonzero and corresponds to the WZW term [58,59].

On the other hand, the $T^{R1}(\eta)$ contributions to the $T(\eta)$ amplitude can be written ($m^2 = ag^2 f_\pi^2$):

$$\begin{cases} T^{R1}(\eta) = c_3 \frac{iem^2}{8\pi^2 f_\pi^3} \left[\frac{T_\rho^0(\eta)}{D_\rho(s)} + \frac{T_\omega^0(\eta)}{D_\omega(s)} + \frac{T_\phi^0(\eta)}{D_\phi(s)} \right] \\ T_\rho^0(\eta) = \epsilon + \frac{2\beta(s)}{z_A} \cos \delta_P \\ \quad + 3 \left[1 - \frac{3\lambda_0^2}{4} - \frac{A_\pm}{6} + \frac{\alpha(s)}{3} + 2\xi_3 \right] \sin \delta_P \\ T_\phi^0(\eta) = - \left[\frac{2\beta(s)}{z_A} \right] \cos \delta_P \\ T_\omega^0(\eta) = - \alpha(s) \sin \delta_P \end{cases}, \quad (9)$$

where $D_\rho(s)$, $D_\omega(s)$, and $D_\phi(s)$ are the indicated inverse vector meson propagators; they are parameterized as defined in Section 9 of [20]. Equation (9) displays the dependency upon the angles $\alpha(s)$ and $\beta(s)$ defining the dynamical vector meson mixing (see Appendix A.4) and upon the parameter defined by the kinetic breaking mechanism (see Appendix A.5) once the Kroll conditions [66] are applied. It is worth remarking that ρ^0 is the only resonant contribution which survives when symmetry-breaking terms are turned off. Moreover, the ω and ϕ contributions are outside the phase space actually available in the η decay.

$T^{R2}(\eta)$, the second resonant contribution, is produced by the non-anomalous $\rho^\pm \eta \pi^\mp$ coupling purely generated by our breaking procedures (see Eq. (3)) and by the $\omega \rho^\pm \pi^\mp$ term of the $VV\eta$ Lagrangian piece (see Appendix C.2.2). Setting $s_{\pm 0} = (p_\pm + q)^2$, q = photon momentum,

we write:

$$\begin{cases} T^{R2}(\eta) = c_3 \frac{iem^2}{8\pi^2 f_\pi^3} T_\rho^\pm(\eta) \left[\frac{1}{D_\pm(s_{+0})} + \frac{1}{D_\pm(s_{-0})} \right] \\ T_\rho^\pm(\eta) = \epsilon - \frac{A_\pm}{2} \sin \delta_P. \end{cases} \quad (10)$$

The $D_\pm(s_{\pm 0})$ s denote the inverse ρ^\pm propagators; the T^{R2} contribution, a pure product of symmetry breakings, cancels out when all symmetries are restored. Finally, the three amplitude pieces just defined depend on the HLS parameter c_3 .

At the chiral point

$$s = s_{+0} = s_{-0} = 0,$$

the vector meson inverse propagators fulfill [20] $D_V(0) = -m_V^2$, with

$$\begin{aligned} m_{\rho^\pm}^2 &= m^2, \quad m_{\rho_0}^2 = m^2(1 + \xi_3)^2, \quad m_\omega^2 = m^2(1 + \xi_0)^2, \\ m_\phi^2 &= m^2 z_V(1 + \xi_0)^2, \end{aligned} \quad (11)$$

where $m^2 = ag^2 f_\pi^2$, the conditions $\alpha(0) = \beta(0) = 0$ being exactly fulfilled.

6 The $\eta' \rightarrow \pi^+ \pi^- \gamma$ amplitude within BHLS₂

The decay process $\eta' \rightarrow \pi^+ \pi^- \gamma$ undergoes a quite similar treatment to those performed for the $\eta \rightarrow \pi^+ \pi^- \gamma$ decay in the preceding section, and so one will avoid duplicating the comments on the η' amplitude already stated on the η amplitude. The three different kinds of contributions to the η' decay amplitude are

$$T(\eta') = T^{NR}(\eta') + T^{R1}(\eta') + T^{R2}(\eta'). \quad (12)$$

The first term, which gathers the $APPP$ and $VPPP$ contributions to the full amplitude $T\eta'$, is given by

$$\begin{aligned} T^{NR}(\eta') &= -\frac{ie}{4\pi^2 f_\pi^3} \left[1 - \frac{3c_3}{2} \right] g_{\eta' \pi^+ \pi^- \gamma} \quad \text{with} \\ g_{\eta' \pi^+ \pi^- \gamma} &= \epsilon' - \left\{ 1 - \frac{A_\pm}{2} - \frac{3\lambda_0^2}{4} \right\} \cos \delta_P \end{aligned} \quad (13)$$

and does not depend on $c_1 - c_2$. On the other hand, the contributions gathered in $T^{R1}(\eta')$ are given by

$$\begin{cases} T^{R1}(\eta') = c_3 \frac{iem^2}{8\pi^2 f_\pi^3} \left[\frac{T_\rho^0(\eta')}{D_\rho(s)} + \frac{T_\omega^0(\eta')}{D_\omega(s)} + \frac{T_\phi^0(\eta')}{D_\phi(s)} \right] \\ T_\rho^0(\eta') = \epsilon' + \frac{2\beta(s)}{z_A} \sin \delta_P \\ \quad - 3 \left[1 - \frac{3\lambda_0^2}{4} - \frac{A_\pm}{6} + \frac{\alpha(s)}{3} + 2\xi_3 \right] \cos \delta_P \\ T_\phi^0(\eta') = - \left[\frac{2\beta(s)}{z_A} \right] \sin \delta_P \\ T_\omega^0(\eta') = + \alpha(s) \cos \delta_P \end{cases} \quad (14)$$

where, as for the η decay, only the ρ^0 term is $\mathcal{O}(\delta^0 = 1)$ in breakings. Finally,

$$\begin{cases} T^{R2}(\eta') = c_3 \frac{iem^2}{8\pi^2 f_\pi^3} T_\rho^\pm(\eta') \left[\frac{1}{D_\pm(s_{+0})} + \frac{1}{D_\pm(s_{-0})} \right], \\ T_\rho^\pm(\eta') = \epsilon' + \frac{A_\pm}{2} \cos \delta_P \end{cases}, \quad (15)$$

which is purely $\mathcal{O}(\delta)$.

The ω contribution in the η' decay must be visible in high-statistics data samples (like [61]) and is worth comparing with its line shape in the $e^+e^- \rightarrow \pi^+\pi^-$ annihilation. Regarding the ϕ contribution, it is somewhat outside the allowed phase space—by $\simeq 60$ MeV. Finally, the influence of higher vector mesons, especially the first radial excitation ρ' , is outside the HLS scope; global fit properties may reveal their actual influence w.r.t. the broken HLS context.

7 BHLS₂ and the WZW box anomalies

Traditionally, the amplitudes associated with the box anomalies are derived from the Wess–Zumino–Witten (WZW)

Lagrangian [58,59]:

$$\mathcal{L}_{WZW} = -i \frac{N_c e}{3\pi^2 f_\pi^3} \epsilon^{\mu\nu\alpha\beta} A_\mu \text{Tr} [Q \partial_\nu P \partial_\alpha P \partial_\beta P], \quad (16)$$

where P is the bare pseudoscalar meson $U(3)$ matrix. This Lagrangian differs from the anomalous $APPP$ Lagrangian piece of the HLS model (see Eq. (86)) by the factor

$$\left[1 - \frac{3}{4}(c_1 - c_2 + c_4) \right]$$

The BHLS₂ η/η' decay amplitudes just defined are expected to coincide with their WZW analogs at the chiral point, where the HLS c_i 's dependencies of the decay amplitudes should cancel out. Their expressions at the chiral point ($s = s_{+0} = s_{-0} = 0$) are given by⁷:

$$\begin{cases} T(\eta) = -\frac{ie}{4\pi^2 f_\pi^3} \left[\epsilon + \left\{ 1 - \frac{A_\pm}{2} - \frac{3\lambda_0^2}{4} \right\} \sin \delta_P \right], \\ T(\eta') = -\frac{ie}{4\pi^2 f_\pi^3} \left[\epsilon' - \left\{ 1 - \frac{A_\pm}{2} - \frac{3\lambda_0^2}{4} \right\} \cos \delta_P \right], \\ T(\pi^0) = +\frac{ie}{4\pi^2 f_\pi^3} \\ \quad \times \left[\left\{ 1 - \frac{A_\pm}{2} - \frac{\lambda_0^2}{3} \right\} - \epsilon \sin \delta_P + \epsilon' \cos \delta_P \right] \end{cases} \quad (17)$$

and coincide with those which can be directly derived from the WZW Lagrangian equation (16) after applying the breaking procedures mentioned in the Appendices.

8 η/η' radiative decays: the BHLS₂ dipion mass spectra

The amplitudes $T(\eta)$ and $T(\eta')$ allow us to describe—within the full EBHLS₂ framework [20,21]—the dipion mass spectra observed in the η/η' radiative decays have been derived in Sects. 5 and 6, respectively; both should be multiplied by the function⁸ $F(s, s_{0+})$ (see Eq. (7)). The differential decay widths can be written as

$$\frac{d^2\Gamma_X}{ds ds_{0+}} = \frac{1}{(2\pi)^3} \frac{1}{32M_X^3} |T_X F(s, s_{0+})|^2, \quad X = \eta, \eta' \quad (18)$$

in terms of, respectively, s , the $(\pi^+\pi^-)$, and s_{0+} , the $(\pi^+\gamma)$ pair invariant masses squared of the η/η' decay products. The accessible invariant mass spectra being functions of only s ,

⁷ The coupling $\pi^0\pi^+\pi^-\gamma$ is involved in the $e^+e^- \rightarrow \pi^0\pi^+\pi^-$ annihilation [20,21].

⁸ The notations $\epsilon(\gamma, q)$ for the photon polarization vector, p^\pm , and q for the pion and photon momenta are generally understood.

this expression should be integrated over s_{0+} :

$$\frac{d\Gamma_X}{ds} = \frac{1}{(2\pi)^3} \frac{1}{32M_X^3} \int_{s_{min}}^{s_{max}} |T_X F(s, s_{0+})|^2 ds_{0+}, \quad (19)$$

$$X = \eta, \eta'$$

where

$$s_{min/max} = \frac{M_X^2 + 2m_\pi^2 - s}{2} \mp p_\pi \frac{M_X^2 - s}{\sqrt{s}} \quad \text{and} \quad (20)$$

$$p_\pi = \frac{\sqrt{s - 4m_\pi^2}}{2}.$$

Both amplitudes $T(\eta)$ and $T(\eta')$, generically referred to as T_X , can be written

$$T_X(s, s_{0+}) = R_X(s) + C_X G(s, s_{0+}) \quad \text{with} \quad (21)$$

$$G(s, s_{0+}) = \frac{1}{D_\rho(s_{0-})} + \frac{1}{D_\rho(s_{0+})},$$

having defined $s_{0\pm} = (q + p^\pm)^2$ related by

$$s_{0-} - m_\pi^2 = (M_X^2 - s) - (s_{0+} - m_\pi^2).$$

$R_X(s)$ collects the contributions previously named $T^{NR}(X)$ and $T^{R1}(X)$ and is (by far) the dominant term, whereas⁹ $T^{R2}(X) = C_X G(s, s_{0+})$ is only $\mathcal{O}(\delta)$ in breakings.

On the other hand, the $[F(s, s_{0+})]^2$ factor in Eq. (19) is

$$[F(s, s_{0+})]^2 = \frac{s}{4}(s_{0+} - m_\pi^2)(s_{0-} - m_\pi^2) - \frac{m_\pi^2}{4}(M_X^2 - s)^2 \quad (22)$$

and can be solely expressed in terms of s and s_{0+} to perform the integration shown in Eq. (19). This leads to *pre-defining* within the fitting code the following integrals:

$$\begin{aligned} I_1(s) &= \int_{s_{min}}^{s_{max}} |F(s, s_{0+})|^2 ds_{0+}, \\ I_2(s) &= \int_{s_{min}}^{s_{max}} |F(s, s_{0+})|^2 |G(s, s_{0+})|^2 ds_{0+} \\ I_3(s) &= \int_{s_{min}}^{s_{max}} |F(s, s_{0+})|^2 \text{Re} [G(s, s_{0+})] ds_{0+}, \\ I_4(s) &= \int_{s_{min}}^{s_{max}} |F(s, s_{0+})|^2 \text{Im} [G(s, s_{0+})] ds_{0+}. \end{aligned} \quad (23)$$

Actually, $I_1(s)$ can be integrated in closed form:

$$I_1(s) = \frac{(M_X^2 - s)^3}{3} \frac{p_\pi^3}{\sqrt{s}} \quad (24)$$

with p_π given in Eq. (20). The three other functions should be integrated numerically within the iterative procedure context

⁹ C_X can be read off the relevant expressions for $T^{R2}(X)$ given in Sects. 5 and 6.

already running to address the $e^+e^- \rightarrow \pi^+\pi^-\pi^0$ annihilation data within the BHLS [18] or BHLS₂ [20,21] frameworks. One then gets

$$\frac{d\Gamma_X}{ds} = \frac{1}{(2\pi)^3} \frac{1}{32M_X^3} \times \left[|R_X(s)|^2 I_1(s) + C_X^2 I_2(s) + 2C_X (\text{Re} [R_X(s) I_3(s) + \text{Im} [R_X(s) I_4(s)]] \right] \tag{25}$$

In the BHLS₂ approach, only leading-order terms in the breaking parameters $\mathcal{O}(\delta)$ (as the C_X term) are addressed, and then terms of order $\mathcal{O}(\delta^2)$ —like the C_X^2 contribution—can be neglected.

The $I_1(s)$ term in Eq. (25) can be rewritten, for subsequent use in the text:

$$\begin{aligned} \frac{d\tilde{\Gamma}_X}{ds} &= \Gamma_0(s) |R_X(s)|^2, \text{ with} \\ \Gamma_0(s) &= \frac{s(M_X^2 - s)^3 [\sigma_\pi(s)]^3}{3 \cdot 2^{11} \pi^3 M_X^3} \text{ and} \\ \sigma_\pi(s) &= \sqrt{1 - \frac{4m_\pi^2}{s}}. \end{aligned} \tag{26}$$

9 Pion form factor in the η/η' radiative decays

The study in [73], also referred to hereafter as SHKMW, has placed a valuable emphasis on the connection between the pion vector form factor $F_\pi(s)$ —as it comes out of the $e^+e^- \rightarrow \pi^+\pi^-$ annihilation process—and the dipion spectra from the $\eta/\eta' \rightarrow \pi^+\pi^-\gamma$ radiative decays. Further works have followed (see, for instance, [74–78] for further reference), generally motivated by a better understanding of the η and η' meson properties regarding their contributions to the light-by-light (LbL) fraction of the muon anomalous magnetic moment a_μ .

(i) It is worthwhile to briefly outline how this connection is established [73]. The pion vector form factor $F_\pi(s)$ and the P -wave $\pi^+\pi^-$ scattering amplitude $T_{\pi\pi}(s)$ are related by

$$\text{Im} [F_\pi(s)] = \sigma_\pi(s) [T_{\pi\pi}(s)]^* F_\pi(s) \Theta(s - 4m_\pi^2), \tag{27}$$

valid along the energy region where the $\pi^+\pi^-$ scattering is *elastic*; $\sigma_\pi(s)$ has been defined just above. Therefore, in this energy region, the pion vector form factor $F_\pi(s)$ and the elastic scattering amplitude $T_{\pi\pi}(s)$ should carry equal phases. The Heaviside function indicates that $F_\pi(s)$ is real below the 2π threshold; the first *significant* inelastic channel being $\omega\pi$, the validity range of Eq. (27) practically extends up to $\simeq 922$ MeV, substantially above the η mass and slightly below the η' mass (by only 36 MeV). Stated another way, the

phase-equality property holds over almost the whole HLS energy range of validity ($\sqrt{s} \leq 1.05$ GeV).

On the other hand, assuming the $\pi^+\pi^-$ scattering is elastic for all $s \geq 4m_\pi^2$, the P -wave amplitude $T_{\pi\pi}(s)$ is written as

$$T_{\pi\pi}(s) = \frac{\sin \delta_{11}(s) e^{i\delta_{11}(s)}}{\sigma_\pi(s)} \tag{28}$$

in terms of the P -wave phase shift $\delta_{11}(s)$, and the solution to Eq. (27) can be expressed in terms of the Omnès function $\Omega(s)$ by

$$\begin{aligned} F_\pi(s) &= K(s)\Omega(s), \text{ where} \\ \Omega(s) &= \exp \left(\frac{s}{\pi} \int_{4m_\pi^2}^\infty \frac{dz}{z} \frac{\delta_{11}(z)}{z - s - i\epsilon} \right), \end{aligned} \tag{29}$$

$K(s)$ being some appropriate real analytic function, required to be free of singularities over the physical region $s \geq 4m_\pi^2$. This expression intends to factor out the non-perturbative contribution to $F_\pi(s)$ contained in the $\Omega(s)$ function, and so the remaining part $K(s)$ (perturbative in the sense of ChPT, at low energy) is expected to behave smoothly and can be well approximated by a polynomial [73] along our region of interest (up to $\simeq m_\phi$). This smooth function $K(s)$ is process-dependent, whereas $\Omega(s)$, being determined by the $\pi\pi$ final state re-scattering phase shifts, represents a more universal part of the vector form factor. It is shown in [74] that a first-degree polynomial $K(s) = 1 + \alpha_\Omega s$ allows us to reach a nice (linear) correlation up to $s \simeq 1$ GeV² between the dipion spectrum from Belle [34] and the $\Omega(s)$ functions derived from the phase shift data from [79], see also [67–69]; a value $\alpha_\Omega \simeq 0.1$ GeV⁻² can be inferred from Figure 1 in [74]. The deterioration of the linear behavior above $s \simeq m_\phi^2$ is actually not unexpected because of rising inelasticities and of the high-mass vector meson influence.

(ii) Assuming the pion pair emerging from the η/η' radiative decays is purely isospin 1 and a P -wave [61,64], its amplitude should carry the same analytic properties as $F_\pi(s)$, i.e., they may only differ by a real analytic function, free of right-hand side singularities. Reference [73] thus proposes to write the differential dipion spectra as

$$\frac{d\bar{\Gamma}_X}{ds} = \Gamma_0(s) |A_X P_X(s) F_\pi(s)|^2, \quad (X = \eta/\eta'), \tag{30}$$

where $\Gamma_0(s)$ has already been defined in Eq. (26), and the A_X 's being appropriate normalization constants. The $P_X(s)$ functions ($P_X(0) = 1$) are remaining correction factors specific to the η and η' radiative decays (in the present case, but are more generally dependent on higher inelastic effects existing at any $\pi\pi$ production vertex), which could both be analyzed within the extended ChPT context [43,45] (see also [80]) and are free of right-hand side singularities.

As just argued regarding the pion vector form factor and its $K(s)$ factor, the $P_X(s)$ functions should satisfac-

torily be approximated by low-degree polynomials [73]. This is what is shown by the bottom panel in Figure 1 of [74], which moreover indicates that $P_\eta(s) = P_{\eta'}(s)$ should likely hold. Of course, procedures to complement this approach by symmetry-breaking effects also have to be invoked, prominently—but not only—the $\rho^0 - \omega$ mixing for the η' decay process.

(iii) The issue is now to relate $d\bar{\Gamma}_X$ (Eq. (30)) and $d\tilde{\Gamma}_X$ (Eq. (26)) within the HLS framework *when no breaking is at work*. Equivalently, this turns out to check whether the $R_X(s)$'s and $F_\pi(s)$ (can) carry the same phase in this case.

Let us consider the pion vector form factor $F_\pi(s)$ as given in [20], discarding terms of order $\mathcal{O}(\delta)$ or higher in breaking parameters; keeping only tree contributions (loop corrections, like the $\rho^0 - \gamma$ transition amplitude, are counted as $\mathcal{O}(\delta)$), and dropping out the \mathcal{L}_{p^4} contributions, one derives ($m^2 = ag^2 f_\pi^2$, the unbroken ρ^0 HK mass.):

$$F_\pi(s) = \left(1 - \frac{a}{2} \left[1 + \frac{m^2}{D_\rho(s)}\right]\right) + \mathcal{O}(\delta). \tag{31}$$

Similarly, the $R_X(s)$ functions in Eq. (26) reduce to

$$\begin{aligned} R_\eta &= -\frac{ie \sin \delta_P}{4\pi^2 f_\pi^3} \left(1 - \frac{3}{2}c_3 \left[1 + \frac{m^2}{D_\rho(s)}\right]\right), \\ R_{\eta'} &= +\frac{ie \cos \delta_P}{4\pi^2 f_\pi^3} \left(1 - \frac{3}{2}c_3 \left[1 + \frac{m^2}{D_\rho(s)}\right]\right) \end{aligned} \tag{32}$$

up to terms of $\mathcal{O}(\delta)$ in breaking parameters.

These equations lead us to define a *no-breaking* reference by requiring the following:

(1) Holding of the vector meson dominance assumption, which implies $a \equiv a_{VMD} = 2$ within the generic HLS model [12, 16], it is worth recalling here (see Section 2 in [21] for details) that the HLS parameter a is not reachable by fit, once the BKY breaking (see Appendix A.2) is at work. Indeed, all Lagrangian terms of interest for our physics depend on the product $a' = a(1 + \Sigma_V)$ and not on each of these parameters separately; therefore, one can freely fix $a = 2$, and then the term $\delta a = a_{VMD} \Sigma_V$ is clearly¹⁰ $\mathcal{O}(\delta)$.

(2) The universality of the ρ phase implies that $R_\eta(s)$, $R_{\eta'}(s)$, and $F_\pi(s)$ share the same phase, and therefore it requires the existence of an “unbroken” value for c_3 . Indeed, imposing $c_3^{ref} = 2/3$ alongside $a_{VMD} = 2$, one can derive a satisfactory no-breaking reference as

$$\begin{aligned} F_\pi(s) &= -\frac{m^2}{D_\rho(s)}, \quad R_\eta = +\frac{ie \sin \delta_P}{4\pi^2 f_\pi^3} \frac{m^2}{D_\rho(s)}, \\ R_{\eta'} &= -\frac{ie \cos \delta_P}{4\pi^2 f_\pi^3} \frac{m^2}{D_\rho(s)}, \end{aligned} \tag{33}$$

¹⁰ In the course of the fitting procedure, it is appropriate to either choose to fit a , fixing $\Sigma_V = 0$ or fix a and fit Σ_V ; we chose the first option.

which should be complemented by $\mathcal{O}(\delta)$ contributions to account for real data.

The issue becomes whether the values returned for a and c_3 from fits to the (real) data differ little enough from a_{VMD} and c_3^{ref} that their differences can be considered $\mathcal{O}(\delta)$ effects. For this purpose, one can refer to the latest published BHLS₂ standard fit results collected in Table 10 of [21], in particular, one finds the following:

- $a = 1.766 \pm 0.001$, which shows a deviation $\delta a = 0.244$ from $a_{VMD} = 2$ corresponding to having $\Sigma_V = 0.122$; and
- $c_3 = 0.742 \pm 0.003$ which deviates by $\delta c_3 = 0.076$ from $c_3^{ref} = 0.667$,

focusing on the favored solution A_- [21] to the Kroll conditions (see Sect. 3)—the A_+ solution actually provides similar values. Thus, δa and δc_3 look small enough to be viewed as departures from, respectively, a_{VMD} and c_3^{ref} and treated as $\mathcal{O}(\delta)$ corrections, on the same footing as the manifest breaking parameters. To our knowledge, it is the first time that an identified physics condition can propose a constraint on one of the FKTUY [13] parameters, namely¹¹ c_3 .

(iv) From what has been just argued, it is clear that within the BHLS₂ context, the $\eta/\eta' \rightarrow \pi^+\pi^-\gamma$ decay amplitudes $T_X(s)$ reported in Sects. 5 and 6 above can actually be written as

$$T_X(s) = B_X F_\pi(s) + \mathcal{O}(\delta), \quad X = \eta/\eta', \tag{34}$$

the B_X 's being definite constants depending on the breaking parameters. $F_\pi(s)$ contains already manifest breaking terms like the ω and ϕ signals with, however, different weights from their analogs in the $T_X(s)$ amplitudes.¹²

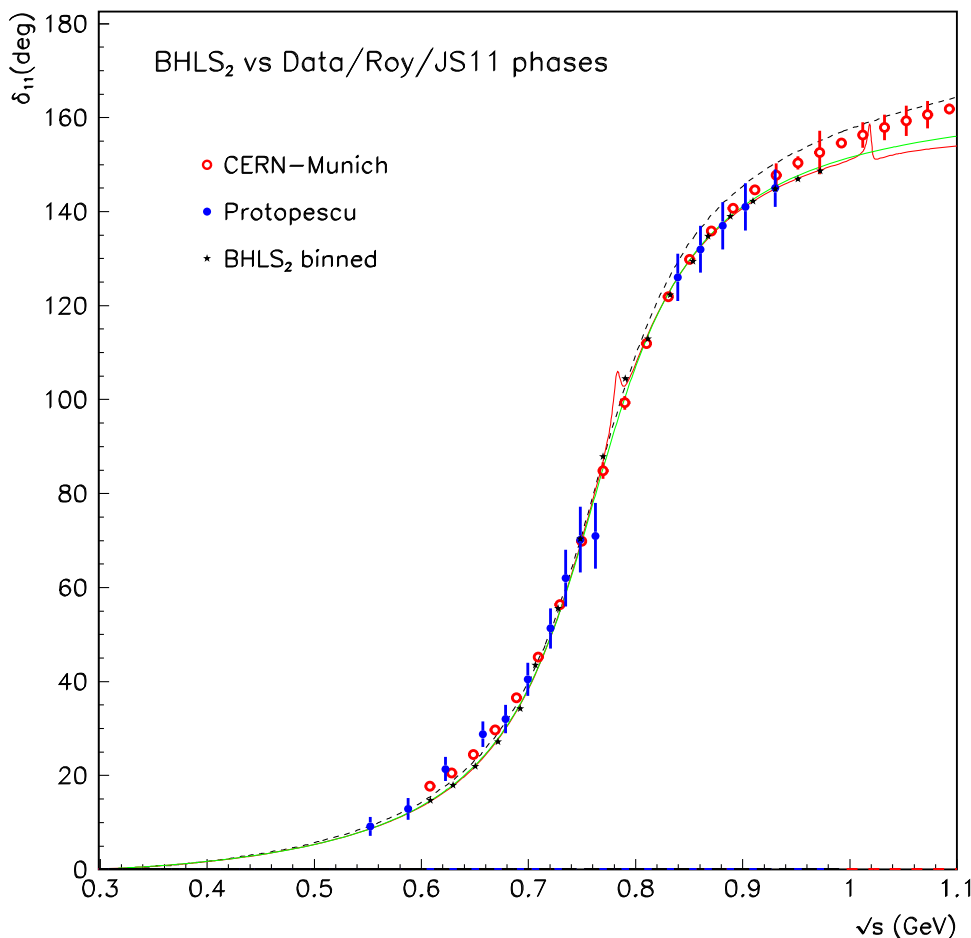
On the other hand, as shown in [20], yielding a fair description of the data samples for $|F_\pi(s)|$ (see Figure 2 and Table 3 in [20]), BHLS₂ also leads to a fair account of the phase shift $\delta_{11}(s)$ over its whole range of validity *without involving any phase shift data sample in its derivation*. This is illustrated by¹³ Fig. 2, which reflects the fair accord reached by the BHLS₂ prediction with the phase derived from the Roy equations [83] or the pion form factor phase of Ref. [84] on the one hand, and the experimental phase shift data from [81, 82] on the other hand. Moreover, the same BHLS₂ spectrum was smeared over 10 MeV bins, to mimic the CERN-Munich spectrum [81] (black star symbols), to clearly show

¹¹ Actually, another condition comes out from the data in analyses performed within the HLS context: $c_3 = c_4$.

¹² For instance, BHLS₂ predicts that the coupling ratio $\omega\pi\pi$ to $\rho^0\pi\pi$ is three times smaller in the η' radiative decay than in the pion vector form factor.

¹³ Reprinted from Figure 10 in [20].

Fig. 2 The δ_{11} phase shift plotted as a function of \sqrt{s} . Besides the data points of [81,82], the dashed black curve is the solution to the Roy equations [83], the green full line shows the phase reconstructed in [84], and the red full line shows the BHLS₂ phase shift exhibiting the ω and ϕ signals. The black stars show the smeared BHLS₂ spectrum (e.g., the red curve)



that the ω and ϕ signals cannot be manifestly observed in the existing data.

All this leads to the conclusion that the SHKMW modification [73] shown in Eq. (30),

$$F_\pi(s) \rightarrow A_X P_X(s) F_\pi(s),$$

also applies in the global BHLS₂ context. In this case, this turns out to perform the change

$$T_X(s) \implies H_X P_X(s) T_X(s)$$

when using the amplitudes constructed in Sects. 5 and 6. Our notations are connected with those in Ref. [73] by writing the following¹⁴:

$$A_X = A_X^0 H_X, \quad H_X \equiv 1 + \delta_X, \quad X = \eta, \eta' \tag{35}$$

as the A_X^0 factors are already accounted for in the T_X amplitudes derived from the BHLS₂ Lagrangian as shown below.

Then the global character of the BHLS₂ fitting context¹⁵ ensures that the non-perturbative effects are suitably accounted for as reflected by Fig. 2.

From now on, the $P_X(s)$ functions are chosen polynomials of the lowest possible degree consistent with a satisfactory fitting. Being beyond the BHLS₂ scope, these functions are supplemented within the fit procedure by performing the change

$$T_X(s) \implies H_X P_X(s) T_X(s), \quad \text{with } P_X(0) = 1, \quad X = \eta, \eta' \tag{36}$$

in Eq. (25) above. Practically, each term in the right-hand side of Eq. (25) gets a factor of $|H_X P_X(s)|^2$, the coefficients of which have to be derived by the global fit, where the $[C_X]^2$ term can be discarded as it is manifestly $\mathcal{O}(\delta^2)$.

¹⁴ Actually, to be formally exact, Ref. [73] writes $A = A_0(1 + \delta)$ for the η meson decay, and $A' = A'_0(1 + \delta')$ for the η' meson, as can be read around their Relations (9).

¹⁵ In this case, its reference set of data samples \mathcal{H}_R [20,21], which already includes most of the existing pion form factor data samples, will be supplemented with the η/η' dipion spectra.

10 Fits of the η/η' radiative decay spectra within BHLS₂

The reference set of data samples \mathcal{H}_R included within the BHLS₂ framework has been presented several times and recently in [20, 21]; it covers the six e^+e^- annihilation channels to $\pi^+\pi^-$, K^+K^- , $K_L K_S$, $\pi^+\pi^-\pi^0$, $\pi^0\gamma$, and $\eta\gamma$, some more decay widths (in particular $\pi^0/\eta/\eta' \rightarrow \gamma\gamma$), and, finally, the dipion mass spectrum in the $\tau \rightarrow \pi\pi\nu$ decay. These represent already the largest set of data (altogether 1366 data points) successfully submitted to a global fit, as reflected by Table 9 in [21]; they will not be discussed here further. It is nevertheless relevant to remember that \mathcal{H}_R encompasses almost all existing samples except for the recent CMD-3 dipion data as already argued in footnote 4, the KLOE08 [40], BaBar [27, 28], and the recent SND [85] dipion spectra because of the strong tension they exhibit with respect to the rest of the (more than 60) \mathcal{H}_R samples. This issue has been thoroughly reexamined in [21].

The present study aims to include also the dipion spectra measured in the η/η' radiative decays within the global BHLS₂ framework. However, it is certainly cautious to avoid using *simultaneously* the η/η' dipion spectra and the $\pi^+\pi^-\pi^0$ annihilation data within global fits as long as a specific study has not assessed some clear statement about process-specific corrections (accounted for by a polynomial) in the latter channel¹⁶ and data.

For the general model dependence of BHLS/BHLS₂ models and also the magnitude of possible biases in the fits, we rely on our previous studies (notably [20] and also [89]) that demonstrated those are limited with respect to other sources of systematics.

More recently, our 2022 publication [21] (see, for example, Section 11.3 therein), which extends BHLS₂ and introduced a comprehensive treatment of the $[\pi^0, \eta, \eta']$ system, includes also a detailed discussion on model dependencies in the new framework (partly by studying model variants)¹⁷. This 2022 study, which in fact prefigured and allowed the present work, reached again the conclusion that model dependence exists but is not a strong source of systematics. It confirmed previous studies which explored systematic differences between BHLS and BHLS₂ types of models (and various subvariants); see, for example, Section 17 in [20].

¹⁶ The studies [86, 87] and the fit results reported in [20, 21] may as well indicate that polynomial corrections are small or effectively absorbed in the parameter values returned by the fits. Anyway, this certainly deserves a devoted work [88].

¹⁷ On the a_μ determination question, since for this purpose we always end using well-constrained, high global and partial probability fits that use *all* the experimental data, this guarantees the fitted pion form factor is very close to the data, and hence that the a_μ is also very close to the integral model-independent determinations from other groups. This remains true when swapping KLOE and BaBar $\pi\pi$ data in the fit.

We explore below eventual new sources of (model and others) systematics, again by studying the fit result dependencies when using model and hypotheses variations (in particular, but not only, for the P_X polynomials), in the same spirit as in our previous works.

It is worthwhile to stress that all the published dipion spectra of the $\eta/\eta' \rightarrow \pi^+\pi^-\gamma$ decays carry an arbitrary normalization; so *they only provide the spectrum line shapes measured by the various experiments*. It follows from this peculiarity that they allow fitting *only* the $P_X(s)$ polynomials, and they are totally insensitive to the H_X parameter values; this issue will be addressed by performing global fits where the corresponding partial widths [taken from the ‘‘Review of Particle Properties’’ (RPP) [70]] are also considered inside the fitting procedure.

10.1 Available dipion spectra from the $\eta/\eta' \rightarrow \pi^+\pi^-\gamma$ decays

Measurements of the dipion spectrum in the $\eta' \rightarrow \pi^+\pi^-\gamma$ decay started long ago, as early as 1975 [49], and several experiments have collected samples of various (but low) statistics motivated by the $\simeq 20$ -MeV shift reported for the ρ^0 peak location compared to its value in $e^+e^- \rightarrow \pi^+\pi^-$ annihilations: JADE [50], CELLO [51], TASSO [52], PLUTO [53], TPC-2 γ [54], ARGUS [55], and Lepton F [56]; the Crystal Barrel Collaboration published in 1997 is the most precise spectrum [57], carrying 7400 events. The breakthrough has come from the BESIII Collaboration [61] which published a 970,000-event spectrum in 2017.

The formerly collected samples have been examined, and their behavior is briefly reported below. Dealing with the uncertainty information provided with these η' samples is generally straightforward, except for the BESIII dipion spectrum [61], for which a spectrum for the energy resolution is provided. It is accounted for by replacing within the minimization procedure the genuine model function value by that of its convolution with the resolution function, assuming the provided resolutions are the standard deviations of Gaussians; the net effect of the BESIII energy resolution information deserves to be shown (see below).

The BESIII data [65] are provided as two 112-data-point spectra, the former giving the numbers of η' event candidates in 10 MeV bins (N_{evt}^i), the latter the estimated numbers of background events (N_{bkg}^i) within the same bins. One has provided our global fitting code with the $N_{signal}^i = N_{evt}^i - N_{bkg}^i$ spectrum; we have assumed the original distributions to be Poissonian and fully correlated by attributing to N_{signal}^i an uncertainty $\sigma_i = \sqrt{N_{evt}^i} + \sqrt{N_{bkg}^i}$; it is shown below that these specific assumptions allow a fair dealing with the BESIII spectrum [61].

On the other hand, the reported dipion spectrum observed in the parent $\eta \rightarrow \pi^+\pi^-\gamma$ decay has undergone much less measurement. Besides former spectra¹⁸ from Layter et al. [62] and Gormley et al. [63], WASA-at-COSY reported for a 14,000-event spectrum [64], whereas the KLOE/KLOE2 Collaboration has collected a 205,000-event spectrum [65]; it should be noted that the WASA dipion spectrum is given with only statistical errors.

It is worth stressing again that the normalization of all these spectra being arbitrary, the theoretical (absolute) distribution scales provided by the BHLS₂ Lagrangian are lost when normalizing to the specific scale of each data set when fitting; stated otherwise, these data samples only allow addressing the fit of the $P_X(s)$ functions ($X = \eta, \eta'$) and *not* of the H_X constants which are canceled out when normalizing the model functions to the experimental spectra.

10.2 η/η' experimental spectra: fits in isolation

The first exercise is thus to explore the degree issue for the $P_X(s)$ polynomials and so does not need to deal with complications due to keeping the constant H_X within the fit procedure. Therefore, fits have been performed, supplementing the reference data set of samples \mathcal{H}_R by either of the experimental η' or η spectra. In this section, one only reports on using the A_- BHLS₂ variant,¹⁹ [21] which will be our working BHLS₂ version.

Regarding the $P_{\eta'}(s)$ polynomial, the results given in the Table just below²⁰ focus on only the BESIII η' sample (112 data points) [61]; indeed, because of their statistics, all the other η' dipion spectra, including the Crystal Barrel one [57], do not exhibit any clear sensitivity to the $P_{\eta'}$ degree and may easily accommodate $P_{\eta'} \equiv 1$:

$P_{\eta'}(s)$ degree	1	2	3
$\chi^2_{BESIII} (N = 112)$	160	99	98
$\chi^2_{TOT} (N = 1187)$	1167	1097	1096
Probability	44.7%	90.6%	90.8%

This clearly points out that, thanks to the statistics reached by the BESIII Collaboration, the first degree for $P_{\eta'}(s)$ can be excluded ($\langle \chi^2 \rangle = 1.43$), and the third degree is obviously useless.

¹⁸ The numerical content of these spectra can only be derived from the paper figures.

¹⁹ Nevertheless, the most relevant results obtained using the A_+ BHLS₂ variant are summarized in the following subsections.

²⁰ The fits which provide these results have been performed with our reference set amputated from the $e^+e^- \rightarrow \pi^+\pi^-\pi^0$ annihilation data. The number of BESIII data points and the total number of fitted data points are given by the N values within parentheses.

Regarding the η data, complementing \mathcal{H}_R with the KLOE/KLOE2 sample (59 data points) [65] alone or together with the WASA sample (37 data points) [64], the picture returned by the fits is much less conclusive, as a first-degree $P_\eta(s)$ provides²¹ $\chi^2(KLOE/KLOE2) = 55$ and $\chi^2(WASA) = 45$, and a second-degree $P_\eta(s)$ yields $\chi^2(KLOE) = 51$ and $\chi^2(WASA) = 51$ with similar fit probabilities, both at the 90% level, as just above. The choice of a minimal degree has been preferred for $P_\eta(s)$.

Therefore, in the following, when different, the polynomials $P_\eta(s)$ and $P_{\eta'}(s)$ are definitely chosen, the former first degree, the latter second degree. The polynomial coefficients returned by the global fits performed with the A_- BHLS₂ variant are discussed below and given in Table 2.

It is worthwhile noting that the degradation of the fit quality observed when assuming a first-degree $P_{\eta'}(s)$ is essentially carried by the the BESIII $\eta'(s)$ data sample itself, with a quite marginal influence on the standard channels of the BHLS₂ framework and on the η dipion spectra. This emphasizes the robustness of the BHLS₂ Lagrangian.

In order to lighten the forthcoming discussion, let us comment on the formerly collected (η/η') dipion spectra listed in the subsection above, which have also been analyzed within the BHLS₂ context; they quite generally yield stable χ^2/N values. Some of them return large χ^2/N values from the global fit procedure, namely, those from TPC-2 γ (69/13), LEPTON-F (45/20), and Layter et al. (60/15). Most of these former samples, however, achieve reasonable χ^2/N values, typically 8/12 (TASSO), 15/21 (CELLO), 23/18 (PLUTO), 20/15 (ARGUS), 11/17 (CRYSTAL BARREL²²), and 13/14 (Gormley et al.) but have a quite negligible impact on the issues examined in the present study. Therefore, one focuses on the high-statistics data samples from BESIII and KLOE/KLOE2; the case for the WASA data set may be nevertheless commented on²¹.

10.3 The η/η' experimental spectra: analysis within the BHLS₂ context

Table 1 collects the relevant fit quality information derived when running global fits within the A_- BHLS₂ variant. The first data column gives the fit information in a global fit performed²³ by discarding the η/η' to provide the BHLS₂ reference fit pattern; using the full \mathcal{H}_R , one would have found the numbers given in the last data column of Table 9 in [21]. The second and third data columns report on the fits performed

²¹ Note that $\chi^2(WASA)$ is always overestimated because of incomplete reported experimental error information.

²² Its data point at 812.5 MeV, soon identified as an outlier, being dropped out; see footnote 21 in [90].

²³ The $e^+e^- \rightarrow \pi^+\pi^-\pi^0$ annihilation data are switched off.

by including η/η' dipion spectra within the fit data set \mathcal{H}_R under the conditions indicated in the top line of Table 1.

The fit information concerning the $e^+e^- \rightarrow \pi^+\pi^-$ annihilation data collected in scan mode (with different detectors at the various Novosibirsk facilities) is displayed in the first data line (the exact sample content behind the wording NSK is explained in [21], for instance). The line KLOE stands for the merging of the KLOE10 [24] and KLOE12 [25] data samples. The spacelike vector pion form factor data merges the NA7 and Fermilab samples [91, 92].

Taking the first data column of Table 1 as a reference, one can clearly conclude that the fit quality obtained when using the η/η' dipion spectra is unchanged and fairly good. Indeed, the χ^2 increase of the NSK set of scan data samples is obviously negligible, and those of the ISR data collected under the name KLOE and spacelike data are unchanged. The description of the data samples in the other channels from BHLS₂ (not shown) is also unchanged.²⁴

Regarding the triangle anomaly sector, the χ^2 information for the $\pi^0/\eta/\eta' \rightarrow \gamma\gamma$ decays are

$$\left\{ \begin{array}{l} \text{BHLS}_2 \text{ } A_- \text{ variant with } P_\eta(s) \neq P_{\eta'}(s) : (\chi_{\pi^0}^2, \chi_\eta^2, \chi_{\eta'}^2) \\ \quad = (1.08, 0.01, 3, 33) \\ \text{BHLS}_2 \text{ } A_- \text{ variant with } P_\eta(s) \equiv P_{\eta'}(s) : (\chi_{\pi^0}^2, \chi_\eta^2, \chi_{\eta'}^2) \\ \quad = (0.73, 0.03, 4.77). \end{array} \right. \quad (37)$$

Thus, the RPP width [70] for $\pi^0 \rightarrow \gamma\gamma$ is reproduced at the $(0.9 \div 1) \sigma$ level, and the one for $\eta \rightarrow \gamma\gamma$ is reconstructed at nearly its RPP value; the width for $\eta' \rightarrow \gamma\gamma$ is found in the range $(1.8 \div 2.2) \sigma$, somewhat larger but still acceptable.

On the other hand, and more importantly, comparing the second and third data columns of Table 1 obviously substantiates the SHKMW conjecture [73] about the uniqueness of the $P_X(s)$ function, e.g., $P_\eta(s) \equiv P_{\eta'}(s)$. One may also note the slight improvement generated by having stated $P_\eta(s) \equiv P_{\eta'}(s)$; this should be due to having provided its curvature to $P_\eta(s)$ which in turn lessens the (already marginal) tension between the KLOE/KLOE2 and BESIII data samples.

Before going on with solely using the A_- variant of the BHLS₂ Lagrangian, it is worthwhile reporting on its A_+ variant behavior. Let us limit this to reporting on the A_+ variant best fit performed assuming $P_\eta(s) \equiv P_{\eta'}(s)$ is of the second degree; one obtains $\chi^2/N(\text{BESIII}) = 110/112$, and the η dipion spectrum from the KLOE/KLOE2 Collaboration yields this ratio at 54/59; for its part, the unfitted WASA sample yields 49/37. The global fit probability is 51.5% only,

to be compared to 90.6 % for the global fit performed under the A_- variant reported in Table 1.

This drop in probability is noticeable, and the cause deserves to be identified; indeed, the $\chi^2(\text{BESIII})$ increases by “only” eight units, whereas the χ^2 for the η dipion spectra are almost unchanged compared to Table 1. Moreover, the usual BHLS₂ channels also benefit from χ^2 's comparable in magnitude to their A_- analogs. Surprisingly, the single place where the disagreement blows up is in the $\gamma\gamma$ decays, as

$$(\chi_{\pi^0}^2, \chi_\eta^2, \chi_{\eta'}^2) = (29.92, 0.34, 0.08);$$

e.g., the $\pi^0 \rightarrow \gamma\gamma$ partial width is at more than 5σ from its accepted value [70], which is by far too large to be acceptable. Indeed, this implies that the A_+ fit central value for the $\pi^0 \rightarrow \gamma\gamma$ partial width is reconstructed at 70% of its present RPP value [70]; this should be brought into balance with the A_- variant, which yields this partial width reconstructed 5% larger than the expected value (7.8 eV).

Therefore, the A_+ variant unexpectedly exhibits a strong tension between the triangle and box anomaly sectors of the BHLS₂ Lagrangian, whereas the A_- variant behaves smoothly in both sectors. Therefore, from now on, we will focus on the A_- variant of BHLS₂ which becomes our reference model; results derived using the A_+ variant are no longer reported *except when explicitly stated*.

Regarding the η spectra, Fig. 3 shows an almost perfect account of the KLOE/KLOE2 spectrum: the BHLS₂ spectrum matches the dipion spectrum from KLOE/KLOE2 [65] on the whole energy range, except for a marginal issue in the 0.45-GeV energy region. Even if its χ^2 value is acceptable, the WASA spectrum [64] may look somewhat distorted with respect to its KLOE/KLOE2 partner, clearly favored by BHLS₂ expectations²¹.

Regarding the η' spectrum, Fig. 4 shows a noticeably fair accord between the BHLS₂ modeling and the BESIII spectrum [61] all along the energy range. The vertical green dotted lines locate the ω mass and thus the $\rho - \omega$ drop-off region, otherwise magnified in the inset. Here, one can observe the effect of convoluting the BHLS₂ model function with energy resolution Gaussians as provided by the BESIII Collaboration: It does perfectly what it is supposed to do, i.e., soften the drop-off to its right line shape with, moreover, a noticeable accuracy. On the rest of the spectrum, the convoluted curve and the underlying model curve superimpose on each other within the thickness of the curves. One should also state that no tension in the $\rho - \omega$ drop-off region is observed in the fits with any of the other dipion spectra submitted to the fit.

²⁴ Their variations are always χ^2 unit fractions.

Table 1 Fit properties of selected dipion data sample sets using the A_- BHLS₂ variant. The fit reported in the first data column is free of η/η' dipion influence. The second data column corresponds to fitting with independent $P_\eta(s)$ and $P_{\eta'}(s)$, whereas the third data column reports on the fit where $P_\eta(s) \equiv P_{\eta'}(s)$ has been imposed. The χ^2/N_{pts} value for the WASA sample, fitted or not, is in the range²¹ (44 – 47) for 37 data points

χ^2/N_{pts} fit configuration (A_-)	No η/η' spectra	$P_\eta(s) \neq P_{\eta'}(s)$	$P_\eta(s) \equiv P_{\eta'}(s)$
NSK $\pi^+\pi^-$ (127)	137/127	139/127	140/127
KLOE $\pi^+\pi^-$ (135)	141/135	140/135	140/135
Spacelike $\pi^+\pi^-$ (59)	64/59	64/59	64/59
η' BESIII (112)	×	100/112	102/112
η KLOE/KLOE2 (59)	×	57/59	55/59
Total χ^2/N_{pts}	995/1075	1156/1246	1154/1246
Fit probability (%)	88.6	89.7	90.6

Fig. 3 The dipion invariant mass spectrum in the $\eta \rightarrow \pi^+\pi^-\gamma$ decay. The blue data points are the KLOE/KLOE2 spectrum, and the green ones display the WASA spectrum. The red curve is the BHLS₂ fit leaving free the $P_\eta(s)$ polynomial. Vertical units are arbitrary

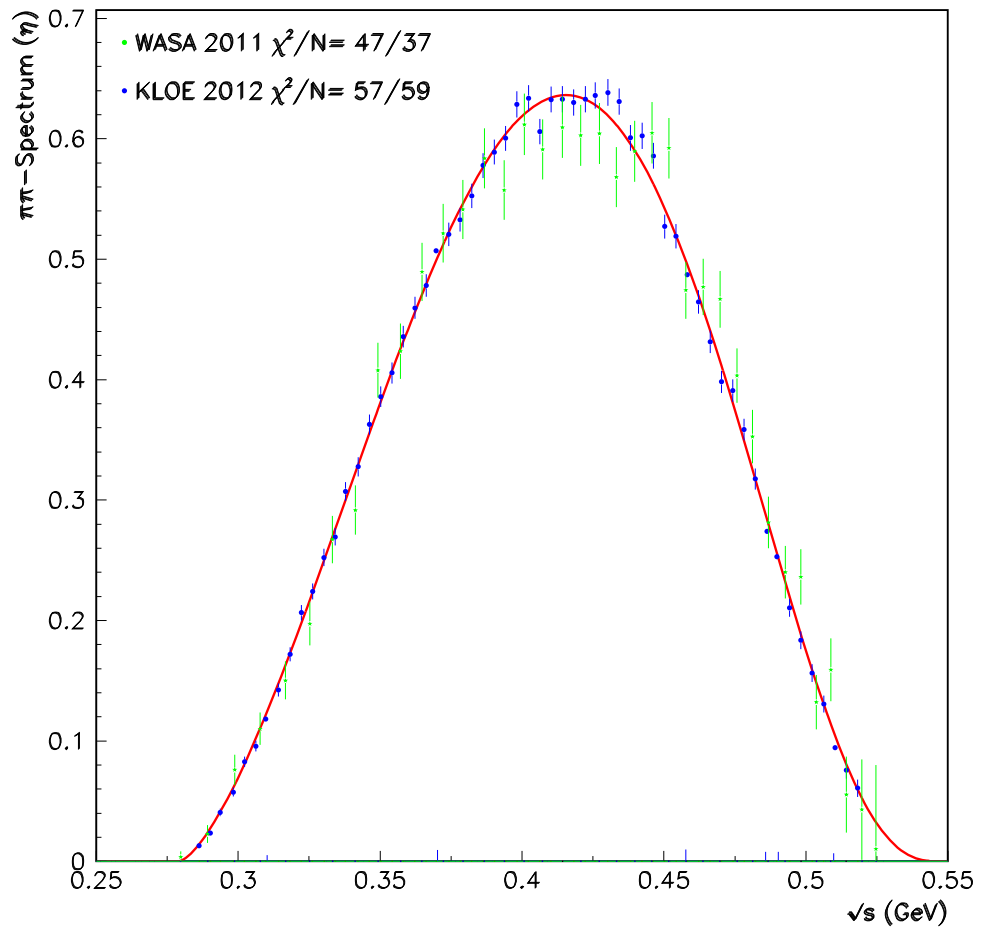
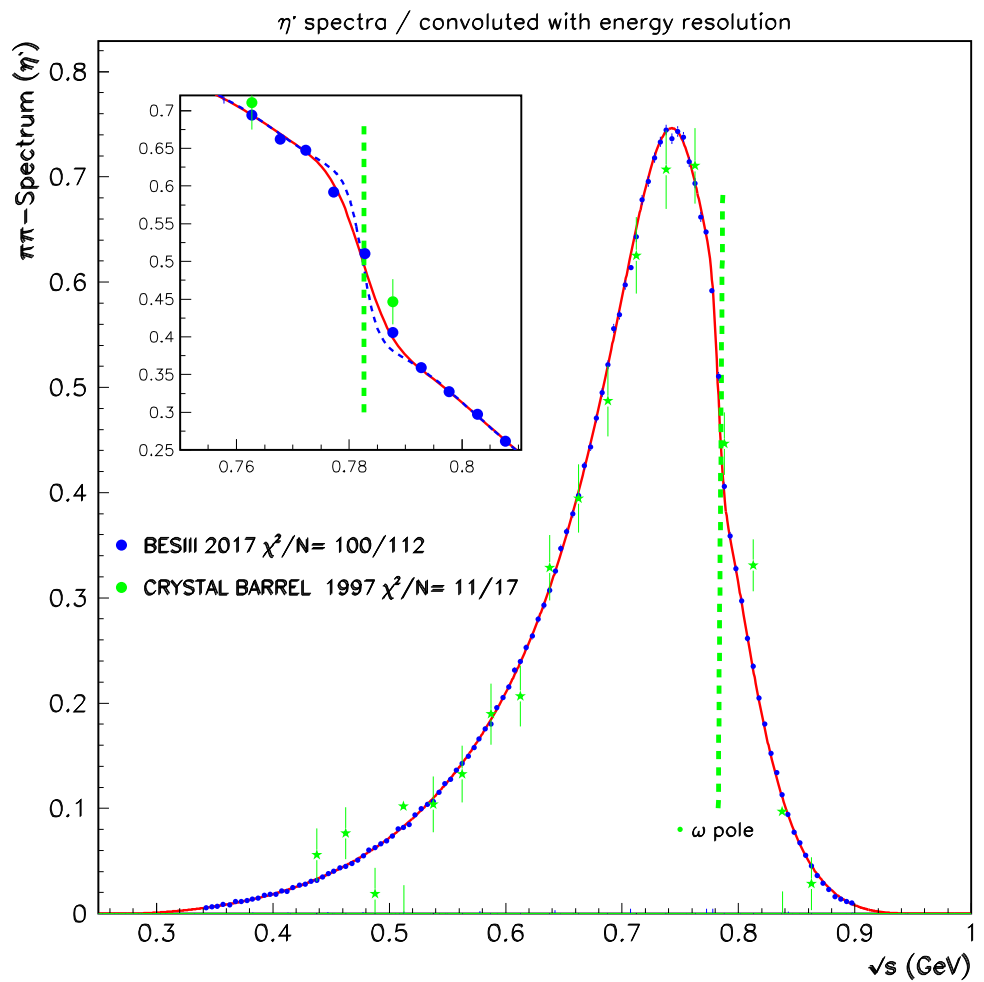


Fig. 4 The dipion invariant mass spectrum in the $\eta' \rightarrow \pi^+\pi^-\gamma$ decay. The blue data points are the BESIII spectrum, and the green ones are those from Crystal Barrel. The red curve is the fit function, i.e., the convolution of the BHLS₂ model function with the energy resolution function assumed Gaussian; the blue curve is the underlying BHLS₂ model function itself. Both curves superimpose over the whole energy range except for the $\rho - \omega$ drop-off region. Vertical units are arbitrary



It is useful to consider the spectra²⁵

$$\overline{P}_X(s) = \left[\frac{d\Gamma_{exp}(s)}{d\sqrt{s}} / \frac{d\Gamma_{theor}(s)}{d\sqrt{s}} \right]_X P_X(s), \quad X = \eta, \eta' \tag{38}$$

to illustrate the behavior of the $P_X(s)$ polynomials under the two assumptions discussed above. As the bracketed term in Eq. (38) fluctuates around 1 and reflects the experimental uncertainty spectrum, the $\overline{P}_X(s)$ spectrum looks to be an appropriate experimentally based evaluation of its corresponding model function $P_X(s)$.

Figure 5 displays the $\overline{P}_{\eta'}(s)$ and $\overline{P}_\eta(s)$ spectra defined just above for the BESIII, KLOE/KLOE2, and WASA spectra together with their model partners $P_{\eta'}(s)$ (second degree) and $P_\eta(s)$ (first degree). As could be inferred from the fit properties shown in Table 1, $P_{\eta'}(s)$ (the red dashed curve in the inset) is also a good evaluation for $\overline{P}_\eta(s)$.

Figure 6 also displays the $\overline{P}_{\eta'}(s)$ and $\overline{P}_\eta(s)$ spectra for the BESIII, KLOE/KLOE2, and WASA data samples but

together with their common model fit function denoted $P_X(s)$, a second-degree polynomial. As reflected by the fit information mentioned in the body of the figure, a fair simultaneous parameterization of the η and η' dipion spectra is reached by only supplying the BHLS₂ model amplitudes with a single second-degree polynomial $P_X(s)$ fulfilling $P_X(0) = 1$.

10.4 $P_X(s)$: BHLS₂ fit results versus others

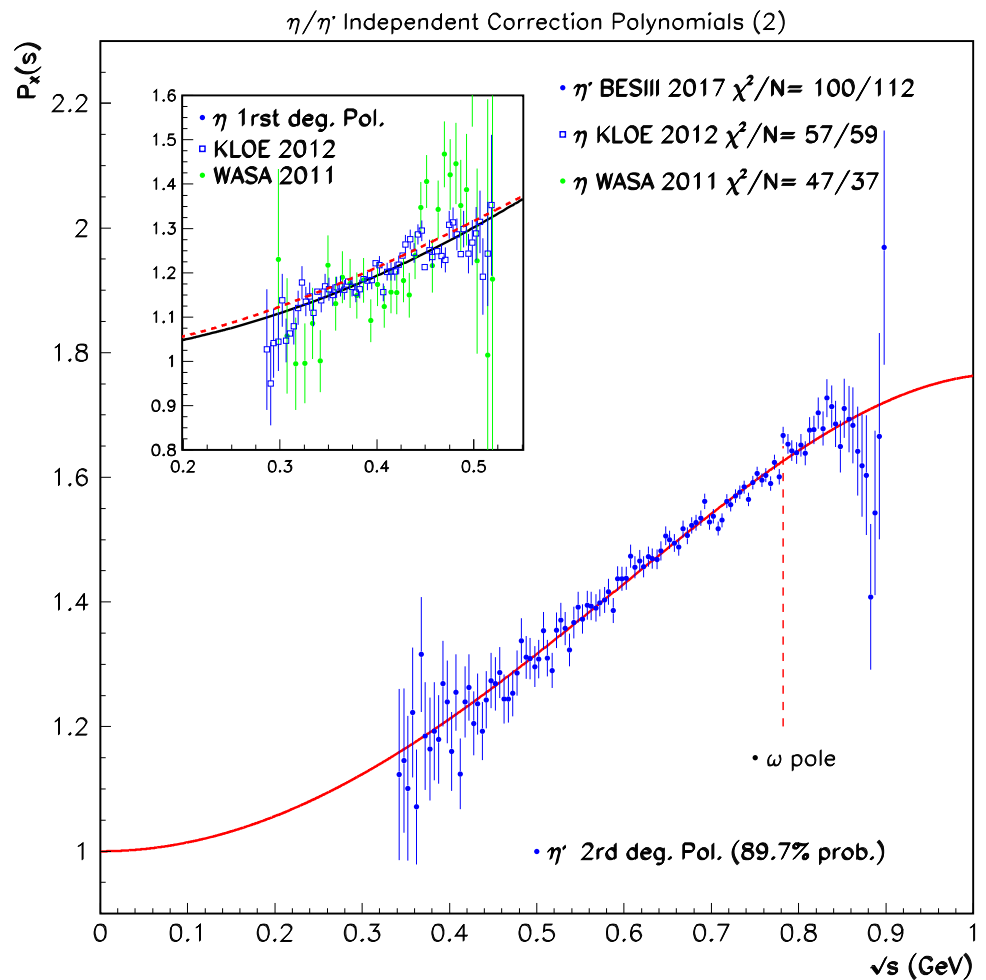
The top bunch in Table 2 displays the values returned for the polynomial coefficients of

$$P_\eta(s) = 1 + \alpha_1 s \quad \text{and} \quad P_{\eta'}(s) = 1 + \alpha'_1 s + \alpha'_2 s^2. \tag{39}$$

When using the same polynomial for the η and η' spectra, it is second degree and denoted $P_X(s)$. It should be noted that the coefficients for $P_{\eta'}(s)$ (second data column) and $P_X(s)$ (third data column) carry numerical values close to each other, i.e., at $\simeq 1 \sigma$ from each other for both the

²⁵ It is, of course, understood that when dealing with the BESIII η' dipion sample, $d\Gamma_{theor}(s)/d\sqrt{s}$ is actually the convolution product of the model function with the BESIII energy resolution function.

Fig. 5 The $\bar{P}_{\eta'}(s)$ and, in the inset, the $\bar{P}_{\eta}(s)$ spectra (Eq. 38). The full red curve and full black curve superimposed to, respectively, $\bar{P}_{\eta'}(s)$ and $\bar{P}_{\eta}(s)$ are, respectively, the $P_{\eta'}(s)$ and $P_{\eta}(s)$ polynomials returned by the fits. The dashed red curve in the inset is also $P_{\eta'}(s)$ but superimposed to the $\bar{P}_{\eta}(s)$ spectrum. Some pieces of fit information are also displayed



first- and second-degree coefficients.²⁶ In the case of having a (single) common function $P_X(s)$, the covariance is $\langle \delta\alpha'_1 \delta\alpha'_2 \rangle = -0.746$.

Regarding the systematics: In the BHLS₂ approach, the statistical and systematic uncertainties provided by the experiments together with their spectra are carefully embodied within the fitting code without any modification; so our reported uncertainties automatically merge both kinds of experimental errors.

On the other hand, the last two data lines in Table 2 clearly illustrate that $\delta a = a - 2$ and $\delta c_3 = c_3 - 2/3$ remain consistent with expectations, i.e., they can be regarded as $\mathbf{O}(\delta)$ breaking parameters. The other fit parameter values are given in Table 3 displayed in the next Sect. 10.5; they are scrutinized in order to detect eventual hints of effects spoiling the BHLS₂ model fit in the 3π channel—where correction polynomials are *not* implemented by now.

- (j) Regarding the $P_{\eta}(s)$ polynomial, it is worth comparing our numerical value for α_1 with those available in the literature. The first published evaluation (GeV^{-2}) of α_1 is the one from the WASA-at-COSY Collaboration ($\alpha_1 = 1.89 \pm 0.25_{stat} \pm 0.59_{syst} \pm 0.02_{th}$) [64], soon followed by $\alpha_1 = 1.96 \pm 0.27_{fit} \pm 0.02_{F\pi}$ [73]; more precise evaluations have been proposed²⁷ since (GeV^{-2}):

$$\begin{aligned} \alpha_1 &= 1.32 \pm 0.08_{stat} \pm 0.10_{syst} \pm 0.02_{th} [65], \\ \alpha_1 &= 1.52 \pm 0.06_{stat} [75]. \end{aligned} \tag{40}$$

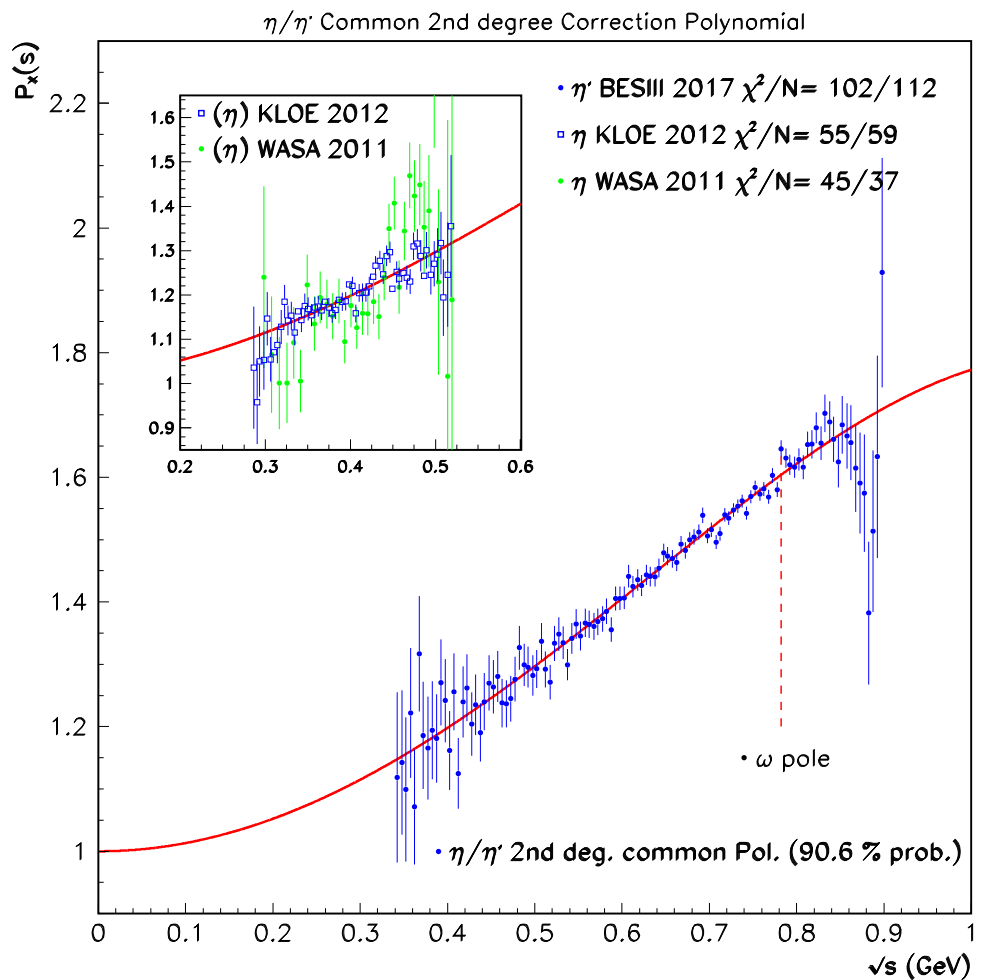
Our own evaluation (reported in Table 2) is in good agreement ($\simeq 1\sigma$) with the KLOE/KLOE2 Collaboration result [65].

- (jj) As far as we know, there are only two evaluations for the $P_{\eta'}(s)$ coefficients available in the literature, the former from the BESIII Collaboration [61]:

²⁶ It might be useful to provide, for completeness, the covariances when $P_{\eta}(s) \neq P_{\eta'}(s)$: Using obvious notations, they are $\langle \delta\alpha_1 \delta\alpha'_1 \rangle = -0.005$, $\langle \delta\alpha_1 \delta\alpha'_2 \rangle = -0.026$, and $\langle \delta\alpha'_1 \delta\alpha'_2 \rangle = -0.812$.

²⁷ Introducing a possible a_2 exchange, Ref. [75] also reports for a smaller value ($\alpha_1 = 1.42 \pm 0.06_{stat}$).

Fig. 6 The $\overline{P}_{\eta'}(s)$ and, in the inset, the $\overline{P}_{\eta}(s)$ spectra (Eq. 38). The full red curve is superimposed on the $\overline{P}_{\eta'}(s)$ and, in the inset, the $\overline{P}_{\eta}(s)$ spectra is their common fit function $P_X(s)$. The ω pole location is indicated. Some pieces of fit information are also displayed



BESIII :

$$\left\{ \begin{array}{l} \alpha'_1(\text{ GeV}^{-2}) = 0.992 \pm 0.039_{stat} \\ \quad \quad \quad \pm 0.067_{syst} \pm 0.163_{th} \\ \alpha'_2(\text{ GeV}^{-4}) = -0.523 \pm 0.039_{stat} \\ \quad \quad \quad \pm 0.066_{syst} \pm 0.181_{th} \end{array} \right\}, \quad (41)$$

the latter from the HHHK group [77, 78]. In their Addendum Table 1, the HHHK group proposes quite comparable values (we quote here the values obtained by the likelihood method):

$$\text{HHHK} : \left\{ \begin{array}{l} \alpha'_1 = 0.714 \pm 0.055 \text{ GeV}^{-2}, \\ \alpha'_2 = -0.412 \pm 0.055 \text{ GeV}^{-4} \end{array} \right\}. \quad (42)$$

Here, one is faced with a surprising pattern: While the BESIII parameterization for $P_X(s)$ is far from the favored A_- variant reported in Table 2, it is in quite remarkable accord with the A_+ solution displayed in the last data column of Table 2; as BESIII does not deal with the intrinsic relationship between the box and the triangle anomalies,

their modeling is not influenced by the $\pi^0 \rightarrow \gamma\gamma$ partial width issue identified in Sect. 10.3 just above.

As a matter of conclusion, within the BHLS₂ framework, it has been shown that the conjecture $P_{\eta'}(s) = P_{\eta}(s)$ is a valid statement at the (high) degree of precision permitted by the spectra from the BESIII and KLOE/KLOE2 Collaborations. Moreover, Table 1 exhibits fair fit probabilities and does not reveal any noticeable tension among the dipion spectra from KLOE/KLOE2 and BESIII on the one hand and, on the other hand, the other channels embodied within the BHLS₂ fit procedure and their data, especially the dipion spectra collected in e^+e^- annihilations.²⁸

10.5 Brief analysis of the BHLS₂ parameter values

Table 3 collects the model parameter values of the BHLS₂ Lagrangian. In order to figure out the effect of the $e^+e^- \rightarrow \pi^+\pi^-\pi^0$ annihilation data on the numerical results, its first

²⁸ Let us recall that KLOE08 [40], BaBar [27, 28], and SND [85] dipion spectra have been discarded because of tensions with the \mathcal{H}_R set.

Table 2 The parameter values from the A_- BHLS₂ variant fit. The first data column reports on the fit using the usual set of data samples \mathcal{H}_R , excluding the e^+e^- annihilation to 3π data. The second and third data columns report on the fits performed on the same amputated \mathcal{H}_R

sample set, completed with the η/η' dipion spectra under the conditions indicated in the top line of the table ($P_X(s) = P_\eta(s) \equiv P_{\eta'}(s)$). The fair probability values can be emphasized. The last data column displays the fit results when using the A_+ variant

Fit parameter value	no η/η'	$P_\eta(s) \neq P_{\eta'}(s)$	$[A_-]: P_X(s)$	$[A_+]: P_X(s)$
α'_1 (GeV ⁻²)	×	1.388 ± 0.072	1.326 ± 0.053	0.953 ± 0.065
α'_2 (GeV ⁻⁴)	×	-0.607 ± 0.055	-0.553 ± 0.048	-0.511 ± 0.052
α_1 (GeV ⁻²)	×	1.169 ± 0.063	×	×
a_{HLS}	1.789 ± 0.001	1.842 ± 0.001	1.821 ± 0.001	1.830 ± 0.001
$(c_3 + c_4)/2$	0.756 ± 0.005	0.773 ± 0.005	0.772 ± 0.004	0.819 ± 0.007
Fit probability (%)	88.6	89.7	90.6	51.4

data column²⁹ displays the fit parameter values derived when they are considered, whereas the second data column provides the same information when they are excluded from the fit procedure. The third and fourth data columns report the fit results when the η/η' dipion spectra are included within the set of data samples \mathcal{H}_R amputated from the 3-pion data.

Besides providing the parameter values themselves, the issue here is to reach an educated guess about unaccounted-for effects in the fit (like P_X polynomial equivalent corrections) in the $e^+e^- \rightarrow \pi^+\pi^-\pi^0$ annihilation process: some effects in this channel could be numerically invisible or be absorbed effectively by the other model parameters.

First of all, the last line in Table 4 clearly shows that one always reaches fair accounts of the spectra submitted to the BHLS₂ global fit. Regarding the parameters collected in the top rows of the table, one observes value differences beyond the reported fit uncertainty, however, with magnitudes consistent with reasonable systematic effects.

The parameters in the lower section of the table look less well behaved. Indeed, regarding ϵ , ϵ' , and ξ_3 , the pieces of information derived by the three fits excluding the 3-pion data are consistent with each other but not with the first column result. The values for ξ_0 look confusing and may only indicate large systematics.

This is in fact reproducing an enduring situation since our previous 2022 publication [21]: there, we also noticed such variations in the isospin-breaking parameters, and also shifts from those same parameter estimations based on meson

mass differences (see Sects. 17 and 21 in [21]).³⁰ This was not the case for the mixing parameters (Section 20 in [21]) which behaved more robustly and were close to other groups' results.

While this situation is not pleasing, we have not investigated yet what could be the origin of these variations, because we feel that (a) their understanding probably needs long investigations; (b) they seem to have little influence on the central subject matter of the present work, which is focused primarily on our first shot at global fitting the η/η' data in the HLS framework, and secondarily on the implications for the a_μ estimation, especially concerning the DR-LQCD discrepancy; and (c) the limited number of independent evaluations of these isospin-breaking parameters from other groups.

Good candidate explanations for this situation could be the effect of higher-order corrections, which may in part be accounted for by the fit and absorbed in these parameters; parametric ambiguities in the fit representation of the model³¹, particularly in the case of parameters which are more indirectly connected to fitted physics observables, or only in combination with other parameters.³²

³⁰ The sign difference between ϵ and ϵ' in the last columns of Table 3 is related to the fact that we are using a fit that leaves ϵ and ϵ' free (corresponding to the A_- solution in the last column of Table 10 and 13 in [21]), which allows for unlike signs (and has the best global fit probability in [21]), compared to the so-called "Condition C" fit that constrains more ϵ and ϵ' , and indirectly forbids a different sign).

³¹ See the discussion after Eq. (32) for a simple example; it can certainly be more complex.

³² Indeed, parameters like ϵ and ϵ' enter in the mixing description with many others (see Eq. 101 and subsequent equations in [21]).

²⁹ Same as the last column in Table 10 in [21].

Table 3 Fit parameter values based on the A_{\perp} BHLS₂ variant: The first data column presents the parameter values when including the 3π spectra only, and the second column provides the same information when the 3π spectra are discarded from the fit procedure. The third and fourth data columns display the fit results when the η/η' spectra are included and the 3π spectra excluded

Fit parameter	3π spectra only	No $\eta/\eta'/3\pi$ spectra	$P_{\eta}(s) \neq P_{\eta'}(s)$	$P_{\eta}(s) \equiv P_{\eta'}(s)$
a_{HLS}	1.766 ± 0.001	1.789 ± 0.001	1.842 ± 0.001	1.821 ± 0.001
g	6.954 ± 0.002	6.334 ± 0.001	6.236 ± 0.001	6.379 ± 0.001
$(c_3 + c_4)/2$	0.742 ± 0.003	0.756 ± 0.005	0.773 ± 0.005	0.772 ± 0.004
θ_P (degrees)	-15.59 ± 0.28	-16.471 ± 0.295	-17.614 ± 0.282	-17.433 ± 0.282
λ_0	0.285 ± 0.009	0.325 ± 0.008	0.339 ± 0.008	0.334 ± 0.008
z_A	1.406 ± 0.004	1.416 ± 0.015	1.418 ± 0.005	1.415 ± 0.005
z_V	1.420 ± 0.001	1.375 ± 0.007	1.304 ± 0.001	1.320 ± 0.001
$\Delta_A \times 10^2$	12.94 ± 4.91	12.191 ± 4.05	10.173 ± 5.39	10.249 ± 5.428
$\epsilon \times 10^2$	3.62 ± 0.30	5.383 ± 0.440	6.456 ± 0.439	6.385 ± 0.411
$\epsilon' \times 10^2$	0.17 ± 0.27	-3.623 ± 0.711	-6.809 ± 0.581	-7.021 ± 0.475
$\xi_0 \times 10^2$	-6.838 ± 0.018	1.178 ± 0.018	1.119 ± 0.013	-0.538 ± 0.014
$\xi_3 \times 10^2$	1.496 ± 0.150	6.082 ± 0.153	6.070 ± 0.136	5.609 ± 0.137
Fit probability (%)	83.5	88.6	89.7	90.6

In this context, the question of the 3-pion data (see the first column), which is not used in the present work, is still open, and is complicated by the fact that no correction polynomial (*à la* P_X) was used in [21].

Nevertheless, there is no obvious hint of significant fit probability spoiling effects in the $e^+e^- \rightarrow \pi^+\pi^-\pi^0$ annihilation process, but it is clear that this process and the way it could be integrated into the fit certainly deserve more scrutiny in future work [88].

10.6 The $T^{R2}(\eta/\eta')$ terms in BHLS₂: the role of ρ^\pm exchanges

Thanks to the breaking mechanisms [20,21] which lead to the BHLS₂ Lagrangian, the derived η/η' decay amplitudes

involve ρ^\pm exchanges as depicted in Fig. 1 by the diagram classes (c1) and (c2). Relying on previous works in the HLS context which have shown that $c_3 = c_4$ is fairly well accepted by the data, this constraint is assumed; as a straightforward consequence [12,16], all diagrams involving direct AVP couplings—all proportional to $(c_3 - c_4)$ —identically vanish, and therefore, the diagram class (c1) contributions also vanish. Nevertheless, the (c2) diagram class, also $\mathcal{O}(\delta)$ in breakings, survives and participates to the decay amplitudes $T_{\eta'}$ and T_η at $\mathcal{O}(\delta)$. Such contributions are not involved in the BHLS₂ vector pion form factor $F_\pi(s)$ expression [20]; they come naturally in the derivation of the amplitude $T(\eta/\eta')$ and are not governed by an additional ad hoc parameter.

Even with $\mathcal{O}(\delta)$ corrections, the $T^{R2}(\eta/\eta')$ amplitudes play a noticeable role within the BHLS₂ context:

Table 4 Main global fit results involving the KLOE+NSK and BaBar+NSK samples collected in $e^+e^- \rightarrow \pi^+\pi^-$ annihilations. On top are displayed the parameters involved in the correction polynomi-

als (see text for details) followed by the contribution to $a_\mu(\pi\pi)$ of the $[2m_\pi, 1.0\text{-GeV}]$ energy range. The lowest bunch provides statistical information relative to the corresponding global fits

Fit parameter	NSK+KLOE	NSK+KLOE	NSK+BaBar	NSK+BaBar
	fit $P_X(s)$ only	fit $P_X(s)$ and H_X	fit $P_X(s)$ only	fit $P_X(s)$ and H_X
H_η	×	0.789 ± 0.017	×	0.797 ± 0.017
$H_{\eta'}$	×	0.671 ± 0.017	×	0.682 ± 0.015
α'_1 (GeV $^{-2}$)	1.326 ± 0.053	1.309 ± 0.055	1.248 ± 0.058	1.241 ± 0.041
α'_2 (GeV $^{-4}$)	-0.553 ± 0.048	-0.562 ± 0.047	-0.535 ± 0.048	-0.560 ± 0.037
$10^{10} \times a_\mu(\pi\pi)$	490.09 ± 0.89	490.15 ± 0.89	494.98 ± 0.91	494.85 ± 0.88
$(\chi^2/N)_{BESIII}$	102/112	99/112	101/112	99/112
$(\chi^2/N)_{KLOE/KLOE2}$	55/59	53/59	55/59	53/59
$(\chi^2/N)_{TOTAL}$	1154/1246	1149/1248	1346/1381	1341/1383
Fit probability (%)	90.6	92.3	55.9	59.4

- (i) They are necessary in order for the full amplitudes $T(\eta/\eta') = T^{NR}(\eta/\eta') + T^{R1}(\eta/\eta') + T^{R2}(\eta/\eta')$ to coincide with their analogs directly derived from the WZW Lagrangian [58,59] at the chiral point³³ $s = s_{0+} = s_{0-} = 0$.
Indeed, at the chiral point, the intensities $T^\pm(\eta/\eta')$ of the $T^{R2}(\eta/\eta')$ amplitudes defined in Sects. 5 and 6 are written as

$$\begin{aligned}
 T^{R2}(\eta) &= -\frac{iec_3}{4\pi^2 f_\pi^3} \left[\epsilon - \frac{A_\pm}{2} \sin \delta_P \right] \quad \text{and} \\
 T^{R2}(\eta') &= -\frac{iec_3}{4\pi^2 f_\pi^3} \left[\epsilon' + \frac{A_\pm}{2} \cos \delta_P \right] \quad (43)
 \end{aligned}$$

and manifestly depend on the FKTUY parameter [13] c_3 . The condition for the amplitudes $T(\eta')$ and $T(\eta)$ to coincide with those derived from the WZW Lagrangian (see Eq. 17) is that all dependencies upon the FKTUY parameters vanish at $s = s_{0+} = s_{0-} = 0$; this condition cannot be fulfilled if dropping out (artificially) the $T^{R2}(\eta/\eta')$ terms from the full-amplitude expressions $T(\eta/\eta')$.

- (ii) To identify the effects of the $T^{R2}(\eta/\eta')$ terms, fits have been performed by discarding them in the full amplitudes and rather fit using $T(\eta/\eta') = T^{NR}(\eta/\eta') + T^{R1}(\eta/\eta')$. The fits have been performed by imposing the constraint $P_\eta(s) = P_{\eta'}(s)$ and return the results collected in the next table.

$T^{R2}(\eta/\eta')$ (off/on)	off	on
χ^2_{BESIII} ($N = 112$)	122	102
$\chi^2_{KLOE/KLOE2}$ ($N = 59$)	57	55
χ^2_{TOTAL} ($N = 1246$)	1187	1154
Probability(%)	73.0	90.6

The χ^2 values indicate that $T^{R2}(\eta)$ can be safely neglected, but also that discarding $T^{R2}(\eta')$ is not safe. The $P_X(s)$ parameterization returned by the fit is

$$\left\{ \begin{aligned}
 \text{A}_-/\text{no TR2} : \alpha'_1 &= 0.437 \pm 0.039 \text{ GeV}^{-2}, \\
 \alpha'_2 &= -0.573 \pm 0.007 \text{ GeV}^{-4} \end{aligned} \right\}, \quad (44)$$

closer to the HHHK results [77,78] recalled in Expressions (42) than to those in Table 2. Therefore, the following is clear from the results collected in Table 2 and the other presented results:

- (1) The η dipion spectrum is essentially insensitive to using or discarding the T^{R2} term in its parameterization; whereas
- (2) the η' dipion spectrum parameterization is significantly degraded if its T^{R2} component is dropped out. This absence may explain the reported failure of the so-called “model-dependent” fit in [61].

In summary, one may conclude that once the polynomial correction and the $\mathcal{O}(\delta)$ T^{R2} contribution predicted by the kinetic breaking of BHLS₂ [21] are considered, the average

³³ One has previously defined $s = (p_+ + p_-)^2$, $s_{0+} = (p_+ + p_0)^2$, and $s_{0-} = (p_- + p_0)^2$.

χ^2 per data point for the η/η' dipion spectra can be considered optimum ($\langle\chi^2\rangle \simeq 1$). Thus, at the level of precision permitted by the presently available η [65] and η' [61] dipion spectra, additional contributions beyond those of the basic vector meson nonet—like the higher-mass vector mesons [61] or the $a_2(1320)$ exchanges [75]—need not be invoked.

10.7 Dealing with the absolute scale of the η/η' dipion spectra

Having determined the η/η' dipion spectrum line shapes by fitting their common factor $P_X(s)$ ($X = \eta/\eta'$), it remains to derive the value of the H_X 's ($X = \eta/\eta'$) to also have their absolute magnitudes. As already noted, the value of the H_X constants can be derived by introducing the accepted values [70] for the $\Gamma(\eta/\eta' \rightarrow \pi^+\pi^-\gamma)$ partial widths into the fitting procedure. This can be (and has been) done, and global fits have been performed in order to get the optimum values for the $\{H_\eta, H_{\eta'}, P_X(s)\}$ triplets.

However, regarding the $\eta/\eta' \rightarrow \pi^+\pi^-\gamma$ decays, each of the published dipion spectra is solely given by its line shape; concerning their normalization, they are tightly related to their partial widths. It happens that the single available “measurement” for each of these decays is the corresponding RPP piece of information [70]. In this case, as just argued, the values for H_X ($X = \eta/\eta'$) can be derived through the fitting code appropriately modified to take the partial widths into account, but also algebraically once the fit to determine the $P_X(s)$ ($X = \eta/\eta'$) function has been performed. In this case, one has, using obvious notations,

$$\begin{aligned} & [\Gamma(\eta/\eta' \rightarrow \pi^+\pi^-\gamma)]_{RPP} \\ & \equiv \int \left[\frac{d\Gamma_X(s)}{d\sqrt{s}} \right]_{exp.} d\sqrt{s} \\ & = H_X^2 \int \left[\frac{d\Gamma_X(s)}{d\sqrt{s}} \right]_{BHLS2} [P_X(s)]^2 d\sqrt{s}, \end{aligned} \quad (45)$$

the integrals being performed over the whole energy range of the $X = \eta/\eta'$ decays, and the fit values for the $\Gamma(\eta/\eta' \rightarrow \pi^+\pi^-\gamma)$ partial widths coincide with the RPP pieces of information.

Two cases have been considered regarding the specific $e^+e^- \rightarrow \pi^+\pi^-$ annihilation sample combinations involved; the first one is $\{\mathcal{H}_R + \eta/\eta'\}$, which corresponds to global fitting with the $\{\text{KLOE, NSK, BESIII, CLEO-c}\}$ combination. Correspondingly, the second case involves the $\{\text{BaBar, NSK, BESIII, CLEO-c}\}$ sample combination. The relevant fit results regarding the correction polynomials are summarized in Table 4.

The average χ^2 per point of the η and η' dipion spectra are clearly insensitive to using either of the KLOE or BaBar $e^+e^- \rightarrow \pi^+\pi^-$ annihilation data within the global fit procedure. The global fit probabilities are instead quite differ-

ent and correspond to our previous BHLS₂ results [20,21]. This insensitivity to the KLOE versus BaBar issue is well reflected by the fit results collected in the top part of Table 4: None of the P_X and H_X parameter central values are observed to differ by more than 1σ in the various fit configurations.

Similarly, as the different $P_X(s)$ parameter values derived from fitting with the various sample combinations look like statistical fluctuations, differences observed between fitting only $P_X(s)$ or the $(P_X(s) \text{ and } H_{\eta/\eta'})$ triplet look like statistical fluctuations. Moreover, defining $\delta_X = H_X - 1$ and focusing, for instance, on the KLOE+NSK combination, one gets

$$\delta_\eta = -0.211 \pm 0.017, \delta_{\eta'} = -0.329 \pm 0.017, \quad (46)$$

which corresponds to, respectively, δ and δ' as defined by Stollenwerk et al. [73], for which these authors derived the values $\delta = -0.22 \pm 0.04$ and $\delta' = -0.40 \pm 0.09$; these are clearly identical to our δ_η and $\delta_{\eta'}$, respectively. As a last remark, it should be noted that once $P_X(s)$ is determined, which implies that both $\frac{d\Gamma_X(s)}{d\sqrt{s}}$ and both BHLS₂ functions are known, Eq. (45) implies that both H_X are not free but are algebraically related.

11 η/η' decays: the muon anomalous magnetic moment

The renewed interest³⁴ in the η/η' physics is intimately related to dealing with the light-by-light contribution to the anomalous magnetic moment (AMM) of the muon. As shown above and previously in [21], the BHLS₂ approach can address accurately several topics related to the η/η' physics, and its results are supported by fair probabilities; these probabilities faithfully reflect the actual behavior of each of the data samples within the global framework, as the error information provided with it is embodied without any ad hoc enlargement inside the fitting code.

11.1 Accuracy of the $P_X(s)$ parameterization

It has been shown above that a single polynomial $P_X(s)$ allows us to address simultaneously both the $\eta/\eta' \rightarrow \pi^+\pi^-\gamma$ decays within the BHLS₂ framework and that the second degree is quite satisfactory. The $P_X(s)$ parameterizations derived using the A_\pm variants of BHLS₂ displayed in Table 2 are based on the choice of the largest set of data samples collected in almost all physics channels covering the HLS energy region (e.g., up to the $\simeq \phi$ mass region) and are consistent with each other. It was also shown that the A_- parameterization is the best favored, but nevertheless, one found it relevant to also provide the A_+ parameterization despite its (sole real) identified failure with the π^0 lifetime

³⁴ See, for instance, [74,93] and the references collected therein.

(or partial width) that A_+ reconstructs at more than 5σ from its commonly accepted value [70].

In this section, one aims to emphasize the reliability of the A_- parameterization by examining carefully how the $P_X(s)$ parameter values evolve while using the various dipion spectra collected in e^+e^- annihilations which are known to exhibit—sometimes severe—inconsistencies among themselves.

A possible fit bias in the parameterizations reported in Table 2 is the choice of the dipion data samples because of their mutual consistency; this issue is examined first. For this purpose, it is useful to define and name some sets of data samples in order to ease the reading.

Basically, the data samples²³ common to the sets of data samples presently embodied within the BHLS₂-based fit procedure are the $\{\pi^0/\eta\}\gamma, K_L K_S, K^+ K^-\}$ e^+e^- annihilation channels, the dipion spectra from the τ decay provided by the ALEPH, CLEO, and BELLE Collaborations, and the pion and kaon spacelike spectra from NA7 [91] and Fermilab [92]; let us, for clarity, name this basic set \mathcal{X}_τ .

Regarding the available $e^+e^- \rightarrow \pi^+\pi^-$ annihilation spectra, one has distinguished four groups³⁵ (two of which being, actually, a one sample “group”): (1) the scan data collected under the name NSK (see [19] for its content), (2) the KLOE (\equiv KLOE10+KLOE12) [24, 25] ISR data sample group, (3) the KLOE08 ISR sample [40], and (4) the BaBar one [27, 28]. For definiteness, the largest set of data samples found consistent with each other and referred to here and before [20, 21] as \mathcal{H}_R gathers the sets \mathcal{X}_τ , NSK, and KLOE just listed. Finally, the set of dipion spectra from the $\eta/\eta' \rightarrow \pi^+\pi^-\gamma$ decays [61, 65] is referred to as η/η' .

The four top lines in Table 5 display the coefficient values of the first- (α'_1) and second-degree (α'_2) terms of the polynomial $P_X(s)$; as indicated in its first column, the corresponding fits differ from each other only by the exact content of the $e^+e^- \rightarrow \pi^+\pi^-$ annihilation spectra sample set submitted to the minimization procedure. Whatever the fit quality, reflected by its corresponding $\langle\chi^2_{\pi\pi}\rangle$ value and its probability, the different values derived for α'_1 as for α'_2 are not distant by more than $(1 \div 2)\sigma$ from each other. It should also be remarked that the parameter values derived in the fit for $\{\mathcal{H}_R + \eta/\eta'\}$ —which includes the KLOE and NSK data sets together—are intermediate between those involving the KLOE and NSK sample sets separately. Therefore, the large spread of probabilities between the fits involving NSK and/or KLOE, and those involving BaBar or KLOE08, does

³⁵ As the more recent dipion spectra from BESIII [29, 30] and Cleo-c [31] accommodate easily any of the groups we are listing, they would not be conclusive and have been put aside for clarity; regarding the SND20 spectrum [41] deeply analyzed in our [21], we have proceeded likewise.

not produce a significant change in the determination of the common η/η' function $P_X(s)$.

The last line in Table 5 displays the $P_X(s)$ coefficients returned by a fit excluding the $e^+e^- \rightarrow \pi^+\pi^-$ annihilation spectra. The linear term coefficient α'_1 is never found distant by more than $\simeq 2\sigma$ from the other corresponding values displayed in the same Table. In contrast, the curvature coefficient α'_2 exhibits a $\simeq (4 \div 5)\sigma$ departure regarding the other reported fit values. Relying on Figs. 5 and 6, one expects the second-degree term (α'_2) to mostly affect the $\rho^0 - \omega$ energy region. This piece of information renders it interesting to compare the pion form factor *predicted* by the fit of the $\{\mathcal{X}_\tau + \eta/\eta'\}$ set³⁶ with the $e^+e^- \rightarrow \pi^+\pi^-$ annihilation data and the fit results derived when fitting the $\{\mathcal{H}_R + \eta/\eta'\}$ set. This is the purpose of Fig. 7.

Comparing the curve in both panels of Fig. 7, the overall agreement between both fits is fairly good, except for the magnitude at the very ρ^0 peak location which may look somewhat underestimated³⁷ by the η' dipion spectrum. Instead, the drop-off location and its intensity are fairly well predicted by the $\{\mathcal{X}_\tau + \eta/\eta'\}$ sample set. This behavior deserves to be confirmed by new precise η' dipion spectra, complementing [61]. So, while within the BHLS₂ framework, the η' decay is accounted for largely independently of the $e^+e^- \rightarrow \pi^+\pi^-$ annihilation process, but this does not prevent its prediction for $F_\pi(s)$ to exhibit a relatively fair accord with the (fully independent) $e^+e^- \rightarrow \pi^+\pi^-$ annihilation spectra.

Still, this accord is not perfect, and one has to contrast the good compatibility of the η/η' samples with the rest of the reference data set (as reflected in the high corresponding fit probability), and also the high probability of the $\{\mathcal{X}_\tau + \eta/\eta'\}$ fit (without the annihilation data contribution), and the visible pion form factor deviation causing the a_μ shift. It is difficult to be categorical at the moment about the nature of this effect on the form factor, which could be due to a variety of causes,³⁸ also because, as discussed in Sect. 11.3 below, it is sometimes difficult to interpret restricted data set fits, which have a more exploratory and confirmatory nature than “full” fits, and in principle, one should trust more our full data set fits, which indeed have no difficulty using the usual data sets in association with the η/η' data.

³⁶ Supplemented by the phase information between the ρ and ω propagators or by the product of branching fractions $\mathcal{B}(\omega \rightarrow e^-e^+) \times \mathcal{B}(\omega \rightarrow \pi^+\pi^-)$ available in the RPP [70].

³⁷ Nevertheless, the line shape is in good correspondence with those of the KLOE12 spectrum included in the $\{\mathcal{H}_R + \eta/\eta'\}$ sample set but slightly smaller than the others.

³⁸ We rechecked our calculations, the various fit information and other aspects but found no anomaly or hints about what could explain the shift. Of course, relatively straightforward causes of the deviation are almost surely excluded by the fact that the full data sets fit works quite well.

Table 5 The $P_X(s)$ parameter values from the A_- BHLS₂ variant fit. The first column indicates which data set combination is submitted to the global fit. $\langle\chi^2_{\pi\pi}\rangle$ indicates the average χ^2 of the timelike $F_\pi(s)$ data points of the sample named in the first column. α'_1 and α'_2 are the coeffi-

cients of the first- and second-degree terms of $P_X(s)$, respectively. The last data column displays the probability of the corresponding global fit

Data set	$\langle\chi^2_{\pi\pi}\rangle$	α'_1	α'_2	Prob. (%)
$\mathcal{X}_\tau + \text{KLOE08} + \eta/\eta'$	1.57	1.294 ± 0.053	-0.379 ± 0.049	61.4
$\mathcal{X}_\tau + \text{BaBar} + \eta/\eta'$	1.20	1.249 ± 0.076	-0.522 ± 0.069	39.6
$\mathcal{X}_\tau + \text{NSK} + \eta/\eta'$	0.98	1.314 ± 0.054	-0.606 ± 0.052	96.6
$\mathcal{X}_\tau + \text{KLOE} + \eta/\eta'$	0.99	1.341 ± 0.054	-0.525 ± 0.050	92.4
$\mathcal{H}_R + \eta/\eta'$	1.07	1.326 ± 0.053	-0.553 ± 0.048	90.6
$\mathcal{X}_\tau + \eta/\eta'$	×	1.453 ± 0.060	-0.792 ± 0.065	96.3

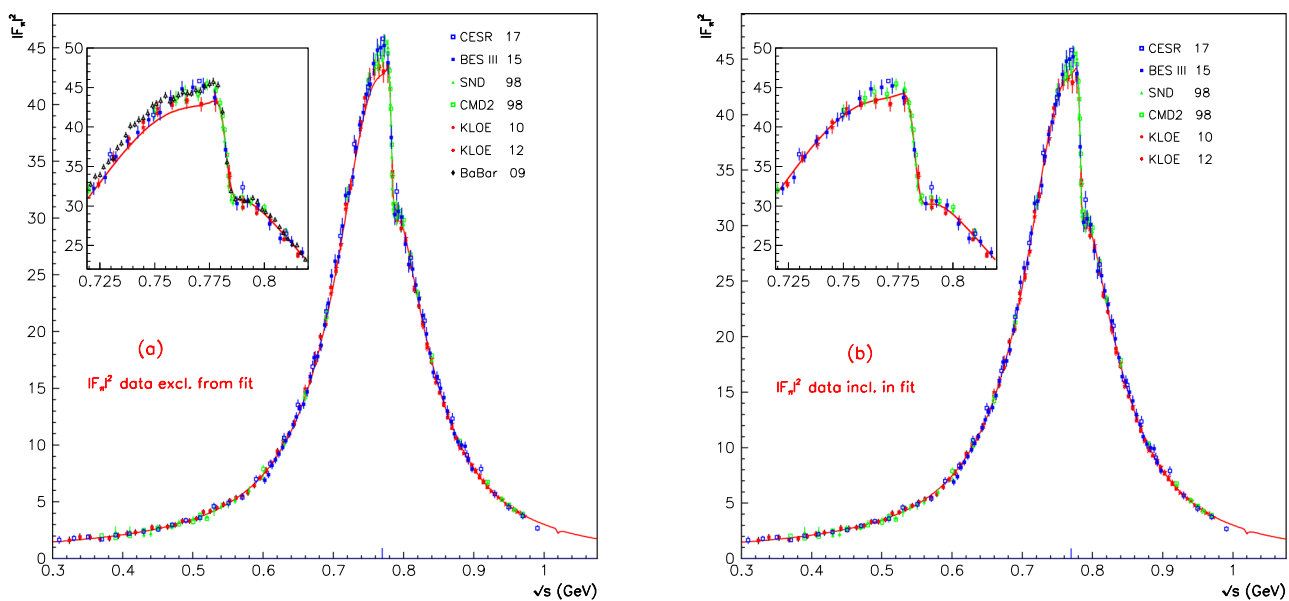


Fig. 7 The curve displayed in the left panel **a** is the pion form factor predicted by fitting the data sample set $\{\mathcal{X}_\tau + \eta/\eta'\}$ and, superimposed, the unfitted pion form factor spectra (including those from BaBar). The

right panel **b** shows the pion form factor derived from fitting the full $\{\mathcal{H}_R + \eta/\eta'\}$ data sample set which includes the KLOE and NSK pion form factors (but not the BaBar spectrum). See the text for comments

In any case, it seems that the a_μ value from valid fits where the $e^+e^- \rightarrow \pi^+\pi^-$ annihilation data are, to some extent, replaced by the η/η' data are much closer to the dispersive estimations than to the LQCD ones. This could indicate that part of the DR-LQCD discrepancy may not depend on experimental or analysis artifacts in the various experiments, since we witness a similar effect for the newly HLS fitted η/η' . If the present study is taken at face value, the DR-LQCD puzzle

seems in fact bolstered, but on the other hand, tentative solutions based on potential purely experimental-level problems could appear less favored (to be clear, we also trust LQCD results).

Based on the current knowledge, other specific interpretations for the DR-LQCD conundrum are speculative (possible effects beyond the Standard Model? $\pi\pi$ loop differences in e^+e^- annihilation channel? See also 11.3.2 below), and in

this light, the same can be stated about the FNAL measurement discrepancy [2] (and even more speculative are eventual causal links between the three a_μ determinations).

Regarding the function $P_X(s)$, awaiting for other theoretical estimates of it, one can conclude that our favored $P_X(s)$ parameterization³⁹ derived from fitting $(\mathcal{H}_R + \eta/\eta')$ provides already a reliable one and benefits from, respectively, a $\simeq 3\%$ and $\simeq 10\%$ precision for, respectively, the linear and the curvature terms.

11.2 The η/η' spectra and HVP estimates

The purpose of Fig. 8 is to elucidate the overall picture of the estimates for $a_\mu(\pi\pi, \sqrt{s} < 1.0 \text{ GeV})$ which emerges from the present work. The top bunch of data points display the values for $a_\mu(\pi\pi, \sqrt{s} \leq 1 \text{ GeV})$ in units of 10^{-10} derived by direct integration of the dipion data taking all dipion spectra, but either excluding the BaBar spectrum or excluding the KLOE spectra; the reason to proceed this way is related to inconsistencies occurring when fitting the pion form factors [21] as reported years prior [42].

The point showing the KNT19 result [6], the usual reference [3], is followed by the evaluation derived from the BHLS₂ global fit involving the $\mathcal{X}_\tau + KLOE + NSK + BABAR$ sample set which contains the same $e^+e^- \rightarrow \pi^+\pi^-$ dipion spectra⁴⁰ as KNT19. The central values derived for $a_\mu(\pi\pi, \sqrt{s} \leq 1 \text{ GeV})$ are substantially identical, reflecting the fact that the normalization uncertainty treatment used to derive the KNT19 evaluation is similar to our own [89]. The BHLS₂ uncertainty is however much improved (by a factor of $\simeq 2$), as can be expected from having performed a (more constraining) global fit; indeed, within a global context, in contrast with KNT19 and others who treat the dipion spectra in a standalone mode, one benefits from also involving the τ dipion spectra and all non- $\pi\pi$ final-state spectra, which play as an increased statistics for all the channels involved by the underlying HLS context, in particular the $\pi\pi$ one. Therefore, comparing KNT19 and our evaluation illustrates that the BHLS₂ Lagrangian approach does not generate biases and that the difference in the central values is essentially due to the data samples chosen to derive motivated physical conclusions.

³⁹ The $P_X(s)$ polynomial may well be interpreted as the lowest-order terms of the Taylor expansion of a more complicated function which does not behave as fast as a power law; for instance, one has checked that the function $U(s) = 1 + 0.5 \log(1 + 4s)$ (i.e., with no free parameter) gives results identical to those derived using the second-degree polynomials $P_X(s)$. Indeed, the probability returned by the fit of the $\{\mathcal{H}_R + \eta/\eta'\}$ data sample set is then 91.7%, and the average χ^2 's per data point are quite favorable: 1.08 for NSK, 1.04 for KLOE, 0.92 for the BESIII η' spectrum, and 0.90 for the η spectrum from KLOE/KLOE2.

⁴⁰ It should be recalled that the corresponding fit probability is low [21] (11.4%), reflecting the KLOE-BaBar tension.

The top two data points of the lowest bunch substantiate numerically the amplitude of the tension between using $\mathcal{X}_\tau + KLOE + NSK$ and $\mathcal{X}_\tau + BABAR + NSK$; both agree with the direct integration results and exhibit a $\simeq 5.4 \times 10^{-10}$ distance between their evaluations of $a_\mu(\pi\pi, \sqrt{s} \leq 1 \text{ GeV})$. In both cases, the first number displayed is the evaluation derived by a standard BHLS₂ fit and is 100% consistent with the results published in [21].

The number within parentheses instead displays the result obtained when adding the η/η' data set defined above according to, respectively, $\mathcal{X}_\tau + KLOE + NSK$ and $\mathcal{X}_\tau + BABAR + NSK$. One should note that the fit probabilities are unchanged when adding the η/η' data set and reflect fairly good fits: 88.7% \rightarrow 90.6% for $\mathcal{X}_\tau + KLOE + NSK (+\eta/\eta')$ and 47.2% \rightarrow 55.9% for $\mathcal{X}_\tau + BABAR + NSK (+\eta/\eta')$. This illustrates that there is no tension between the $e^+e^- \rightarrow \pi^+\pi^-$ dipion spectra and those derived from the (η/η') decays, as the probability difference between the fits involving the two data sample sets is not degraded by including the (η/η') samples. The corresponding central values are very similar too, confirming that there are no bad surprises with the η/η' data and the new Lagrangian terms describing them, at least in the $\mathcal{X}_\tau + KLOE + NSK$ and $\mathcal{X}_\tau + BABAR + NSK$ cases.

11.3 The case for the τ data

11.3.1 Fitting the τ data

Among the data set combinations that look interesting to explore and fit, and in addition to the ones mentioned above, the quasi “standalone” fitting of the τ decay-specific data, in the spirit of what was achieved in our previous works [18], [19], and [89]⁴¹ for the BHLS model, seems in order.

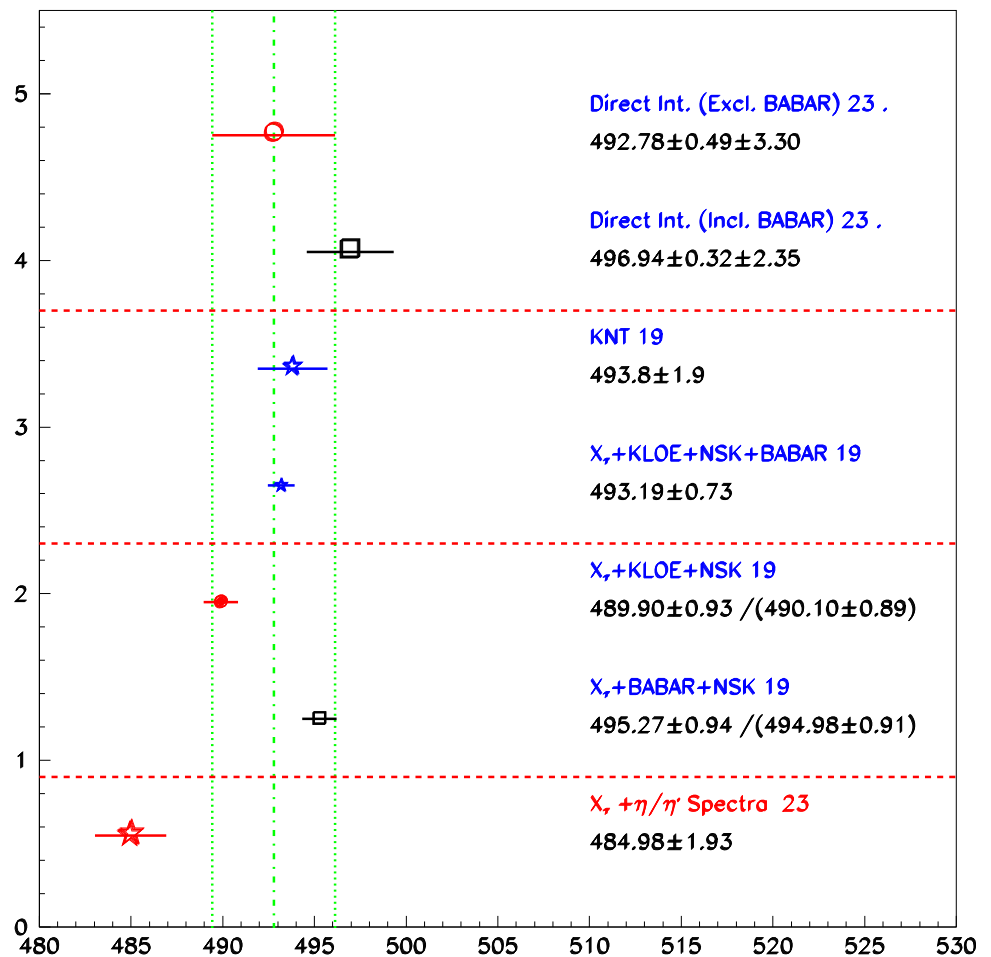
Since the inception of the BHLS₂ type of models [20], we are unable to reach a satisfactory convergence (and good global probability) for such a fit, using the same type of complementary simple ($\pi\pi$ -independent) RPP data that was used for BHLS (with some tentative variations in these data choices, and also in the MINUIT fit handling). We made additional tries⁴² by adding in the fitted data set spacelike $\pi\pi$ data (the idea being to constrain the fit behavior around $s = 0$, while mostly preserving independence from the annihilation $\pi\pi$ information, due also to the limited statistical weight of the spacelike data sets), but to no avail. So, whereas the working quasi “standalone” τ fit in the BHLS framework allowed us to nicely reconstruct the full pion vector form factor⁴³ (including in the near spacelike region), and vice versa

⁴¹ See Section 7.1 and Figure 4 in the last reference for example.

⁴² Recently, for some of them.

⁴³ By also using some simple complementary RPP information; see details in our previous [19], Section 4.1.

Fig. 8 $a_\mu(\pi\pi, \sqrt{s} < 1.0 \text{ GeV})$ in units of 10^{-10} for various data sample combinations. The top two data points display the values derived by a direct integration of all the dipion spectra (when including BaBar, KLOE is excluded) [94]. The point tagged by KNT19 [6] is a usual (external) reference; the following point is derived using BHLS₂ with the indicated (largest) content of $e^+e^- \rightarrow \pi^+\pi^-$ spectra. The two following points show our fit results for two indicated combinations of data samples; within parentheses, one also displays the results obtained by also including the η/η' samples within the global fit procedure. The small magnitude of the BHLS₂-derived uncertainties should be noted (see text). The bottom entry in this figure exhibits the prediction derived for $a_\mu(\pi\pi, \sqrt{s} < 1.0 \text{ GeV})$ when all annihilation to dipion data are discarded from the fit. The growth of its uncertainty reflects the drastic reduction of the statistics involved in the corresponding fit



for the dipion spectra in τ decays, using only the τ data for the former and only the annihilation $\pi\pi$ data for the latter, BHLS₂ does not seem to behave in the same way.

While this could seem disappointing, the importance of not being able to fit the τ data in “standalone” form should be put into perspective. Indeed, several considerations are relevant:

- (i) Compared to BHLS, in BHLS₂ more general methods are employed to break symmetries (covariant derivative, kinetic breaking, for example); while those allow for a more consistent and more powerful way to parameterize the breakings, it seems that BHLS₂ is differently constrained in the τ sector. This could have the unfortunate effect of spoiling the BHLS₂ standalone τ fit convergence (due to secondary false minima, for example).
- (ii) While the standalone τ fit does not work in BHLS₂, we stress that the global fit, involving the full range of usual data sets (plus the τ and the new η/η' data), is well behaved and returns good probabilities, as reported above. This means BHLS₂, when correctly constrained,

describes adequately the data, and that the involved data sets, including the τ , are statistically compatible⁴⁴

- (iii) While it is advisable to perform partial data fits (like the τ one, and also the $\mathcal{X}_\tau + \eta/\eta'$ fit), there is no guarantee that fits will continue to converge while discarding data sets (without changing the model). It is difficult with relatively complicated and parametrically intricate models like BHLS₂ to predict the minimal set of data allowing sound convergence, and in practice, one resorts to the empirical method of trying to fit, hoping for good convergence and probability.⁴⁵ So while many workers use partial fits to explore sensitivities (of a_μ , for example) relative to the data set composition, in some cases, the meaning of those fits should be pondered. The min-

⁴⁴ The BHLS τ standalone fit was demonstrated at a time (around 2012) where various groups were doing and discussing this type of a_μ estimations (in particular due to the “ τ puzzle”), so some effort was invested into the study of this fit.

⁴⁵ This is indeed an example of some type of model dependence, and probably of the price to pay for having a global model encompassing all sorts of data.

imal acceptability requirement is of course that partial fits behave correctly and yield probabilities comparable to the full data set fits.

Apart from the well-known variations in the fitted data sets (like replacing KLOE by BaBar data, Fig. 8), in this work, we explored two interesting partial fits: the $\mathcal{X}_\tau + \eta/\eta'$ fit and the standalone τ fit. The former fit has good convergence and good probability, which is not the case for the latter (here, we confirmed our previous observations). This is why we kept the $\mathcal{X}_\tau + \eta/\eta'$ fit and discarded the incomplete τ fit, and give no a_μ estimation from this last fit.

Again, we emphasize that the role of these partial fits should not be overestimated: the real benchmarks for data compatibility and model adequacy are the full fits.

A worry could be that in full fits, data sets with lower statistical weight may be of little influence when fitted together with large and precise data sets (BaBar, KLOE, etc.). In these regards and in the a_μ determination case at least, we can think of two reasons to be reassured: (a) we consider only fits with high probability, meaning high *global* χ^2 probability which practically guarantees that the fitted pion form factor will be close to the data, and hence to the usual dispersive estimations; (b) we require also good *local* (partial) χ^2 probability in the various sectors/data sets in the function to be minimized, which de facto eliminates full fits which describe poorly a particular data set, and also allows sometimes to detect discrepancies between data sets.

Still, in view also of the recent renewed interest for the τ decay data, we have not completely abandoned the idea of demonstrating a τ quasi-standalone BHLS₂ fit, but the present lack of success in this endeavor certainly indicates an unknown level of difficulty.

11.3.2 τ data and a_μ

To broaden the discussion on the τ decay data, we repeat the comment conveyed in Subsection 21.3 of [20], where we put forward the idea that the QCD-QED interference at work in the neutral current (NC) $\pi^+\pi^-$ channel may cause a shift of the data with respect to the LQCD result. While in the neutral channel (NC) process $e^+e^- \rightarrow \pi^+\pi^-$, experiments measure the photon propagator, at leading order in lattice QCD one is calculating the pure QCD hadronic current two-point correlator, free of external QED corrections. In the charged current (CC) $\tau^\pm \rightarrow \pi^\pm\pi^0\nu_\tau$ decay, in contrast, one measures the W propagator in the quasi-static limit, and the ρ^+ meson does not mix with a photon exchange (also, no HVP subtraction correction needs to be applied), and the hadronic blob exhibited in the τ data is naturally much more directly related to the LQCD HVP than the one in the NC data. Actually, some recent τ data-driven analyses [95–97] find results such as $a_\mu^{HVP-LO}[\tau] = 704.1_{4.0}^{+4.1} \times 10^{-10}$, which

also is close to the dispersive results [98] of $a_\mu^{HVP-LO}[\tau] = 705.3 \pm 4.5[689.8 \pm 5.2] \times 10^{-10}$ (result excluding τ data in brackets).

When combining e^+e^- and τ data in HVP calculations, usually, the τ data are corrected towards matching the e^+e^- ones, where in the latter the QCD-QED mixing is inherent. A part of the QCD-QED mix-up is the $\rho^0 - \gamma$ [84] mixing. Besides having corrected the τ spectra by the commonly accepted isospin-breaking effects, other corrections like the $\rho^0 - \gamma$ mixing or the mass and width shift between ρ^0 and ρ^\pm can be applied to the I=1 component of $\pi^+\pi^-$ data in order to reduce the QED contamination of the latter.⁴⁶ In 2008, Belle [34] already, after applying standard (commonly accepted) isospin-breaking corrections, obtained the τ data-driven result $a_\mu^{\pi\pi}[2m_\pi, 1.8 \text{ GeV}] = (523.5 \pm 1.5(\text{exp.}) \pm 2.6(\text{Br.}) \pm 2.5(\text{isospin})) \times 10^{-10}$ (τ data from Belle), which was compared to the e^+e^- data-driven NSK result $a_\mu^{\pi\pi}[2m_\pi, 1.8 \text{ GeV}] = (504.6 \pm 3.1(\text{exp.}) \pm 0.9.6(\text{rad})) \times 10^{-10}$ (e^+e^- : CMD2, SND). The difference is 18.9×10^{-10} , and if applied to dispersive result $a_\mu^{HVP-LO}[e^+e^-] = (694.79 \pm 4.18) \times 10^{-10}$ [94], one gets 713.7×10^{-10} , and we note that with $a_\mu^{HVP-LO} = 718.2 \times 10^{-10}$, we would have the coincidence of theory and experiment in the muon $g - 2$: $a_\mu^{\text{exp.}} = a_\mu^{\text{th.}}$. Recently, the CMD-3 Collaboration [99], for the range 0.327 to 1.2 GeV, obtained $a_\mu^{\text{had};LO}(2\pi, \text{CMD3}) = (526.0 \pm 4.2) \times 10^{-10}$, to be compared to $(506.0 \pm 3.4) \times 10^{-10}$ reported in the white paper document. Again, the difference shifts the WP value $a_\mu^{HVP-LO}[e^+e^-] = (693.1 \pm 4.0) \times 10^{-10}$ to $(713.1 \pm 4.7) \times 10^{-10}$. We note that the CMD-3 result, clearly at variance with all previous $e^+e^- \rightarrow \pi^+\pi^-$ results, has been obtained by applying a new RLA-based generalized vector dominance model (GVDM) correction [100], whereas other experiments apply scalar QED to perform QED corrections. Using older $\pi\pi$ data, our HLS global fits (standalone or not) showed no incompatibility between the τ data and the annihilation $\pi\pi$ data, which seems to shift the problem away from a pure τ data incompatibility with other main data sets but rather towards a questioning of the relation between a_μ and the pion form factor as we know it.

11.4 η/η' -based evaluations of the HVP

If, as conjectured long ago [73], an accurate enough determination of the function $P_X(s)$ can be provided (by extended ChPT [43–45], possibly), dipion spectra from the η' decay may provide a new way to estimate the dipion contribution to

⁴⁶ In HLS, however, and as a consequence of using the extended BKY isospin-breaking mechanism, we showed that the data is better described by the induced difference in the universal vector coupling constant g appearing in the anomalous and non-anomalous parts of the Lagrangian (see [18], Section 12, for example).

the muon HVP up to $\simeq 1$ GeV. The present work has shown that phenomenology is able to provide already a function $P_X(s)$ carrying a noticeable precision, and moreover, it has also been shown that a unique function accommodates easily the available η and η' high-precision dipion spectra simultaneously.

Indeed, within the BHLS₂ context [20,21], the amplitudes for the $\eta/\eta' \rightarrow \pi^+\pi^-\gamma$ decays and for the $e^+e^- \rightarrow \pi^+\pi^-$ annihilation proceed from the same Lagrangian and do not call for a special treatment of their common dominant neutral ρ meson signal. Moreover, once the $P_X(s)$ effects are factored out, the derivation of both amplitudes from the same Lagrangian is unchanged.

On the other hand, discrepancies revealed by comparing with each other the dipion spectra collected in scan mode (NSK) and the various samples collected in ISR mode by KLOE [24,25,40] and BaBar [27,28] has not resulted in a really satisfactory solution; the recent SND20 [41]—and even more, presumably, the new CMD3 [7] data—seems rather to darken the picture.

Therefore, getting high-statistics dipion spectra independent of the e^+e^- annihilation mechanism, carrying different kinds of systematics, may helpfully contribute to a more satisfactory understanding of the crucial $\pi^+\pi^-$ contribution to the muon HVP.

For the time being, the limited number of high-statistics η [65] and η' [61] dipion spectra allow us to already derive the prediction for $a_\mu(\pi\pi, \sqrt{s} < 1.0$ GeV) displayed in the bottom of Fig. 8, namely,

$$a_\mu(\pi\pi, \sqrt{s} \leq 1 \text{ GeV}) = (484.98 \pm 1.93) \times 10^{-10} \quad (47)$$

with a 96.3% fit probability, and is distant from its estimate based on fitting the \mathcal{H}_R data sample set⁴⁷ by 2.6σ (conservatively). Therefore, additional high-statistics η/η' data samples can put more light on the issue, clearly located in the $\rho^0 - \omega$ invariant mass region.

12 Concluding remarks

The present work has shown that besides the already reported e^-e^+ annihilation spectra, some decay modes (especially the $P \rightarrow \gamma\gamma$ modes) or τ dipion spectra [20,21], BHLS₂ can encompass the dipion spectra from the η and η' decays; however, to reach this result, one has to invoke a (common) correction polynomial—not a part of the HLS model—as inferred by the SHKMW group in [73].

In this context, BHLS₂ offers a fairly good simultaneous fit of the η and η' dipion spectra together with the e^+e^-

annihilations into $\pi^+\pi^-/K\bar{K}/\pi^0\gamma/\eta\gamma$ final states and the $\tau^\pm \rightarrow \pi^\pm\pi^0\nu_\tau$ decay also addressed by the BHLS₂ framework in our previous [20,21].

This proves that once the $P_X(s)$ correction is accounted for, the BESIII η' spectrum [61] does not need more information that that already present in BHLS₂ to get a satisfactory picture; the picture is found as fair for the η spectrum reported in [65]—and, actually, even for those in [64]. The role of the charged ρ meson—a natural feature of BHLS₂, [21], never considered elsewhere—has been shown to provide a fair treatment of the $\eta' \rightarrow \pi^+\pi^-\gamma$ dipion spectrum.

This turns out to state that most of the parameters needed to write out the relevant decay amplitudes are not free but are numerically shared with the other channels embodied within the same BHLS₂ framework. This is an additional step in the proof in which a unified effective Lagrangian can fairly describe the low-energy physics up to and including the ϕ mass region.

One has first shown that the η and η' dipion spectra are well fitted with specific low-degree polynomials supplementing the amplitudes derived from the BHLS₂ Lagrangian. In a second step, it has been proved that, actually, the same second-degree polynomial $P_X(s)$ is involved in the considered η and η' decays, as inferred in [73]. As already noted, the ρ^\pm exchange implied by the kinetic breaking defined in [21] is shown to enhance the global fit quality. The polynomial coefficients have been derived from our fits with fair precision and found that they remain stable when varying the fit conditions (see Table 5).

It should be noted that the picture revealed by comparing both panels of Fig. 7 suggests that the traditionally used dipion spectra carry a line shape compatible with the η' dipion spectrum. Thus, higher statistics on this can be a helpful tool in the present controversy concerning the dispersive approaches and LQCD, due to the different systematics affecting the η' dipion spectrum, certainly independent of those involved in the $e^-e^+ \rightarrow \pi^+\pi^-$ annihilation. At its level of accuracy, the present η' dipion spectrum [61] rather favors the DR prediction, as shown in Fig. 8; this could indicate that the DR-LQCD a_μ discrepancy is not entirely related to experimental biases, since it appears also in the independent η/η' data, but could rather be a misunderstood effect in dispersive estimations for processes involving pion pairs.⁴⁸ However, better statistics and a finer binning in the $\rho^0 - \omega$ energy region look mandatory for a competing estimate of the muon $a_\mu(\pi^+\pi^-, \sqrt{s} < 1.0$ GeV). This may motivate our colleagues to enlarge the available η' dipion sample by analyzing the already existing data or by collecting new samples at other detectors.

⁴⁷ It is interesting to note that the distance between this prediction and the solution derived using NSK+KLOE is almost equal to the distance between the NSK+KLOE and NSK+BaBar solutions.

⁴⁸ It should be noted also that, in our global fit, the present η/η' data do not impact the appraisal of the BaBar/KLOE discrepancy.

Acknowledgements We gratefully acknowledge Andrzej Kupsc, Uppsala University, for having provided the KLOE/KLOE2 and the BESIII dipion spectra; additional information on these has also been quite helpful. The CNRS/IN2P3 Computing Center (Lyon - France) is also gratefully acknowledged for having provided the computing and data-processing resources needed for this work.

Data Availability Statement This manuscript has no associated data. [Authors' comment: Data sharing not applicable to this article as no datasets were generated during the current study.]

Open Access This article is licensed under a Creative Commons Attribution 4.0 International License, which permits use, sharing, adaptation, distribution and reproduction in any medium or format, as long as you give appropriate credit to the original author(s) and the source, provide a link to the Creative Commons licence, and indicate if changes were made. The images or other third party material in this article are included in the article's Creative Commons licence, unless indicated otherwise in a credit line to the material. If material is not included in the article's Creative Commons licence and your intended use is not permitted by statutory regulation or exceeds the permitted use, you will need to obtain permission directly from the copyright holder. To view a copy of this licence, visit <http://creativecommons.org/licenses/by/4.0/>. Funded by SCOAP³.

Appendices

A Brief outline of the HLS/BHLS₂ approach

For the reader's convenience, it appears worthwhile to avoid too much cross-references and briefly collect here the various ingredients which participate in the definition and working of our symmetry-broken hidden local symmetry (HLS) model which is spread out into several references. The HLS model admits a non-anomalous sector [12] and also an anomalous sector [13]—see also [16]. To make this approach a successful tool in its physical realm, the HLS model should undergo symmetry-breaking mechanisms. The salient features of the broken version named BHLS₂ which underlie the present study can be found, recalled, or defined, in⁴⁹ [20,21]. As it grounds the present study, the anomalous sector of the HLS model [13,16] is mostly discussed in the body of the text.

A.1 The unbroken non-anomalous HLS Lagrangian

The non-anomalous HLS Lagrangian is a generalization of the ChPT Lagrangian [101,102] which can be written [16] as

$$\begin{aligned} \mathcal{L}_{\text{chiral}} &= \frac{f_\pi^2}{4} \text{Tr} \left[\partial_\mu U \partial^\mu U^\dagger \right] \\ &= -\frac{f_\pi^2}{4} \text{Tr} \left[\partial_\mu \xi_L \xi_L^\dagger - \partial_\mu \xi_R \xi_R^\dagger \right]^2, \end{aligned} \quad (48)$$

⁴⁹ For full details, the interested reader is referred to these articles, where former references can also be found.

where f_π ($= 92.42$ MeV) is the pion decay constant, and

$$\xi_{R/L}(x) = \exp[\pm i P(x)/f_\pi] \implies U(x) = \xi_L^\dagger(x) \xi_R(x), \quad (49)$$

when working in the so-called unitary gauge, which removes a scalar field term in the definition of $\xi_{R/L}(x)$; $P(x)$ is the usual pseudoscalar (PS) field matrix. Ignoring in this reminder the weak sector [16,20], the HLS approach turns out to replace in Eq. (48) the usual derivative by the covariant derivative:

$$D_\mu \xi_{R/L} = \partial_\mu \xi_{R/L} - ig V_\mu \xi_{R/L} + ie \xi_{R/L} A_\mu Q, \quad (50)$$

where A_μ is the photon field, $Q = \text{Diag}[2/3, -1/3, -1/3]$ is the quark charge matrix, and V_μ is the vector field matrix; the expressions for P and⁵⁰ V are the usual ones—fulfilling the $U(3)$ flavor symmetry—and can be found in [16,18,103], for example. In this way, the first HLS Lagrangian piece named \mathcal{L}_A is derived from Eq. (49). However, a second piece— \mathcal{L}_V —can be defined, which vanishes in the inverse substitution $D_\mu \rightarrow \partial_\mu$. The two pieces are written as

$$\begin{aligned} \mathcal{L}_A &= -\frac{f_\pi^2}{4} \text{Tr} \left[D_\mu \xi_L \xi_L^\dagger - D_\mu \xi_R \xi_R^\dagger \right]^2, \\ \mathcal{L}_V &= -\frac{f_\pi^2}{4} \text{Tr} \left[D_\mu \xi_L \xi_L^\dagger + D_\mu \xi_R \xi_R^\dagger \right]^2, \end{aligned} \quad (51)$$

and the full non-anomalous HLS Lagrangian is written as

$$\mathcal{L}_{\text{HLS}} = \mathcal{L}_A + a \mathcal{L}_V, \quad (52)$$

where a is a free parameter specific to the HLS approach [16]. This (unbroken) HLS Lagrangian can be found expanded in [103].

A.2 Breaking the HLS Lagrangian I: the BKY mechanism

The first breaking mechanism for the HLS Lagrangian has been proposed in [104]; one uses a modified version of it given in [103] in order to avoid identified undesirable properties of the original proposal [105]. Originally, the BKY mechanism was intended to only break the $U(3)$ symmetry of the HLS Lagrangian; it has been extended following the lines of [106] to also cover isospin-breaking effects.

Defining $L = D_\mu \xi_L \xi_L^\dagger$ and $R = D_\mu \xi_R \xi_R^\dagger$, the (modified and extended) BKY breaking is implemented in the BHLS₂ framework by modifying Eq. (51) as follows:

$$\begin{aligned} \mathcal{L}_A &= -\frac{f_\pi^2}{4} \text{Tr} [(L - R) X_A]^2, \\ \mathcal{L}_V &= -\frac{f_\pi^2}{4} \text{Tr} [(L + R) X_V]^2, \end{aligned} \quad (53)$$

⁵⁰ In the V matrix the ρ , ω and ϕ fields correspond to the so-called ideal fields.

where the constant matrices $X_{A/V}$ provide departures from the unit matrix; they have been parameterized as $X_{A/V} = \text{Diag}(q_{A/V}, y_{A/V}, z_{A/V})$. In practice, one prefers setting $q_{A/V} = 1 + (\Sigma_{A/V} + \Delta_{A/V})/2$ and $y_{A/V} = 1 + (\Sigma_{A/V} - \Delta_{A/V})/2$. As z_A and z_V are affecting the $s\bar{s}$ entries, their departure from 1 can be (and are found) large compared to $q_{A/V}$ and $y_{A/V}$ —which refer to, respectively, the $u\bar{u}$ and $d\bar{d}$ entries [18,20,21].

Within the BHLS₂ context opened in [20], it has been shown that the diagonalization of the vector meson mass term implies $\Delta_V = 0$; on the other hand, it has also been proved [20] that Σ_V is actually out of reach and can be fixed to zero without any loss of generality. Therefore, the BKY-breaking mechanism introduces three free parameters: z_A and Δ_A tightly related with the ratio f_K/f_π and z_V with the Higgs–Kibble ϕ meson mass.

A.3 Breaking the HLS Lagrangian II: the covariant derivative (CD) breaking

The main ingredient in the HLS approach is the covariant derivative as displayed in Eq. (50), complemented when relevant by W and Z^0 terms [16]. Thus, a relevant breaking mechanism can be chosen affecting the covariant derivative itself; this can be done by replacing Eq. (50) by

$$D_\mu \xi_{R/L} = \partial_\mu \xi_{R/L} - ig \left[V_\mu^I + \delta V_\mu \right] \xi_{R/L} + ie \xi_{R/L} A_\mu Q, \tag{54}$$

where δV_μ can be chosen to break the $U(3)_V$ symmetry in a controlled way. Breaking the universality of the vector coupling g is an interesting tool; a priori one may think that breaking nonet symmetry (i.e., along the Gell–Mann matrix T^0) can be performed independently of breaking the $SU(3)_V$ symmetry (i.e., along the Gell–Mann matrix T^8); the diagonalization of the vector meson mass term and the expected values of the pion and kaon form factors at the chiral point prevent such a freedom of choice [20].

Identifying the field combinations associated with each of the canonical Gell–Mann T_a $U(3)$ matrix basis, one is led to define the following components which can participate to δV_μ separately or together:

$$\begin{cases} \delta V_\mu^0 = \frac{\xi_0}{\sqrt{2}} \left[\frac{\sqrt{2}\omega_\mu^I + \Phi_\mu^I}{3} \right] \text{Diag}[1, 1, 1], \\ \delta V_\mu^8 = \frac{\xi_8}{\sqrt{2}} \left[\frac{\omega_\mu^I - \sqrt{2}\Phi_\mu^I}{3\sqrt{2}} \right] \text{Diag}[1, 1, -2], \\ \delta V_\mu^3 = \frac{\xi_3}{\sqrt{2}} \left[\frac{\rho_\mu^0}{\sqrt{2}} \right] \text{Diag}[1, -1, 0], \end{cases} \tag{55}$$

in terms of the usual ideal field combinations; the CD-breaking term is

$$\delta V_\mu = \delta V_\mu^0 + \delta V_\mu^8 + \delta V_\mu^3.$$

The (free) breaking parameters ξ_0 , ξ_8 , and ξ_3 are only requested to be real in order that δV_μ is hermitian as V_μ^I itself. Clearly, δV_μ^0 defines a breaking of the nonet symmetry down to $SU(3)_V \times U(1)_V$, δV_μ^8 rather expresses the breaking of the $SU(3)_V$ symmetry, while δV_μ^3 is related to a direct breaking of isospin symmetry in the vector sector.

As mentioned above, it happens that the ξ parameters introduced by Eq. (55) should fulfill [20] $\xi_0 = \xi_8$, and so that the CD breaking only involves two new free parameters. This means that within BHLS₂, one cannot solely break nonet symmetry, which should be accompanied by a $SU(3)$ breaking of similar intensity.

A.4 Breaking the HLS Lagrangian III: dynamical vector meson mixing

The unbroken HLS Lagrangian already exhibits couplings for $\rho_I/\omega_I/\phi_I \rightarrow K^+K^-/K^0\bar{K}^0$ transitions; this property is naturally transferred to all its broken versions. This implies that at one-loop order, the $\rho^0/\omega/\phi$ squared mass matrix exhibits non-diagonal entries, and thus, the ideal vector fields are no longer mass eigenstates.

At one-loop order, the squared mass matrix of the $\rho^0/\omega/\phi$ system can be written as

$$M^2(s) = M_0^2(s) + \delta M^2(s), \tag{56}$$

where the dependence upon the momentum squared s flowing through the vector lines is made explicit. After the BKY and CD breakings just sketched, the vector meson masses are written⁵¹ as

$$\begin{cases} m_{\rho^0}^2 = m^2 [1 + \Sigma_V + 2 \xi_3], \\ m_\omega^2 = m^2 \left[1 + \Sigma_V + \frac{4}{3} \xi_0 + \frac{2}{3} \xi_8 \right] \\ \quad = m^2 [1 + \Sigma_V + 2 \xi_0], \\ m_\phi^2 = m^2 z_V \left[1 + \frac{2}{3} \xi_0 + \frac{4}{3} \xi_8 \right] = m^2 z_V [1 + 2 \xi_0]. \end{cases} \tag{57}$$

in terms of the various breaking parameters; Σ_V has been kept for convenience. The $M_0^2(s)$ matrix occurring in Eq. (56) is thus written as

$$M_0^2(s) = \text{Diag}(m_{\rho^0}^2 + \Pi_{\pi\pi}(s), m_\omega^2, m_\phi^2). \tag{58}$$

and is diagonal; $\Pi_{\pi\pi}(s)$ is the pion loop and includes the $\rho\pi^+\pi^-$ coupling squared.

⁵¹ One should note that within BHLS₂, the charged and neutral ρ mesons carry different masses as $m_{\rho^\pm}^2 = m^2 (1 + \Sigma_V)$.

The expression for $\delta M^2(s)$ is slightly more involved. Having defined the (ρ^0, ω, ϕ) renormalized fields, generally indexed by R (i.e., those which diagonalize the vector meson mass term), one can derive the $\mathcal{V}_R^i \rightarrow \mathcal{V}_R^j$ transitions ($i, j = \rho^0, \omega, \phi$). For this purpose, having defined $\Pi_{\pm}(s)$ and $\Pi_0(s)$, respectively, the *amputated* charged and neutral kaon loops, the transition amplitudes ($i, j = \rho^0, \omega, \phi$) are written as

$$\delta M_{i,j}^2(s) = g_{K^+K^-}^i g_{K^+K^-}^j \Pi_{\pm}(s) + g_{K^0\bar{K}^0}^i g_{K^0\bar{K}^0}^j \Pi_0(s), \tag{59}$$

where the $g_{K\bar{K}}$ coupling constants are displayed in Section 10 of [20].

The *physical* ρ^0, ω, ϕ are the eigenvectors of the full squared mass matrix $M^2(s)$; they are related to their *renormalized* partners by

$$\begin{pmatrix} \rho_R \\ \omega_R \\ \Phi_R \end{pmatrix} = \begin{pmatrix} 1 & -\alpha(s) & \beta(s) \\ \alpha(s) & 1 & \gamma(s) \\ -\beta(s) & -\gamma(s) & 1 \end{pmatrix} \begin{pmatrix} \rho_{Phys} \\ \omega_{Phys} \\ \Phi_{Phys} \end{pmatrix} \tag{60}$$

The three complex angles occurring here are combinations of the $\delta M^2(s)$ matrix elements and of the eigenvalues of the full $M^2(s)$ matrix, as displayed in Subsection 10.2 of [20].

It is worth remarking that the dynamical mixing just sketched has provided the first solution [17, 18] to the long-standing puzzle “ e^+e^- versus τ ” [98, 107, 108], as it generates a s -dependent difference between the $\rho^{\pm} - W^{\pm}$ and $\rho^0 - \gamma$ transition amplitudes.

A.5 The kinetic breaking and the $[\pi^0, \eta, \eta']$ system

This section is mostly aimed at reviewing the notations used in the body of the paper; these essentially deal with the pseudoscalar meson (PS) sector of the HLS model.

The full pseudoscalar meson kinetic energy term of the BHLS₂ Lagrangian [21] is written as

$$\mathcal{L}_{kin} = \text{Tr} [\partial P_{bare} X_A \partial P_{bare} X_A] + 2 \{ \text{Tr} [X_H \partial P_{bare}] \}^2, \tag{61}$$

where P_{bare} is the PS *bare* field matrix. The first term is already broken by the BKY mechanism applied to the \mathcal{L}_A HLS Lagrangian piece (see Eq. 53 in Appendix A), and the second one expresses the so-called kinetic breaking generalizing the 'tHooft mechanism [71]. It has been shown in [21] that an appropriate choice for the X_H matrix is

$$X_H = \lambda_0 T_0 + \lambda_3 T_3 + \lambda_8 T_8 \tag{62}$$

in terms of the canonical $U(3)$ Gell–Mann matrices ($T_0 = I/\sqrt{6}$, $\text{Tr}[T_a T_b] = \delta_{ab}/2$) with real λ_i coefficients in close correspondence with the CD breaking term δV affecting the vector sector (see Appendix A.3). This choice manifestly allows for isospin symmetry breaking, nonet symmetry breaking (the so-called 't Hooft term [71]), and $SU(3)$ breaking.

It is useful to introduce the vector of PS fields as

$$\mathcal{V}_{any} = (\pi_{any}^3, \eta_{any}^0, \eta_{any}^8) \quad \text{where } any = (bare, R1, R) \tag{63}$$

to clarify the component indexing.

The diagonalization of the kinetic energy Eq. (61) which leads from the *bare* PS fields to their renormalized partners (hereafter indexed by R) is performed in two steps. The intermediate step (from *bare* to to $R1$ fields) turns out to diagonalize $\text{Tr} [\partial P_{bare} X_A \partial P_{bare} X_A]$ and to define the W transformation matrix as

$$W = \begin{pmatrix} 1 & -\frac{\Delta_A}{\sqrt{6}} & -\frac{\Delta_A}{2\sqrt{3}} \\ -\frac{\Delta_A}{\sqrt{6}} & B & A \\ -\frac{\Delta_A}{2\sqrt{3}} & A & C \end{pmatrix} \tag{64}$$

which depends on the BKY breaking parameter Δ_A and via

$$A = \sqrt{2} \frac{z_A - 1}{3z_A}, \quad B = \frac{2z_A + 1}{3z_A}, \quad C = \frac{z_A + 2}{3z_A} \tag{65}$$

on the other BKY breaking parameter z_A (see Appendix A.2 above).

In order to achieve the diagonalization of the (full) kinetic energy term of the BHLS₂ Lagrangian, one still has to define the linear transform which relates the intermediate $R1$ and final R renormalized PS fields (see Eq. (28) in [21]). Given the (co-)vector

$$a^t = (\lambda_3, \lambda_0 B + \lambda_8 A, \lambda_0 A + \lambda_8 C), \tag{66}$$

one can then prove [21] that Eq. (61) becomes canonical (at first order in breakings) when expressed in terms of the \mathcal{V}_R fields defined by

$$\mathcal{V}_{bare} = W \cdot \left[1 - \frac{1}{2} a \cdot a^t \right] \cdot \mathcal{V}_R. \tag{67}$$

However, the \mathcal{V}_R fields are not still the PS mass eigenstates denoted by the triplet (π^0, η, η') . One expects these *physical* states to be related with the \mathcal{V}_R fields via a three-dimensional rotation and thus three angles. Adopting the Leutwyler parameterization [109], one has

$$\begin{pmatrix} \pi_R^3 \\ \eta_R^8 \\ \eta_R^0 \end{pmatrix} = \begin{pmatrix} 1 & -\epsilon & -\epsilon' \\ \epsilon \cos \theta_P + \epsilon' \sin \theta_P & \cos \theta_P & \sin \theta_P \\ -\epsilon \sin \theta_P + \epsilon' \cos \theta_P & -\sin \theta_P & \cos \theta_P \end{pmatrix} \begin{pmatrix} \pi^0 \\ \eta \\ \eta' \end{pmatrix} \tag{68}$$

to relate the R fields which diagonalize the kinetic energy to the physical (i.e., mass eigenstates) neutral PS fields. The three angles (ϵ , ϵ' , and even θ_P) are assumed $\mathcal{O}(\delta)$ perturbations; nevertheless, for clarity, the so-called third mixing angle [72] is not treated as manifestly small.

On the other hand, the ‘‘angles’’ ϵ and ϵ' are related with the light quark masses, and it is worth stating that they are expected to have like signs (see the discussion in [21]).

B Erratum: the VPP/APP interaction pieces in BHLS₂

It is worthwhile to list the VPP and APP interaction terms of the BHLS₂ Lagrangian, corrected when needed, related with the present study, i.e., the charged and neutral pion fields, the η and η' mesons. We have

$$\begin{aligned} \mathcal{L}_{\pi^-\pi^+} &= ie \left[1 - \frac{a}{2}(1 + \Sigma_V) \right] A \cdot \pi^- \overleftrightarrow{\partial} \pi^+ \\ &\quad + \frac{ia g}{2} (1 + \Sigma_V) [1 + \xi_3] \rho_I^0 \cdot \pi^- \overleftrightarrow{\partial} \pi^+ \\ \mathcal{L}_{\pi^0\pi^\pm} &= \frac{ia g}{2} (1 + \Sigma_V) \left(1 - \frac{\lambda_3^2}{2} \right) \\ &\quad \left[\rho^- \cdot \pi^+ \overleftrightarrow{\partial} \pi^0 - \rho^+ \cdot \pi^- \overleftrightarrow{\partial} \pi^0 \right] \\ \mathcal{L}_{\eta\pi^\pm} &= -\frac{ia g}{2} \left[\left\{ \frac{1}{2\sqrt{3}} \Delta_A + \frac{\lambda_3 \tilde{\lambda}_8}{2} \right\} \cos \theta_P \right. \\ &\quad \left. - \left\{ \frac{1}{\sqrt{6}} \Delta_A + \frac{\lambda_3 \tilde{\lambda}_0}{2} \right\} \sin \theta_P + \epsilon \right] \\ &\quad [1 + \Sigma_V] \left[\rho^- \cdot \pi^+ \overleftrightarrow{\partial} \eta - \rho^+ \cdot \pi^- \overleftrightarrow{\partial} \eta \right] \\ \mathcal{L}_{\eta'\pi^\pm} &= -\frac{ia g}{2} \left[\left\{ \frac{1}{\sqrt{6}} \Delta_A + \frac{\lambda_3 \tilde{\lambda}_0}{2} \right\} \cos \theta_P \right. \\ &\quad \left. + \left\{ \frac{1}{2\sqrt{3}} \Delta_A + \frac{\lambda_3 \tilde{\lambda}_8}{2} \right\} \sin \theta_P + \epsilon' \right] \\ &\quad [1 + \Sigma_V] \left[\rho^- \cdot \pi^+ \overleftrightarrow{\partial} \eta' - \rho^+ \cdot \pi^- \overleftrightarrow{\partial} \eta' \right] \end{aligned} \tag{69}$$

The last two Lagrangian pieces supersede the corresponding formulae displayed in Eq. (45) of [21]; they were given for completeness but unused. In the present study, they should be considered.

In the expressions above, the kinetic breaking parameters occur; besides λ_3 , one also has

$$\tilde{\lambda}_0 = \lambda_0 B + \lambda_8 A, \quad \tilde{\lambda}_8 = \lambda_0 A + \lambda_8 C, \tag{70}$$

where A , B , and C have also been mentioned in the Appendix A.5 just above. On the other hand, we have chosen here

to keep the Σ_V parameter for clarity. However, it has been shown in [21] that it is out of reach and can be fixed to zero without any loss of generality.

C A_\pm solutions: the AAP and VVP Lagrangians

It is worthwhile displaying the anomalous BHLS₂ Lagrangian pieces associated with the so-called triangle anomalies, having imposed the Kroll conditions [66], examined in full details in [21] and briefly sketched in Sect. 3. Using obvious notations, these anomalous pieces are derived from the following [13, 16]:

$$\begin{cases} \mathcal{L}_{VVP} = -\frac{N_c g^2}{4\pi^2 f_\pi} c_3 \epsilon^{\mu\nu\alpha\beta} \text{Tr}[\partial_\mu V_\nu \partial_\alpha V_\beta P] \\ \mathcal{L}_{AAP} = -\frac{N_c e^2}{4\pi^2 f_\pi} (1 - c_4) \epsilon^{\mu\nu\alpha\beta} \partial_\mu A_\nu \partial_\alpha A_\beta \text{Tr}[Q^2 P] \\ \mathcal{L}_{AVP} = -\frac{N_c g e}{8\pi^2 f_\pi} (c_4 - c_3) \epsilon^{\mu\nu\alpha\beta} \partial_\mu A_\nu \text{Tr}[\{\partial_\alpha V_\beta, Q\} P]. \end{cases} \tag{71}$$

The phenomenology examined so far with the broken variants of the HLS model never led to us consider a nonzero $c_3 - c_4$; therefore, one assumes $c_3 = c_4$, which turns out to discard the \mathcal{L}_{AVP} Lagrangian piece.

Unless otherwise stated, the neutral vector fields displayed here are the so-called ideal combinations generally named ρ^I , ω^I , and ϕ^I . The transformation which connects the *bare* vector fields to their *physical* partners is treated in [20] and briefly mentioned in Appendix A above.

We also recall here the definition for δ_P :

$$\begin{cases} \sin \delta_P = \frac{1}{\sqrt{3}} (\sqrt{2} \sin \theta_P - \cos \theta_P), \\ \cos \delta_P = \frac{1}{\sqrt{3}} (\sqrt{2} \cos \theta_P + \sin \theta_P) \end{cases} \tag{72}$$

and ($d_\pm \equiv \pm 1$)

$$A_\pm = \Delta_A + d_\pm \lambda_0^2. \tag{73}$$

used below.

C.1 The AAP Lagrangian

The AAP Lagrangian defined in the header just above where Q is the quark charge matrix and P the $U(3)$ symmetric matrix of the bare pseudoscalar fields is given for definiteness:

$$\left\{ \begin{aligned} g_{\pi^0\gamma\gamma} &= \frac{1}{6} \left\{ 1 - \frac{5}{6} A_{\pm} - \frac{\lambda_0^2}{3} \right\} \\ &\quad - \frac{\epsilon}{18z_A} \left\{ 5z_A \sin \delta_P + \sqrt{2} \cos \delta_P \right\} \\ &\quad - \frac{\epsilon'}{18z_A} \left\{ \sqrt{2} \sin \delta_P - 5z_A \cos \delta_P \right\}, \\ g_{\eta\gamma\gamma} &= -\frac{\epsilon}{6} - \frac{\sqrt{2}}{18z_A} \cos \delta_P \\ &\quad + \frac{1}{12} \left\{ A_{\pm} + \frac{5}{6} (3\lambda_0^2 - 4) \right\} \sin \delta_P \\ g_{\eta'\gamma\gamma} &= -\frac{\epsilon'}{6} - \frac{\sqrt{2}}{18z_A} \sin \delta_P \\ &\quad - \frac{1}{12} \left\{ A_{\pm} + \frac{5}{6} (3\lambda_0^2 - 4) \right\} \cos \delta_P. \end{aligned} \right. \tag{74}$$

The coupling constants for the physical mesons $P_0\gamma\gamma$ ($P_0 = \pi^0, \eta, \eta'$) are given by

$$G_{P_0\gamma\gamma} = -\frac{3\alpha_{em}}{\pi f_{\pi}} (1 - c_4) g_{P_0\gamma\gamma}, \tag{75}$$

and the AAP Lagrangian can also be written as

$$\mathcal{L}_{AAP_0} = G_{P_0\gamma\gamma} P_0 \epsilon^{\mu\nu\alpha\beta} \partial_{\mu} A_{\nu} \partial_{\alpha} A_{\beta} \text{ for each of } P_0 = \pi^0, \eta, \eta'. \tag{76}$$

C.2 The VVP Lagrangian

The VVP Lagrangian is given by

$$\begin{aligned} \mathcal{L}_{VVP} &= -\frac{3g^2}{4\pi^2 f_{\pi}} c_3 \epsilon^{\mu\nu\alpha\beta} \text{Tr} [\partial_{\mu} V_{\nu} \partial_{\alpha} V_{\beta} P], \\ C &= -\frac{N_c g^2 c_3}{4\pi^2 f_{\pi}}. \end{aligned} \tag{77}$$

C.2.1 The $VV\pi$ Lagrangians

The $VV\pi$ Lagrangians relevant for our phenomenology are given by

$$\begin{aligned} \mathcal{L}_{VVP}(\pi^{\pm}) &= \frac{C}{2} \epsilon^{\mu\nu\alpha\beta} \left\{ \left[\left(1 + \frac{2\xi_0 + \xi_8}{3} \right) \partial_{\mu} \omega_{\nu}^I \right. \right. \\ &\quad \left. \left. + \frac{\sqrt{2}}{3} (\xi_0 - \xi_8) \partial_{\mu} \phi_{\nu}^I \right] \right. \\ &\quad \left. \times \left[\partial_{\alpha} \rho_{\beta}^+ \pi^- + \partial_{\alpha} \rho_{\beta}^- \pi^+ \right] \right\} \end{aligned} \tag{78}$$

and:

$$\begin{aligned} \mathcal{L}_{VVP}(\pi^0) &= \frac{C}{2} \epsilon^{\mu\nu\alpha\beta} \left\{ G_0 \partial_{\mu} \rho_{\nu}^I \partial_{\alpha} \omega_{\beta}^I + G_1 \left[2\partial_{\mu} \rho_{\nu}^- \partial_{\alpha} \rho_{\beta}^+ \right. \right. \\ &\quad \left. \left. + \partial_{\mu} \rho_{\nu}^I \partial_{\alpha} \rho_{\beta}^I + \partial_{\mu} \omega_{\nu}^I \partial_{\alpha} \omega_{\beta}^I \right] \right. \\ &\quad \left. + G_2 \partial_{\mu} \phi_{\nu}^I \partial_{\alpha} \phi_{\beta}^I + G_3 \partial_{\mu} \rho_{\nu}^I \partial_{\alpha} \phi_{\beta}^I \right\} \pi^0 \end{aligned} \tag{79}$$

where:

$$\left\{ \begin{aligned} G_0 &= \left[1 - \frac{\lambda_0^2}{3} + \frac{2\xi_0 + \xi_8}{3} + \xi_3 \right] \\ G_1 &= -\frac{A_{\pm}}{4} + \frac{1}{2} [\epsilon' \cos \delta_P - \epsilon \sin \delta_P] \\ G_2 &= -\frac{1}{z_A \sqrt{2}} [\epsilon' \sin \delta_P + \epsilon \cos \delta_P] \\ G_3 &= \frac{\sqrt{2}}{3} (\xi_0 - \xi_8). \end{aligned} \right. \tag{80}$$

Actually, one imposes $\xi_0 = \xi_8$, so that, always, $G_3 = 0$.

C.2.2 The $VV\eta$ Lagrangian

The $VV\eta$ Lagrangian is given by

$$\begin{aligned} \mathcal{L}_{VVP}(\eta) &= \frac{C}{2} \epsilon^{\mu\nu\alpha\beta} \left\{ K_1 \partial_{\mu} \rho_{\nu}^- \partial_{\alpha} \rho_{\beta}^+ + K_2 \partial_{\mu} \rho_{\nu}^I \partial_{\alpha} \rho_{\beta}^I \right. \\ &\quad \left. + K_3 \partial_{\mu} \omega_{\nu}^I \partial_{\alpha} \omega_{\beta}^I + K_4 \partial_{\mu} \phi_{\nu}^I \partial_{\alpha} \phi_{\beta}^I \right. \\ &\quad \left. + K_5 \partial_{\mu} \omega_{\nu}^I \partial_{\alpha} \phi_{\beta}^I + K_6 \partial_{\mu} \rho_{\nu}^I \partial_{\alpha} \omega_{\beta}^I \right\} \eta. \end{aligned} \tag{81}$$

Having defined⁵²

$$\left\{ H_2 = \frac{1}{8} [3\lambda_0^2 - 4], H_3 = -\frac{\sqrt{2}}{6z_A} [(3 + 2\xi_0 + 4\xi_8)] \right\} \tag{82}$$

the $VV\eta$ couplings become:

$$\left\{ \begin{aligned} K_1 &= 2H_2 \sin \delta_P, & K_2 &= (H_2 - \xi_3) \sin \delta_P \\ K_3 &= \left[H_2 - \frac{2\xi_0 + \xi_8}{3} \right] \sin \delta_P, & K_4 &= H_3 \cos \delta_P \\ K_5 &= -\frac{(\xi_0 - \xi_8)}{3z_A} [2 \cos \delta_P + z_A \sqrt{2} \sin \delta_P], \\ K_6 &= \frac{A_{\pm}}{2} \sin \delta_P - \epsilon \end{aligned} \right. \tag{83}$$

Actually, similarly to just above, the K_5 term drops out in the practical BHLS₂ context.

C.2.3 The $VV\eta'$ Lagrangian

The $VV\eta'$ Lagrangian is given by

$$\begin{aligned} \mathcal{L}_{VVP}(\eta') &= \frac{C}{2} \epsilon^{\mu\nu\alpha\beta} \left\{ K'_1 \partial_{\mu} \rho_{\nu}^- \partial_{\alpha} \rho_{\beta}^+ + K'_2 \partial_{\mu} \rho_{\nu}^I \partial_{\alpha} \rho_{\beta}^I \right. \\ &\quad \left. + K'_3 \partial_{\mu} \omega_{\nu}^I \partial_{\alpha} \omega_{\beta}^I + K'_4 \partial_{\mu} \phi_{\nu}^I \partial_{\alpha} \phi_{\beta}^I \right. \\ &\quad \left. + K'_5 \partial_{\mu} \omega_{\nu}^I \partial_{\alpha} \phi_{\beta}^I + K'_6 \partial_{\mu} \rho_{\nu}^I \partial_{\alpha} \omega_{\beta}^I \right\} \eta' \end{aligned} \tag{84}$$

⁵² Referring to [21], the Kroll conditions turn out to fix $H_1 = 0$.

the $VV\eta'$ couplings being

$$\begin{cases} K'_1 = -2H_2 \cos \delta_P, & K'_2 = -(H_2 - \xi_3) \cos \delta_P \\ K'_3 = -\left[H_2 - \frac{2\xi_0 + \xi_8}{3}\right] \cos \delta_P, & K'_4 = H_3 \sin \delta_P \\ K'_5 = -\frac{(\xi_0 - \xi_8)}{3z_A} \left[-z_A \sqrt{2} \cos \delta_P + 2 \sin \delta_P\right], \\ K'_6 = -\frac{A_{\pm}}{2} \cos \delta_P - \epsilon' \end{cases} \tag{85}$$

where also the K'_5 term drops out in the practical BHLS₂ context, where $\xi_0 = \xi_8$. The H_i functions occurring here have been defined in our previous paper and have been mentioned in the subsection just above— H_1 vanishes thanks to having requested the Kroll conditions.

One should also note that the $VV\eta'$ couplings are related to the $VV\eta$ couplings and can be derived by making in the $VV\eta$ couplings

$$\{\sin \delta_P \rightarrow -\cos \delta_P \text{ and } \cos \delta_P \rightarrow \sin \delta_P\}.$$

D A_{\pm} solutions: the $APPP$ and $VPPP$ Lagrangians

Besides the Lagrangian pieces associated with the triangle anomalies mentioned in the Appendix just above, those associated with the so-called box anomalies play an important role in the $\eta/\eta' \rightarrow \pi^+\pi^-\gamma$ decays and in the $e^+e^- \rightarrow \pi^+\pi^-\pi^0$ annihilation thoroughly considered in our [21]. We find it helpful to provide their expressions while the Kroll conditions are applied. The $APPP$ and $VPPP$ Lagrangian pieces introduce a new HLS parameter ($c_1 - c_2$) which is not fixed by the model and should be derived from fits.

As for the VVP interactions mentioned in Appendix C, the neutral vector fields occurring in the $VPPP$ interaction Lagrangian are their ideal combinations; they should be expressed in terms of *physical* vector fields as developed in [20] in practical applications.

D.1 The $APPP$ Lagrangian

The $APPP$ Lagrangian is given by

$$\begin{aligned} \mathcal{L}_{APPP} &= D \epsilon^{\mu\nu\alpha\beta} A_{\mu} \text{Tr} [Q \partial_{\nu} P \partial_{\alpha} P \partial_{\beta} P], \\ D &= -i \frac{N_c e}{3\pi^2 f_{\pi}^3} \left[1 - \frac{3}{4}(c_1 - c_2 + c_4)\right]. \end{aligned} \tag{86}$$

Regarding the phenomenology we address, the relevant $APPP$ Lagrangian piece to be considered is

$$\begin{aligned} \mathcal{L}_{APPP}^1 &= D \epsilon^{\mu\nu\alpha\beta} A_{\mu} \left\{ g_{\gamma\pi^0} \partial_{\nu} \pi^0 + g_{\gamma\eta} \partial_{\nu} \eta + g_{\gamma\eta'} \partial_{\nu} \eta' \right\} \\ &\quad \partial_{\alpha} \pi^- \partial_{\beta} \pi^+, \end{aligned} \tag{87}$$

in terms of fully renormalized PS fields. Requiring the A_{\pm} Kroll conditions, these $g_{\gamma P}$ couplings can be written as

$$\begin{cases} g_{\gamma\pi^0} = -\frac{1}{4} \left[1 - \frac{A_{\pm}}{2} - \frac{\lambda_0^2}{3} - \epsilon \sin \delta_P + \epsilon' \cos \delta_P \right] \\ g_{\gamma\eta} = \left[1 - \frac{A_{\pm}}{2} - \frac{3\lambda_0^2}{4} \right] \frac{\sin \delta_P}{4} + \frac{\epsilon}{4} \\ g_{\gamma\eta'} = -\left[1 - \frac{A_{\pm}}{2} - \frac{3\lambda_0^2}{4} \right] \frac{\cos \delta_P}{4} + \frac{\epsilon'}{4}, \end{cases} \tag{88}$$

keeping only the leading-order terms in the breakings.

D.2 The $VPPP$ Lagrangian

The $VPPP$ anomalous HLS Lagrangian is

$$\begin{aligned} \mathcal{L}_{VPPP} &= -i \frac{N_c g}{4\pi^2 f_{\pi}^3} (c_1 - c_2 - c_3) \epsilon^{\mu\nu\alpha\beta} \\ &\quad \text{Tr} [V_{\mu} \partial_{\nu} P \partial_{\alpha} P \partial_{\beta} P] \end{aligned} \tag{89}$$

where the c_i are the FKTUY parameters not fixed by the model. N_c is the number of colors fixed to 3. The V and P field matrices are the bare ones.

The relevant part of \mathcal{L}_{VPPP} within the present context is

$$\begin{cases} \mathcal{L}_{VPPP}^{\pi^+\pi^-} \\ = E \epsilon^{\mu\nu\alpha\beta} \left\{ \left[g_{\rho\pi}^0 \partial_{\nu} \pi^0 + g_{\rho\eta}^0 \partial_{\nu} \eta + g_{\rho\eta'}^0 \partial_{\nu} \eta' \right] \rho_{\mu}^I \right. \\ \quad + \left[g_{\omega\pi}^0 \partial_{\nu} \pi^0 + g_{\omega\eta}^0 \partial_{\nu} \eta + g_{\omega\eta'}^0 \partial_{\nu} \eta' \right] \omega_{\mu}^I \\ \quad \left. + g_{\phi\pi}^0 \partial_{\nu} \pi^0 \phi_{\mu}^I \right\} \partial_{\alpha} \pi^- \partial_{\beta} \pi^+ \\ \text{with } E = -i \frac{3g(c_1 - c_2 - c_3)}{4\pi^2 f_{\pi}^3} \end{cases} \tag{90}$$

in terms of the *physical* pseudoscalar fields. Keeping only the A_{\pm} solutions and the leading-order breaking terms, the couplings just defined are

$$\begin{cases} g_{\rho\pi^0}^0 = \frac{1}{4} \left[\frac{A_{\pm}}{2} + \epsilon \sin \delta_P - \epsilon' \cos \delta_P \right] \\ g_{\rho\eta}^0 = \frac{1}{4} \left[1 + \xi_3 - \frac{3}{4} \lambda_0^2 \right] \sin \delta_P \\ g_{\rho\eta'}^0 = -\frac{1}{4} \left[1 + \xi_3 - \frac{3}{4} \lambda_0^2 \right] \cos \delta_P \end{cases} \tag{91}$$

and:

$$\begin{cases} g_{\omega\pi^0}^0 = -\frac{3}{4} \left[1 + \frac{2\xi_0 + \xi_8}{3} - \frac{1}{3} \lambda_0^2 \right] \\ g_{\omega\eta}^0 = \frac{3}{4} \left\{ \epsilon - \frac{A_{\pm}}{2} \sin \delta_P \right\} \\ g_{\omega\eta'}^0 = \frac{3}{4} \left\{ \epsilon' + \frac{A_{\pm}}{2} \cos \delta_P \right\} \\ g_{\phi\pi}^0 = -\frac{\sqrt{2}}{4} [\xi_0 - \xi_8], \quad g_{\phi\eta}^0 = 0, \quad g_{\phi\eta'}^0 = 0. \end{cases} \tag{92}$$

As pseudoscalar meson form factor values at origin imply [20] $\xi_0 = \xi_8$, one observes that no term involving ϕ^I survives at leading order in breakings.

References

- B. Abi et al., Measurement of the positive muon anomalous magnetic moment to 0.46 ppm (2021). [arXiv:2104.03281](#)
- Muon $g-2$, D.P. Aguillard et al., Measurement of the positive muon anomalous magnetic moment to 0.20 ppm (2023). [arXiv:2308.06230](#)
- T. Aoyama et al., The anomalous magnetic moment of the muon in the Standard Model. *Phys. Rep.* **887**, 1 (2020). [arXiv:2006.04822](#)
- B.L. Roberts, Status of the Fermilab muon ($g-2$) experiment. *Chin. Phys. C* **34**, 741 (2010). [arXiv:1001.2898](#)
- M. Davier, A. Hoecker, B. Malaescu, Z. Zhang, Reevaluation of the hadronic contributions to the muon $g-2$ and to alpha(MZ). *Eur. Phys. J. C* **71**, 1515 (2011). [arXiv:1010.4180](#)
- A. Keshavarzi, D. Nomura, T. Teubner, Muon $g-2$ and $\alpha(M_Z^2)$: a new data-based analysis. *Phys. Rev. D* **97**, 114025 (2018). [arXiv:1802.02995](#)
- CMD-3, F.V. Ignatov et al., Measurement of the $e^+e^- \rightarrow \pi^+\pi^-$ cross section from threshold to 1.2 GeV with the CMD-3 detector (2023). [arXiv:2302.08834](#)
- R. Alemany, M. Davier, A. Hocker, Improved determination of the hadronic contribution to the muon ($g-2$) and to alpha(M(Z)**2) using new data from hadronic tau decays. *Eur. Phys. J. C* **2**, 123 (1998). [arXiv:hep-ph/9703220](#)
- G. Ecker, J. Gasser, A. Pich, E. de Rafael, The role of resonances in chiral perturbation theory. *Nucl. Phys. B* **321**, 311 (1989)
- G. Ecker, J. Gasser, H. Leutwyler, A. Pich, E. de Rafael, Chiral Lagrangians for massive spin 1 fields. *Phys. Lett. B* **223**, 425 (1989)
- U.G. Meissner, Low-energy hadron physics from effective chiral lagrangians with vector mesons. *Phys. Rep.* **161**, 213 (1988)
- M. Bando, T. Kugo, K. Yamawaki, Nonlinear realization and hidden local symmetries. *Phys. Rep.* **164**, 217 (1988)
- T. Fujiwara, T. Kugo, H. Terao, S. Uehara, K. Yamawaki, Non-abelian anomaly and vector mesons as dynamical gauge bosons of hidden local symmetries. *Prog. Theor. Phys.* **73**, 926 (1985)
- V.V. Anashin, Measurement of R between 1.84 and 3.05 GeV at the KEDR detector. *Phys. Lett. B* **770**, 174 (2017). [arXiv:1610.02827](#)
- BES, M. Ablikim et al., R value measurements for e^+e^- annihilation at 2.60-GeV, 3.07-GeV and 3.65-GeV. *Phys. Lett. B* **677**, 239 (2009). [arXiv:0903.0900](#)
- M. Harada, K. Yamawaki, Hidden local symmetry at loop: a new perspective of composite gauge boson and chiral phase transition. *Phys. Rep.* **381**, 1 (2003). [arXiv:hep-ph/0302103](#)
- M. Benayoun, P. David, L. DelBuono, O. Leitner, H.B. O'Connell, The dipion mass spectrum in e^+e^- annihilation and tau decay: a dynamical (ρ^0 , ω , ϕ) mixing approach. *Eur. Phys. J. C* **55**, 199 (2008). [arXiv:hep-ph/0711.4482](#)
- M. Benayoun, P. David, L. DelBuono, F. Jegerlehner, Upgraded breaking of the HLS model: a full solution to the $\tau^- - e^+e^-$ and ϕ decay issues and its consequences on $g-2$ VMD estimates. *Eur. Phys. J. C* **72**, 1848 (2012). [arXiv:1106.1315](#)
- M. Benayoun, P. David, L. DelBuono, F. Jegerlehner, An update of the HLS estimate of the muon $g-2$. *Eur. Phys. J. C* **73**, 2453 (2013). [arXiv:1210.7184](#)
- M. Benayoun, L. Delbuono, F. Jegerlehner, BHLS₂, a new breaking of the HLS model and its phenomenology. *Eur. Phys. J. C* **80**, 81 (2020). [arXiv:1903.11034](#) [Erratum: *Eur. Phys. J. C* **80**, 244 (2020)]
- M. Benayoun, L. DelBuono, F. Jegerlehner, BHLS₂ upgrade: τ spectra, muon HVP and the [π^0 , η , η'] system. *Eur. Phys. J. C* **82**, 184 (2022). [arXiv:2105.13018](#)
- R.R. Akhmetshin et al., Measurement of the $e^+e^- \rightarrow \pi^+\pi^-$ cross section with the CMD-2 detector in the 370-MeV–520-MeV cm energy range. *JETP Lett.* **84**, 413 (2006). [arXiv:hep-ex/0610016](#)
- M.N. Achasov et al., Update of the $e^+e^- \rightarrow \pi^+\pi^-$ cross section measured by SND detector in the energy region 400-MeV $< \sqrt{s} < 1000$ -MeV. *J. Exp. Theor. Phys.* **103**, 380 (2006). [arXiv:hep-ex/0605013](#)
- KLOE, F. Ambrosino et al., Measurement of $\sigma(e^+e^- \rightarrow \pi^+\pi^-)$ from threshold to 0.85 GeV² using initial state radiation with the KLOE detector. *Phys. Lett. B* **700**, 102 (2011). [arXiv:1006.5313](#)
- KLOE Collaboration, D. Babusci et al., Precision measurement of $\sigma(e^+e^- \rightarrow \pi^+\pi^- \gamma)/\sigma(e^+e^- \rightarrow \mu^+\mu^- \gamma)$ and determination of the $\pi^+\pi^-$ contribution to the muon anomaly with the KLOE detector. *Phys. Lett. B* **720**, 336 (2013). [arXiv:1212.4524](#)
- KLOE-2, A. Anastasi et al., Combination of KLOE $\sigma(e^+e^- \rightarrow \pi^+\pi^- \gamma(\gamma))$ measurements and determination of $a_\mu^{\pi^+\pi^-}$ in the energy range 0.10 $< s < 0.95$ GeV². *JHEP* **03**, 173 (2018). [arXiv:1711.03085](#)
- BABAR, B. Aubert et al., Precise measurement of the $e^+e^- \rightarrow \pi^+\pi^- (\gamma)$ cross section with the Initial State Radiation method at BABAR. *Phys. Rev. Lett.* **103**, 231801 (2009). [arXiv:0908.3589](#)
- BABAR Collaboration, J. Lees et al., Precise measurement of the $e^+e^- \rightarrow \pi^+\pi^- (\gamma)$ cross section with the initial-state radiation method at BABAR. *Phys. Rev. D* **86**, 032013 (2012). [arXiv:1205.2228](#)
- BESIII, M. Ablikim et al., Measurement of the $e^+e^- \rightarrow \pi^+\pi^-$ cross section between 600 and 900 MeV using initial state radiation (2015). [arXiv:1507.08188](#)
- BESIII, M. Ablikim et al., Erratum to "Measurement of the $e^+e^- \rightarrow \pi^+\pi^-$ cross section between 600 and 900 MeV using initial state radiation". [arXiv:2009.05011](#) (2020)
- T. Xiao, S. Dobbs, A. Tomaradze, K.K. Seth, G. Bonvicini, Precision measurement of the hadronic contribution to the muon anomalous magnetic moment (2017). [arXiv:1712.04530](#)
- ALEPH, S. Schael et al., Branching ratios and spectral functions of tau decays: final ALEPH measurements and physics implications. *Phys. Rep.* **421**, 191 (2005). [arXiv:hep-ex/0506072](#)
- CLEO, S. Anderson et al., Hadronic structure in the decay $\tau^- \rightarrow \pi^- \pi^0 \nu_\tau$. *Phys. Rev. D* **61**, 112002 (2000). [arXiv:hep-ex/9910046](#)
- Belle, M. Fujikawa et al., High-statistics study of the $\tau^- \rightarrow \pi^- \pi^0 \nu_\tau$ decay. *Phys. Rev. D* **78**, 072006 (2008). [arXiv:0805.3773](#)
- S. Borsanyi Budapest-Marseille-Wuppertal, Hadronic vacuum polarization contribution to the anomalous magnetic moments of leptons from first principles. *Phys. Rev. Lett.* **121**, 022002 (2018). [arXiv:1711.04980](#)
- S. Borsanyi et al., Leading hadronic contribution to the muon magnetic moment from lattice QCD (2020). [arXiv:2002.12347](#)
- A. Gerardin et al., The leading hadronic contribution to $(g-2)_\mu$ from lattice QCD with $N_f = 2+1$ flavours of O(a) improved Wilson quarks. *Phys. Rev. D* **100**, 014510 (2019). [arXiv:1904.03120](#)
- M. Cè et al., Window observable for the hadronic vacuum polarization contribution to the muon $g-2$ from lattice QCD. *Phys. Rev. D* **106**, 114502 (2022). [arXiv:2206.06582](#)
- RBC, UKQCD, T. Blum et al., Calculation of the hadronic vacuum polarization contribution to the muon anomalous magnetic moment. *Phys. Rev. Lett.* **121**, 022003 (2018). [arXiv:1801.07224](#)
- KLOE, G. Venanzoni et al., A precise new KLOE measurement of $|F_\pi|^2$ with ISR events and determination of $\pi\pi$ contribution

- to a_μ for $0.592 < M_{\pi\pi} < 0.975$ GeV. AIP Conf. Proc. **1182**, 665 (2009). [arXiv:0906.4331](#)
41. SND, M. Achasov et al., Measurement of the $e^+e^- \rightarrow \pi^+\pi^-$ process cross section with the SND detector at the VEPP-2000 collider in the energy region $0.525 < \sqrt{s} < 0.883$ GeV (2020). [arXiv:2004.00263](#)
 42. M. Benayoun, Impact of the recent KLOE data samples on the estimate for the muon $g - 2$. Int. J. Mod. Phys. Conf. Ser. **35**, 1460416 (2014)
 43. R. Kaiser, H. Leutwyler, Large N_c in chiral perturbation theory. Eur. Phys. J. C **17**, 623 (2000). [arXiv:hep-ph/0007101](#)
 44. R. Kaiser, H. Leutwyler, in Adelaide 1998, Nonperturbative methods in quantum field theory, 15, Pseudoscalar decay constants at large N_c (2001). [arXiv:hep-ph/9806336](#)
 45. H. Leutwyler, On the $1/N$ -expansion in chiral perturbation theory. Nucl. Phys. Proc. Suppl. **64**, 223 (1998). [arXiv:hep-ph/9709408](#)
 46. T. Feldmann, P. Kroll, B. Stech, Mixing and decay constants of pseudoscalar mesons: the sequel. Phys. Lett. B **449**, 339 (1999). [arXiv:hep-ph/9812269](#)
 47. T. Feldmann, P. Kroll, B. Stech, Mixing and decay constants of pseudoscalar mesons. Phys. Rev. D **58**, 114006 (1998). [arXiv:hep-ph/9802409](#)
 48. T. Feldmann, Quark structure of pseudoscalar mesons. Int. J. Mod. Phys. A **15**, 159 (2000). [arXiv:hep-ph/9907491](#)
 49. A. Grigorian et al., Charge conjugation invariance in $\eta'(958) \rightarrow \pi^+\pi^-\gamma$. Nucl. Phys. B **91**, 232 (1975)
 50. JADE, W. Bartel et al., A measurement of the reaction $e^+e^- \rightarrow e^+e^-\eta'$ and the radiative width $\Gamma(\eta' \rightarrow \gamma\gamma)$ at PETRA. Phys. Lett. B **113**, 190 (1982)
 51. CELLO, H.J. Behrend et al., Determination of the radiative widths of the η' and A_2 from two photon exchange production. Phys. Lett. B **114**, 378 (1982) [Erratum: Phys. Lett. B **125**, 518 (1983)]
 52. TASSO, M. Althoff et al., Measurement of the radiative width of the η' (958) in two photon interactions. Phys. Lett. B **147**, 487 (1984)
 53. PLUTO, C. Berger et al., Measurement of exclusive η' production in $\gamma\gamma$ reactions. Phys. Lett. B **142**, 125 (1984)
 54. TPC/Two Gamma, H. Aihara et al., A study of η' formation in photon-photon collisions. Phys. Rev. D **35**, 2650 (1987)
 55. ARGUS, H. Albrecht et al., Measurement of $\eta' \rightarrow \pi^+\pi^-\gamma$ in $\gamma\gamma$ collisions. Phys. Lett. B **199**, 457 (1987)
 56. Lepton F, S.I. Bitukov et al., Study of the radiative decay $\eta' \rightarrow \pi^+\pi^-\gamma$. Z. Phys. C **50**, 451 (1991)
 57. Crystal Barrel, A. Abele et al., Measurement of the decay distribution of $\eta' \rightarrow \pi^+\pi^-\gamma$ and evidence for the box anomaly. Phys. Lett. B **402**, 195 (1997)
 58. J. Wess, B. Zumino, Consequences of anomalous Ward identities. Phys. Lett. B **37**, 95 (1971)
 59. E. Witten, Global aspects of current algebra. Nucl. Phys. B **223**, 422 (1983)
 60. M. Benayoun, P. David, L. DelBuono, P. Leruste, H.B. O'Connell, Anomalous η/η' decays: the triangle and box anomalies. Eur. Phys. J. C **31**, 525 (2003). [arXiv:nucl-th/0306078](#)
 61. BESIII, M. Ablikim et al., Precision study of $\eta' \rightarrow \gamma\pi^+\pi^-$ decay dynamics. Phys. Rev. Lett. **120**, 242003 (2018). [arXiv:1712.01525](#)
 62. J.G. Layter et al., Study of dalitz-plot distributions of the decays $\eta \rightarrow \pi^+\pi^-\pi^0$ and $\eta \rightarrow \pi^+\pi^-\gamma$. Phys. Rev. D **7**, 2565 (1973)
 63. M. Gormley et al., Experimental determination of the dalitz-plot distribution of the decays $\eta \rightarrow \pi^+\pi^-\pi^0$ and $\eta \rightarrow \pi^+\pi^-\gamma$, and the branching ratio $\eta \rightarrow \pi^+\pi^-\gamma$. Phys. Rev. D **2**, 501 (1970)
 64. WASA-at-COSY, P. Adlarson et al., Exclusive measurement of the $\eta \rightarrow \pi^+\pi^-\gamma$ decay. Phys. Lett. B **707**, 243 (2012). [arXiv:1107.5277](#)
 65. KLOE, D. Babusci et al., Measurement of $\Gamma(\eta \rightarrow \pi^+\pi^-\gamma)/\Gamma(\eta \rightarrow \pi^+\pi^-\pi^0)$ with the KLOE detector. Phys. Lett. B **718**, 910 (2013). [arXiv:1209.4611](#)
 66. P. Kroll, Isospin symmetry breaking through $\pi^0 - \eta - \eta'$ mixing. Mod. Phys. Lett. A **20**, 2667 (2005). [arXiv:hep-ph/0509031](#)
 67. H. Leutwyler, Electromagnetic form-factor of the pion, in *Continuous Advances in QCD 2002 / ARKADYFEST (honoring the 60th birthday of Prof. Arkady Vainshtein)*, pp. 23–40 (2002). [arXiv:hep-ph/0212324](#)
 68. G. Colangelo, Hadronic contributions to a_μ below one GeV. Nucl. Phys. B Proc. Suppl. **131**, 185 (2004). [arXiv:hep-ph/0312017](#)
 69. G. Colangelo, Chiral symmetry, $\pi\pi$ scattering and $\alpha(\mu)$. Nucl. Phys. B Proc. Suppl. **162**, 256 (2006)
 70. Particle Data Group, R.L. Workman et al., Review of Particle Physics (RPP). Prog. Theor. Exp. Phys. **2022**, 083C01 (2022)
 71. G. 't Hooft, How instantons solve the U(1) problem. Phys. Rep. **142**, 357 (1986)
 72. M. Benayoun, L. DelBuono, H.B. O'Connell, VMD, the WZW Lagrangian and ChPT: the third mixing angle. Eur. Phys. J. C **17**, 593 (2000). [arXiv:hep-ph/9905350](#)
 73. F. Stollenwerk, C. Hanhart, A. Kupsc, U.G. Meissner, A. Wirzba, Model-independent approach to $\eta \rightarrow \pi^+\pi^-\gamma$ and $\eta' \rightarrow \pi^+\pi^-\gamma$. Phys. Lett. B **707**, 184 (2012). [arXiv:1108.2419](#)
 74. C. Hanhart, A. Kupsc, U.G. Meißner, F. Stollenwerk, and A. Wirzba, Dispersive analysis for $\eta \rightarrow \gamma\gamma^*$. Eur. Phys. J. C **73**, 2668 (2013). [arXiv:1307.5654](#) [Erratum: Eur. Phys. J. C **75**, 242 (2015)]
 75. B. Kubis, J. Pleliter, Anomalous decay and scattering processes of the η meson. Eur. Phys. J. C **75**, 283 (2015). [arXiv:1504.02588](#)
 76. L.-Y. Dai, X.-W. Kang, U.-G. Meißner, X.-Y. Song, D.-L. Yao, Amplitude analysis of the anomalous decay $\eta' \rightarrow \pi^+\pi^-\gamma$. Phys. Rev. D **97**, 036012 (2018). [arXiv:1712.02119](#)
 77. S. Holz, C. Hanhart, M. Hoferichter, B. Kubis, A dispersive analysis of $\eta' \rightarrow \pi^+\pi^-\gamma$ and $\eta' \rightarrow \ell^+\ell^-\gamma$. Eur. Phys. J. C **82**, 434 (2022). [arXiv:2202.05846](#)
 78. S. Holz, C. Hanhart, M. Hoferichter, B. Kubis, Addendum: A dispersive analysis of $\eta' \rightarrow \pi^+\pi^-\gamma$ and $\eta' \rightarrow \ell^+\ell^-\gamma$. Eur. Phys. J. C **82**, 1159 (2022)
 79. R. Garcia-Martin, R. Kaminski, J.R. Pelaez, J. Ruiz de Elvira, F.J. Yndurain et al., The Pion-pion scattering amplitude. IV: Improved analysis with once subtracted Roy-like equations up to 1100 MeV. Phys. Rev. D **83**, 074004 (2011). [arXiv:1102.2183](#)
 80. J. Bijnens, A. Bramon, F. Cornet, Three pseudoscalar photon interactions in chiral perturbation theory. Phys. Lett. B **237**, 488 (1990)
 81. B. Hyams et al., $\pi\pi$ phase shift analysis from 600-MeV to 1900-MeV. Nucl. Phys. B **64**, 134 (1973)
 82. S.D. Protopopescu, $\pi\pi$ partial wave analysis from reactions $\pi^+p \rightarrow \pi^+\pi^-\Delta^{++}$ and $\pi^+p \rightarrow K^+K^-\Delta^{++}$ at 7.1-GeV/c. Phys. Rev. D **7**, 1279 (1973)
 83. B. Ananthanarayan, G. Colangelo, J. Gasser, H. Leutwyler, Roy equation analysis of pi pi scattering. Phys. Rep. **353**, 207 (2001). [arXiv:hep-ph/0005297](#)
 84. F. Jegerlehner, R. Szafron, $\rho^0 - \gamma$ mixing in the neutral channel pion form factor $|F_\pi|^2$ and its role in comparing e^+e^- with τ spectral functions. Eur. Phys. J. C **71**, 1632 (2011). [arXiv:1101.2872](#)
 85. SND, M. Achasov et al., Measurement of the $e^+e^- \rightarrow \pi^+\pi^-$ process cross section with the SND detector at the VEPP-2000 collider in the energy region $0.525 < \sqrt{s} < 0.883$ GeV. [arXiv:2004.00263](#) (2020)
 86. M. Hoferichter, B.-L. Hoid, B. Kubis, Three-pion contribution to hadronic vacuum polarization. JHEP **08**, 137 (2019). [arXiv:1907.01556](#)
 87. M. Hoferichter, B.-L. Hoid, B. Kubis, D. Schuh, Isospin-breaking effects in the three-pion contribution to hadronic vacuum polarization. JHEP **08**, 208 (2023). [arXiv:2307.02546](#)

88. D. Stamen, T. Isken, B. Kubis, M. Mikhasenko, M. Niehus, Analysis of rescattering effects in 3π final states. [arXiv:2212.11767](https://arxiv.org/abs/2212.11767) (2022)
89. M. Benayoun, P. David, L. DelBuono, F. Jegerlehner, Muon $g - 2$ estimates: can one trust effective Lagrangians and global fits? *Eur. Phys. J. C* **75**, 613 (2015). [arXiv:1507.02943](https://arxiv.org/abs/1507.02943)
90. M. Benayoun, P. David, L. DelBuono, O. Leitner et al., A global treatment of VMD physics up to the ϕ : I. e^+e^- annihilations, anomalies and vector meson partial widths. *Eur. Phys. J. C* **65**, 211 (2010). [arXiv:0907.4047](https://arxiv.org/abs/0907.4047)
91. NA7, S.R. Amendolia et al., A measurement of the space-like pion electromagnetic form-factor. *Nucl. Phys. B* **277**, 168 (1986)
92. E.B. Dally et al., Elastic scattering measurement of the negative pion radius. *Phys. Rev. Lett.* **48**, 375 (1982)
93. L. Gan, B. Kubis, E. Passemar, S. Tulin, Precision tests of fundamental physics with η and η' mesons. *Phys. Rep.* **945**, 1 (2022). [arXiv:2007.00664](https://arxiv.org/abs/2007.00664)
94. F. Jegerlehner, The effective fine structure constant and other SM running couplings. <https://people.physik.hu-berlin.de/~fjeger/alphaQED23.pdf> (2023)
95. J.A. Miranda, P. Roig, New τ -based evaluation of the hadronic contribution to the vacuum polarization piece of the muon anomalous magnetic moment. *Phys. Rev. D* **102**, 114017 (2020). [arXiv:2007.11019](https://arxiv.org/abs/2007.11019)
96. P. Masjuan, A. Miranda, P. Roig, [arXiv:2305.20005](https://arxiv.org/abs/2305.20005) (2023)
97. P. Masjuan, A. Miranda, P. Roig, Tau data-driven evaluation of the Hadronic Vacuum Polarization, in *26th High-Energy Physics International Conference in QCD*. [arXiv:2310.14102](https://arxiv.org/abs/2310.14102) (2023)
98. M. Davier et al., The discrepancy between τ and e^+e^- spectral functions revisited and the consequences for the muon magnetic anomaly. *Eur. Phys. J. C* **66**, 127 (2010). [arXiv:0906.5443](https://arxiv.org/abs/0906.5443)
99. F. Ignatov et al., Recent results from CMD-3. *EPJ Web Conf.* **212**, 04001 (2019)
100. F. Ignatov, R.N. Lee, *Phys. Lett. B* **833**, 137283 (2022). [arXiv:2204.12235](https://arxiv.org/abs/2204.12235)
101. J. Gasser, H. Leutwyler, Chiral perturbation theory to one loop. *Ann. Phys.* **158**, 142 (1984)
102. J. Gasser, H. Leutwyler, Chiral perturbation theory: expansions in the mass of the strange quark. *Nucl. Phys. B* **250**, 465 (1985)
103. M. Benayoun, H.B. O'Connell, SU(3) breaking and hidden local symmetry. *Phys. Rev. D* **58**, 074006 (1998). [arXiv:hep-ph/9804391](https://arxiv.org/abs/hep-ph/9804391)
104. M. Bando, T. Kugo, K. Yamawaki, On the vector mesons as dynamical gauge bosons of hidden local symmetries. *Nucl. Phys. B* **259**, 493 (1985)
105. A. Bramon, A. Grau, G. Pancheri, Effective chiral lagrangians with an SU(3) broken vector meson sector. *Phys. Lett. B* **345**, 263 (1995). [arXiv:hep-ph/9411269](https://arxiv.org/abs/hep-ph/9411269)
106. M. Hashimoto, Hidden local symmetry for anomalous processes with isospin/SU(3) breaking effects. *Phys. Rev. D* **54**, 5611 (1996). [arXiv:hep-ph/9605422](https://arxiv.org/abs/hep-ph/9605422)
107. M. Davier, A. Hoecker, B. Malaescu, Z. Zhang, Reevaluation of the hadronic contributions to the muon $g-2$ and to $\alpha(MZ)$. *Eur. Phys. J. C* **71**, 1515 (2011). [arXiv:1010.4180](https://arxiv.org/abs/1010.4180)
108. M. Benayoun, The HLS approach to $(g - 2)_\mu$: a solution to the τ versus e^+e^- puzzle. *EPJ Web Conf.* **118**, 01001 (2016). [arXiv:1511.01329](https://arxiv.org/abs/1511.01329)
109. H. Leutwyler, Implications of $\eta-\eta'$ mixing for the decay $\eta \rightarrow 3\pi$. *Phys. Lett. B* **374**, 181 (1996). [arXiv:hep-ph/9601236](https://arxiv.org/abs/hep-ph/9601236)